Università degli Studi di Palermo

AREA RICERCA E TRASFERIMENTO TECNOLOGICO
SETTORE DOTTORATI E CONTRATTI PER LA RICERCA
U. O. DOTTORATI DI RICERCA

UNIONE EUROPEA
Fondo Sociale Europeo

Ministero dell'Università e della Ricerca

PON REACT EU
RICERCA E INNOVAZIONE

Dottorato in Tecnologie e Scienze per la Salute dell'Uomo
Dipartimento di Scienze e Tecnologie Biologiche Chimiche e Farmaceutiche (STEBICEF)
Settore Scientifico Disciplinare BIO/18

Proteomic-based approach to investigate the role of iRhoms in cancer

IL DOTTORE
DONATELLA PIA SPANO'

IL COORDINATORE
PROF. BRUNO GIUSEPPE PIGNATARO

IL TUTOR
PROF. SALVATORE FEO

CO TUTOR
DOTT. SIMONE DARIO SCILABRA

CICLO XXXVII PON R&I 2014-2020
ANNO CONSEGUIMENTO TITOLO 2025

AREA RICERCA E TRASFERIMENTO TECNOLOGICO
SETTORE DOTTORATI E CONTRATTI PER LA RICERCA
U. O. DOTTORATI DI RICERCA

UNIONE EUROPEA
Fondo Sociale Europeo

Ministero dell'Università e della Ricerca

PON REACT EU
RICERCA E INNOVAZIONE

Dottorato in Tecnologie e Scienze per la Salute dell'Uomo
Dipartimento di Scienze e Tecnologie Biologiche Chimiche e Farmaceutiche (STEBICEF)
Settore Scientifico Disciplinare BIO/18

Proteomic-based approach to investigate the role of iRhoms in cancer

IL DOTTORE
DONATELLA PIA SPANO'

IL COORDINATORE
PROF. BRUNO GIUSEPPE PIGNATARO

IL TUTOR
PROF. SALVATORE FEO

CO TUTOR
DOTT. SIMONE DARIO SCILABRA

CICLO XXXVII PON R&I 2014-2020
ANNO CONSEGUIMENTO TITOLO 2025

A mia mamma Marianna
e
A mia sorella Florentina

The Power of Tiny Gains

	$1^{365} = 1$
1% better every day	$(1.01)^{365} = 37.78$
1% worse every day	$(0.99)^{365} = 0.03$

James Clear, *Atomic Habits*

Table of contents

Acknowledgements

A PhD is much more than a pursuit of knowledge. It is a deep journey that transforms the way we think, question, and approach the world. It is often challenging, but every challenge is an opportunity to adapt and evolve. In this journey, the support of tutors, peers, and colleagues is indispensable.

I would like to thank my PhD co-supervisor Dr. Simone Dario Scilabra for his invaluable mentorship since my internship in his research group. His indispensable advice and support during my challenging scientific journey helped to bring out the best in me and focus my efforts to achieve the best results from my work. He taught me all aspects of a research journey, from planning experiments and writing scientific papers to preparing posters and presentations, with great patience, guiding me to develop the skills necessary for achieving successful research outcomes.

I would like also to thank my PhD supervisor Prof. Salvatore Feo, for his priceless guidance throughout my studies, and for his endurance and expertise, which have been invaluable to my academic journey.

I wish to express my deepest gratitude to former and present members from Scilabra's group: Dr. Matteo Calligaris, Dr. Simone Bonelli, Margot Lo Pinto, Elisabetta Scalia, Maria Chiara Puccio, Dr. Oriana Lo Re, Andrea Capodici and Camilla Mangini. Working alongside such dedicated and talented young individuals has been both inspiring and enriching.

I am deeply grateful to ISMETT researchers Dr. Gioacchin Iannolo, Dr. Rosaria Tinnirello and Dr. Giovanni Zito for motivating me and supporting me daily in managing lab research life.

A special thanks to Dr. Carl P. Blobel and his research group – Dr. Gisela Weskamp, Qura-Tul-Ain (Annie) Khan, Dr. Minakshi Rana, and Alejandra Vela Moreno – for giving me the opportunity to join his lab in New York City, for the invaluable mentorship and willingness to fully support my research.

Finally, I would like to thank my mum Marianna and my sister Florentina, to whom my PhD thesis is dedicated. Thanks for your unconditional love and support for letting me pursue my dream of becoming a researcher. Your presence and your understanding have been essential for motivating me to move forward and help me through all the steps.

Preface

This PhD project was funded by

PON R&I 2014/2020 per lo sviluppo delle Azioni IV.4 “Dottorati e contratti di ricerca su tematiche dell'innovazione”.

Published on Cellular and Molecular Life Sciences

Calligaris M, Spanò DP, Bonelli S, Müller SA, Carcione C, D'apolito D, Amico G, Miele M, Di Bella M, Zito G, Nuti E, Rossello A, Blobel CP, Lichtenthaler SF, Scilabra SD. iRhom2 regulates ectodomain shedding and surface expression of the major histocompatibility complex (MHC) class I. Cell Mol Life Sci. 2024 Apr 4;81(1):163. doi: 10.1007/s00018-024-05201-7. PMID: 38570362; PMCID: PMC10991058.

This manuscript includes parts of Chapter 4 and related Materials and Methods.

Abstract

ADAM17 (A Disintegrin and Metalloprotease 17), also known as tumour necrosis factor-alpha converting enzyme (TACE), is a cell surface enzyme that belongs to the ADAM family of proteases. It is involved in shedding of over 80 different substrates, including growth factors (e.g. the epidermal growth factor receptor EGFR–ligands), cytokines (e.g. tumour necrosis factor-α –TNF), adhesion molecules, endocytic receptors and others. ADAM17 plays a crucial role in numerous biological processes but if dysregulated, leads to several pathologies, such as auto-inflammatory disorders and cancer. ADAM17 facilitates cancer progression by promoting cell proliferation, survival, migration and invasion. For instance, its action on EGFR ligands can activate downstream signalling pathways like MAPK and PI3K, which are often impaired in cancer. Additionally, the cleavage of TNF contributes to inflammation, creating a pro-tumour microenvironment. The maturation, trafficking and function of ADAM17 are controlled by the seven-membrane-spanning proteins iRhom1 and iRhom2. At the cell surface, iRhoms can integrate the stimuli leading to ADAM17 activation, functioning as the regulatory subunit of an iRhom/ADAM17 catalytic complex. While iRhom1 and iRhom2 share largely redundant roles in facilitating ADAM17 maturation, they differ significantly in their regulation of substrate selectivity. Evidence suggests that iRhom2 can support the stimulated shedding of most ADAM17 substrates, whereas iRhom1 appears to enable stimulated shedding for only a limited subset of substrates, such as TGFα.

On these premises, I conducted an unbiased mass spectrometry-based analysis to investigate in a systematic manner the sheddome resulting from the activity of iRhom1/ADAM17 or iRhom2/ADAM17 catalytic complexes. I found that the shedding of most ADAM17 substrates was supported by both iRhoms in murine and human fibroblasts. However, in the human fibroblast system, the efficiency of substrate shedding varied depending on whether ADAM17 was associated with iRhom1 or iRhom2, resulting in a continuum ranging from substrates preferentially cleaved by the iRhom1/ADAM17 complex to those preferentially cleaved by the iRhom2/ADAM17 complex.

In addition to enabling a systematic investigation of substrate selectivity, this approach identified several novel ADAM17 substrates, including SIRPα, MXRA8 and the major histocompatibility complex class I (MHC-I). Validation of MHC-I shedding by orthogonal methods, such as Western blotting and flow cytometry, demonstrated that iRhom2 regulated its surface levels through mechanisms beyond shedding. The loss of iRhom2 impaired MHC-I stability and trafficking to the cell surface in various cancer cell lines, including leukaemia

and chondrosarcoma. MHC-I, a transmembrane protein expressed in all eukaryotic nucleated cells, plays a key role in the presentation of foreign antigens, such as mutated oncogenic proteins, to the immune system. Its loss from the cell surface is of significant relevance in cancer, as it represents one of the immune evasion mechanisms adopted by several cancers, such as pancreatic ductal adenocarcinoma (PDAC).

In conclusion, this PhD project offered useful prompts for future investigation into iRhom/ADAM17 biology, particularly in the context of cancer. It identified novel ADAM17 substrates with established roles in cancer progression, such as SIRPα and MHC-I. Notably, it uncovered a key regulatory mechanism of MHC-I that modulates its surface levels in cancer cells. This mechanism may play a significant role in how PDAC evades immune surveillance during cancer progression. The finding that iRhom2 enhances MHC-I levels at the cell surface highlights its potential as a therapeutic target to improve the efficacy of immunotherapy, particularly in poorly immunogenic cancers (cold tumours) like PDAC. Preliminary results on three PDAC cell lines with increasing aggressiveness – PaTU8902, Panc1, AsPC1 – showed that surface levels of MHC-I decreased lacking iRhom2 and rescued when iRhom2 is present. Investigating iRhom2 regulation of MHC-I, along with its counterpart iRhom1, in PDAC is my follow-up project.

List of Figures

List of Tables

Chapter One:
Introduction

1.1 Ectodomain shedding

Membrane proteins participate in various physiological and pathological processes, playing a key role both in health and disease [1]. Several paracrine signalling proteins, including growth factors and cytokines, are initially synthesized as membrane-bound pro-proteins, that need to be released from the cell surface in order to start cell responses. The mechanism by which these pro-protein signalling molecules are liberated into the extracellular milieu involves their proteolytic cleavage, which results in the release of their extracellular domain (ectodomain) in the extracellular milieu. This proteolytic process is known as ectodomain shedding (hereafter referred to as *shedding*) (Figure 1), which is an irreversible post-translational modification that not only controls the release of signalling molecules, but also broadly regulates the function of membrane proteins [1,2].

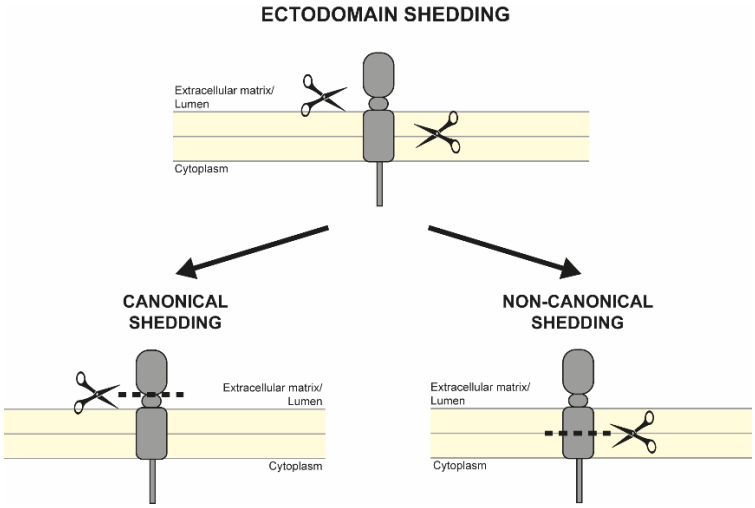

Figure 1: Schematic representation of ectodomain shedding. *Adapted from Lichtenthaler S. F. et al 2018*.

In addition to signalling proteins, membrane proteins frequently serve as receptors that bind specific ligands to initiate intracellular signalling cascades. In this context, receptor shedding acts as a key regulatory mechanism by reducing receptor availability at the cell surface, thereby attenuating downstream signalling. Beyond receptors, membrane proteins also mediate cell–cell adhesion and cell–extracellular matrix (ECM) interactions. Shedding of these adhesion molecules modulates their surface levels and, consequently, influences dynamic processes such as cell migration and invasion. Furthermore, membrane proteins function in transport and catalysis, and their shedding can impact various cellular processes, including endocytosis, proteolysis, glycosylation, and other regulatory mechanisms [1,2].

Shedding of transmembrane proteins is mediated by a specialised protease – referred to as a *sheddase* [1,2]. The proteolytic cleavage typically occurs close to the transmembrane (TM) domain, leading to the release of the entire extracellular portion of the protein, but in some cases, it occurs at more distal sites, resulting in the release of shorter fragments of the extracellular region. This process is known as "canonical shedding" [1]. However, some proteases cleave within the TM domain, mediating a process known as "non-canonical shedding". Notably, shedding is not restricted to the plasma membrane. It can also occur at

the membranes of intracellular organelles, such as the Golgi apparatus or endosomes [1]. In these cases, distinct from cell surface shedding, the ectodomain is released into the lumen of the organelle. Vesicles originating from these compartments subsequently fuse with the plasma membrane, releasing their luminal contents, including the shed ectodomains, into the extracellular space [3,4].

Many membrane proteins undergo a two-step cleavage, in which shedding acts as the first step, followed by "regulated intramembrane proteolysis" (RIP). During RIP, cleavage occurs within the transmembrane (TM) domain. As a result, the intracellular domain (ICD) may be released from the membrane and translocate into the nucleus to function as a transcriptional regulator [5,6]. Considering its broad involvement, ectodomain shedding contributes to maintain cellular and tissue homeostasis, from embryo development to cell death [7]. Dysregulation of this process could lead to numerous pathological conditions, such as inflammatory disorders, autoimmune disease, and cancers [1,2,7,8].

1.2 Sheddases

As mentioned above, ectodomain shedding is mediated by a specialized group of proteases, called "sheddases". Depending on the position of the cleavage site in the substrates' amino acidic sequence, sheddases can be divided in canonical sheddases and non-canonical sheddases.

Regardless of differences in membrane protein topology, which includes single-span transmembrane proteins (type I, with the N-terminus in the extracellular/lumenal domain, and type II, with the N-terminus intracellular), GPI-anchored proteins, and multipass proteins, we refer to canonical sheddases as those that cleave at the juxtamembrane (JM) domain, in close proximity to the cell membrane [1,9]. These sheddases are typically membrane-bound and include a disintegrin and metalloproteases (ADAMs) [7,10], β-site APP cleaving enzymes (BACE) [11], and membrane-type matrix metalloproteases (MT-MMPs) [12]. Also belonging to the group of membrane-bound canonical sheddases are meprin β [13], pro-protein convertases [14], and transmembrane serine proteases [15,16].

An increasing number of soluble proteases have also been identified as mediators of canonical shedding. For instance, several secreted MMPs [17,18] can function as canonical sheddases, along with legumain [19,20] and cathepsins S and L [21]. Furthermore, the concept of canonical shedding has broadened in recent years to include cleavages occurring at more distal sites within the ectodomain of transmembrane proteins, rather than strictly near the cell surface.

Table 1: List of canonical and non-canonical mammalian sheddases. *Adapted from Lichtenthaler S. F. et al 2018*.

Sheddase type	Protease family	Protease type	Catalytic mechanism	Cellular localization	References
Canonical sheddase	**ADAM proteases**	Membrane-anchored, type I	Metalloproteases	Plasma membrane	7,10
	BACE proteases	Membrane-anchored, type I	Aspartyl proteases	Trans-Golgi network and endosome	11
	MT-MMPs	Membrane-anchored, type I or GPI-anchored	Metalloproteases	Plasma membrane	12
	Meprin β	Membrane-anchored, type I	Metalloproteases	Plasma membrane	13
	Pro-protein convertases	Membrane-anchored, type I or soluble	Serine proteases	Late secretory pathway	14
	Transmembrane serine proteases	Membrane-anchored, type II	Serine proteases	Plasma membrane	15,16
	MMPs	Soluble	Metalloproteases	Extracellular space	17,18
	Legumain (δ-secretase)	Soluble	Cysteine protease	Lysosome, extracellular space	19,20
	Cathepsins S and L	Soluble	Cysteine proteases	Extracellular space	21
Non-canonical sheddase	**Rhomboids**	Integral multipass TM protein	Serine proteases	Golgi, plasma membrane, endosomes, ER	22,23
	SPP/SPPL family	Integral multipass TM protein	Aspartyl proteases	ER, lysosomes, cell surface, Golgi	24
	Presenilin/ɣ-secretase	Integral multipass TM protein	Aspartyl protease	Plasma membrane, endosomes	25

Unlike canonical sheddases, which cleave membrane proteins at juxtamembrane extracellular sites, non-canonical sheddases cleave within the transmembrane (TM) domain [1]. These proteases were initially thought to function exclusively in RIP and to require prior ectodomain shedding by canonical sheddases to access their substrates. However, recent evidence demonstrates that these sheddases can directly cleave full-length substrates, resulting in the release of the ectodomain into the extracellular space. Sheddases in this group

include rhomboid proteases [22,23], SPP/SPPL family [24], and γ-secretase in complex with presenilin-1 or -2 [25]. Notably, the primary function of some of these proteases is not ectodomain shedding. Nevertheless, they can also act as sheddases under certain physiological or pathological contexts. Due to this dual functionality, they are often referred to as "part-time" sheddases, in contrast to "full-time" sheddases, such as ADAMs and BACE proteases, whose main biological role is indeed regulating ectodomain [1].

All currently known families of canonical and non-canonical sheddases, their catalytic mechanism and typical cellular localization, are listed in Table 1.

1.2.1 Canonical sheddases

1.2.1.1 ADAM proteases

A Disintegrin and Metalloproteases (ADAMs) are membrane-tethered proteases with their catalytic domain extruding into the extracellular compartment [7,10,26].

ADAMs were initially identified as the heterodimeric protein fertilin – consisting of ADAM1 and ADAM2 [27–29]. Since their discovery, they have been found in a wide variety of mammalian tissues, as well as in non-mammalian organisms such as *Xenopus laevis* [30], *Drosophila melanogaster*[31], *Caenorhabditis elegans* [32], and *Schizosaccharomyces pombe* [33]. Up to date, 30 ADAM family members have been recognized in mammals, although about half of them possess a functional metalloprotease domain and display proteolytic activity (ADAM8, 9, 10, 12, 15, 17, 19, 20, 21, 28, 30, and 33) [26].

In terms of structure, ADAMs typically comprise a series of conserved and characteristic protein domains: a pro-domain, a metalloprotease domain, a disintegrin domain, a cysteine-rich region, an EGF-like domain, a transmembrane domain and a cytoplasmic domain [34,35]. ADAMs are commonly synthesized as inactive zymogens, in which the pro-domain binds to the catalytic domain and inhibits its activity. In addition to ensure proper folding of the protease during biosynthesis, the pro-domain impedes premature or aberrant proteolytic activity along the secretory pathway. Activation of ADAMs occurs either through conformational changes or proteolytic removal of the pro-domain, thereby exposing the catalytic site and enabling substrate cleavage at the cell surface or within endosomal compartments [36,37]. Active ADAMs metalloprotease domain contains the conserved catalytic motif **HEXGHXXGXXHD**, which consists in three histidines (H) coordinating a zinc ion (Zn^{2+}), two glycines (G), and one glutamic acid (E) that acts as the active-site residue required for proteolytic activity [38,39]. Following the catalytic domain, ADAMs possess a disintegrin domain, a cysteine-rich domain, a transmembrane region and a cytoplasmic (intracellular) tail. The disintegrin domain is named for its high sequence similarity to snake

venom disintegrins [40,41] – short, soluble proteins that typically contain an Arg-Gly-Asp (RGD) motif for integrins binding. Among human ADAMs, only ADAM15 possess an RGD sequence [42], while ADAM12 has been demonstrated to bind integrins through non-canonical RGD sequence [43]. Even without RGD, some ADAMs may influence integrin function being involved in cell–cell and cell–matrix interactions and adhesion processes [44]. The cysteine-rich domain, named for its multiple conserved cysteine residues that form stabilizing disulfide bonds, plays a key role in maintaining the tertiary structure of ADAM proteases and contributes to substrate recognition [45]. The transmembrane domain of ADAMs functions as a membrane anchor and the cytoplasmic tail usually contains phosphorylation sites and proline-rich sequences that may serve as Src homology 3 (SH3) ligand domains [46]. SH3 domains are present in cytoskeletal proteins and in signalling molecules [47], indeed, different descriptive interaction studies have shown engagements with SH3 domain-containing proteins and ADAMs cytoplasmic tail, such as ADAM9 [48], ADAM10 [49], ADAM12 [50], and ADAM15 [48,51,52]. Most of these studies applied a proteome-wide phage display screening coupled with pull-down assays and co-immunoprecipitations and identified several SH3 domain-containing partners that are mainly involved in intracellular trafficking and endocytosis, including endophilins, sorting nexins (e.g. SNX9, SNX18, SNX30, and SNX33), and the adaptor protein Grb2, but also in signal transduction, as non-receptor tyrosine kinases (e.g. Src, Lck, Fyn, Abl). These observations collectively suggest a potential role for ADAMs as scaffolds or mediators of intracellular signal transduction, although this function has still not been conclusively demonstrated *in vitro* and *in vivo*, with no substantial updates since 2015. To date, a single *in vivo* study explored the role of ADAM17 cytotail in regulating its activity, by using CRISPR-Cas9 knock-in mice lacking this region (ADAM17Δcyto). Although viable, the mice showed developmental defects due to reduced EGFR signalling, since ADAM17 is the major regulator EGFR signalling in development [53]. Lacking of the cytotail ADAM17Δcyto led to lower protein levels and impaired EGFR-ligand shedding, suggesting the cytoplasmic domain supports ADAM17 stability, likely via interaction with an unknown stabilizing factor [54].

ADAM regulation. ADAMs are regulated at multiple levels, including transcriptional, post-transcriptional, epigenetic, and post-translational mechanisms. In addition, ADAM activity is directly modulated by TIMP-3, one of the four mammalian tissue inhibitor of metalloproteinases (TIMPs) [55]. TIMP-3 inserts into the catalytic cleft and coordinates the catalytic zinc ion (Zn^{2+}), thereby blocking the protease activity. While TIMP-3 inhibits most of ADAMs, such as ADAM17 and ADAM10, with high affinity, exhibiting inhibition

constants (K_i) in the low nanomolar range, TIMP-1, -2, and -4 exhibit little to no inhibitory activity against this group of proteases under physiological conditions [56,57].

Inactive ADAMs. In addition to catalytically active ADAMs, the human genome encodes 11 inactive ADAM family members that either completely lack the metalloprotease catalytic domain or carry mutations in key residues of the catalytic motif. This group of pseudoproteases includes ADAM2, ADAM7, ADAM18, ADAM20, ADAM21, ADAM29, and ADAM32, which are predominantly expressed in the testis and are involved in sperm development, maturation, and fertilization (notably, the role of several of these inactive ADAMs still remain poorly characterized). Another subset, including ADAM11, ADAM22, ADAM23, and ADAM30, is highly expressed in the brain and has been implicated in neurogenesis, synaptic organization, neuronal signaling and may play roles in neurological disorders [7,34].

1.2.1.2 BACE proteases

This family includes two type-I transmembrane aspartyl proteases, BACE1 and BACE2. BACE1 was identified as the sheddase responsible for the cleavage of amyloid precursor protein (APP), a critical step leading to the generation of the amyloid-beta (Aβ) peptide and development of Alzheimer's disease [58–60]. BACE2, which also cleaves APP, is expressed in several brain cell types, such as neurons, oligodendrocytes, and astrocytes, although at significantly lower levels than BACE1, and it is mainly expressed in peripheral tissues, where it plays specific roles in melanocytes[61] and pancreatic β-cells [62]. BACE1 and BACE share a 59% amino acidic sequence similarity, and the same structural domain organization [63].

Similar to ADAMs, BACE proteases contain a pro-domain which is removed enzymatically by furin-like protein in Golgi [64], and, along with a series of N-glycosylation at four asparagine residues (N153, N172, N223, and N354), contribute to the correct trafficking and maturation to exert their protease activity [65]. The catalytic domain of BACE proteases, which is taken together by three disulfide bridges, contains the two catalytic aspartate residues (D93 and D289 in BACE1). As aspartyl proteases, BACE1 and BACE2 reach their maximal catalytic activity under acidic conditions, with an optimal at pH 4.5 [66,67]. Thus, while both proteases localize on the plasma membrane, they are predominantly active in the endosomal compartments. BACE1 and BACE2 are anchored to the membrane through a 21-residue helical transmembrane domain, and possess a short cytoplasmic C-terminal domain with a dileucine sorting signal (495DDISLL500) [63], whose post-translational

modifications determine trafficking either to the secretory pathway and endosome internalization [68], or even lysosomal degradation. [69], as it has been described for BACE1.

Other than APP, a number of proteins have been shown to be shed by BACE1, highlighting a wider role in brain function. Kuhn et al. used a proteomic-based approach called Secretome Protein Enrichment with Click Sugars (SPECS) [70], which consists of metabolic labelling of newly synthesized cellular glycoproteins – predominantly secreted and shed – by incorporating azido sugars. Then, these azide-labeled glycoproteins are tagged via copper-free click chemistry biotinylation [71], enriched through streptavidin pull-down and analysed by high-resolution mass spectrometry. This technique facilitates the identification of secreted glycoproteins from complex media, such as serum-containing culture conditions, by addressing key limitations of secretome analysis: low abundance of secretome proteins, high background from serum proteins like albumin, and contamination from intracellular proteins released by apoptotic cells. For instance, BACE1-mediated sheds over 30 different transmembrane proteins in the brain, thereby modulating a number of neural processes. By using SPECS, it was shown that BACE1 sheds over 30 different transmembrane proteins in the brain, thereby modulating a number of neural processes. For instance, BACE1-mediated shedding of neuroregulin 1 (NRG1), close homologue of neural cell adhesion molecule L1 (CHL1) and L1 cell adhesion molecule (L1CAM) contributes to neuronal development [72] and axonal organization [73], respectively. BACE1 activity on seizure-related protein 6 (SEZ6) is important for synaptic plasticity, function and motor coordination [74,75]. Interestingly, a more recent finding revealed a role for BACE1 on neuroinflammatory modulation of IL-6 signalling through cleavage of the glycoprotein gp130 [76].

Differently from BACE1, BACE2-mediated shedding is more prominent in systemic tissues, for example pancreas, where it is highly expressed, and its substrate repertoire is more restricted. By using targeted approaches and similar proteomics-based methods, only 55 transmembrane proteins have been shown to be shed by BACE2 [77]. One of these is the transmembrane protein 27 (TMEM27), which is involved in insulin exocytosis along with components of the SNARE complex [78]. BACE2 proteolytic processing of TMEM27 regulates its levels on the cell surface, since accumulation of TMEM27 causes aberrant release of insulin, leading to type 2 diabetes [79]. A distinct role of BACE2 consists in the shedding of pigment cell-specific melanocyte protein (PMEL17) [61], a TM protein whose processing leads to maturation of pigmented melanosome of hair, skin and mucosa [80].

1.2.1.3 MT-MMPs

Membrane-type matrix metalloproteinases (MT-MMPs) are a subgroup of the matrix metalloproteinases (MMPs), a family of proteases that plays a key role in the turnover of the extracellular matrix. There are six MT-MMPs in humans: MT1-MMP, MT2-MMP, MT3-MMP, MT4-MMP, MT5-MMP, and MT6-MMP [12]. They share a conserved domain structure comprising a pro-domain, a catalytic domain, a hinge (linker-1) region, a hemopexin-like (HPX) domain, and a stalk region (linker-2). MT1-, MT2-, MT3-, and MT5-MMP are tethered to the plasma membrane through a TM domain, followed by a cytoplasmic domain, while MT4- and MT6-MMP are associated to the membrane through a hydrophobic GPI-anchor [12].

Other than participates on extracellular matrix (ECM) and tissue remodelling components, through processing of collagen and fibronectin [12], MT-MMPs are also sheddases of membrane-bound proteins, thereby regulating cell signalling, migration and adhesion [81].

MT1-MMP, the most extensively studied, was demonstrated to shed the glycoprotein CD44[82], the heparan sulfate proteoglycans Syndecan-1 and Syndecan-4 [83], and α3 integrin [84], resulting in modulation of cell-ECM interaction and facilitating tumour invasion. Along with MT2- and MT3-MMP – despite less-well characterized –, MT1-MMP shedding of Discoidin domain receptor 1 (DDR1) attenuates collagen I- and IV-induced receptor phosphorylation, thereby regulating cell-collagen signal transduction pathways [85]. MT1-MMP was shown to be a positive modulator of FGF-signaling during intramembranous ossification, in that MT1-mediated shedding of ADAM9 protects FGFR2 from its ectodomain shedding [86].

MT5-MMP is highly expressed in neuronal cells [87]. Other than regulating neuronal growth and function, it shed APP acting as η-secretase, releasing a short fragment sAPPη [88]. The remaining membrane-bound fragment could be subsequently cleaved either by α- or β-secretase producing Aη-α or Aη-β peptides, respectively, leading to a lowered neuronal activity and impaired synaptic function [88].

1.2.1.4 Meprin β

Meprin β is a type I transmembrane metalloproteinase that, like ADAMs, belong to the family of metzincins [13]. It is synthesized as a zymogen that consists of an N-terminal pro-domain, followed by a zinc-binding catalytic domain (CAT), a meprin A5 protein tyrosine phosphatase μ domain (MAM), a tumour necrosis factor receptor-associated factor homology domain (TRAF), an EGF-like domain, a transmembrane domain, and a C-terminal

cytosolic domain. Meprin β is processed in the Golgi apparatus by the pro-protein convertase furin, which cleaves off the pro-domain, enabling its trafficking to the plasma membrane [89]. In terms of structure, mature meprin β forms homodimers or hetero-oligomers, when in complex with its isoform meprin α, linked by disulphide bridges [90,91].

Despite being discovered in 1980 [92–94], its role in biological processes and physiological functions is still not well understood. Meprin β is more abundant in kidney and intestine, in particular in the microvilli-rich region on the apical surface of epithelial cells [95–97], where it is responsible for the shedding of different cell adhesion molecules, such as E-cadherin and tenascin-C [98]. During ischaemia/reperfusion injury (IRI), meprin β migrates to the basolateral tubular basement membrane[99,100] and starts an exacerbate shedding, causing the degradation of basement membrane components, leukocytes infiltration and release of pro-inflammatory cytokines [101,102].

Noteworthy, meprin β in the brain is also responsible for APP shedding in the brain. It was reported as an alternative β-secretase for releasing different Aβ species from cleavage sites identical or close to the known β-secretase cleavage [103].

1.2.1.5 Pro-protein convertases

Pro-protein convertases (PCs) are a family of soluble serine proteases related to bacterial subtilisin [104], whose major role is to cleave pro-domain from secreted or membrane-tethered proteins, in order to their proper activation and trafficking to the correct cellular localization [14]. This family comprises nine members, PC1/3, PC2, furin, PC4, PC5/6, PACE4, PC7, SKI-1/S1P, and PCSK9, but the most well studied is furin, given its ubiquitous expression [105,106].

Structurally, PCs share a pro-segment, that could be either autocatalytically removed or cleaved off by other proteases, a catalytic domain typical of subtilisin-like serine protease family, and P-domain, involved in enzymatic stability and protein–protein interactions [107].

Despite pro-domain cleavage is not considered shedding, some PCs can actually perform ectodomain shedding for selected substrates, acting as "part-time" sheddases. Among all members, furin and SKI-1/S1P are the best characterized in terms of shedding activity. For example, furin sheds MT5-MMP, into a cleavage site proximal to its TM domain [108]. Although the biological impact of this event is not fully understood, it suggests that furin may modulate pericellular proteolysis by regulating the availability of membrane-tethered enzymes. Moreover, furin was reported to process TGF-β1 and TGF-β2 precursor molecules and, consequently promoting cell proliferation and migration, suggesting its relevance in developmental processes and pathological conditions, including cancer progression [109].

Interestingly, subtilisin/kexin-isozyme 1 (SKI-1/S1P) is the only family member that primarily functions as a sheddase [110]. Two known substrates are transcription factors SREBP, involved in cholesterol homeostasis, and ATF6, which is proteolytically activated during the endoplasmic reticulum (ER) unfolded protein response (UPR). Both SREBP and ATF6 are further RIPped by site-2 protease, highlighting SKI-1/S1P plays an initial role into a two-step proteolytic cascade that culminates in the release of their N-terminal transcriptionally active domains [5].

1.2.1.6 Transmembrane serine proteases

Transmembrane serine proteases (TTPs) are type II TM "part-time" sheddades still understudied [1,111]. TTPs are produced as zymogens, whose pro-domain is irreversibly removed by autocatalysis or heterocatalysis [111,112]. The extracellular chymotrypsin/trypsin-like domain contains the serine protease active site (DHS), followed by a TM domain and a cytoplasmic domain [112,113].

Although traditionally associated with pro-protein activation and tissue remodelling, several TTSPs also mediate ectodomain shedding.

Transmembrane serine protease 2 (TMPRSS2) was identified as the sheddase of the SARS-CoV-2 surface glycoprotein (Spike), ameliorating virus entry efficiency and infectiousness [114].

Matriptase was reported to shed APP within the amyloid β domain, thus reducing amyloid plaques formation [115]. Matriptase also cleaves EpCAM, that physiologically modulates epithelial adhesion, but unrestrained matriptase activity on EpCAM has been shown to correlates with intestinal epithelial dysplasia [116].

Matriptase and Hepsin, another member of TTPs, mediates ectodomain shedding of TMEFF2 when overexpressed in prostate cancer, thereby showing a role in cancer progression [117].

1.2.1.7 MMPs

Canonical sheddases are mostly membrane-bound proteases. However, some of them are soluble, targeting substrates that are typically released. Matrix metalloproteases (MMPs) are secreted sheddases involved in ECM remodelling [17,118]. As previously mentioned, all the six MT-MMPs belong to this family, but seventeen out of twenty-three lack membrane anchoring (MMP-1, MMP-2, MMP-3, MMP-7, MMP-8, MMP-9, MMP-10, MMP-12, MMP-13, MMP-19, MMP-20, MMP-21, MMP-23A/B, MMP-26, MMP-27) [81].

Likewise, their domain structure comprises a pro-domain, a catalytic site, a hinge region, and a HPX domain [18]. Based on substrate specificity, sequence and domain organization, MMPs can be divided into four main groups: collagenases, gelatinases, stromelysins, and matrilysins [18].

Accumulating evidence shows that several secreted MMPs can also mediate ectodomain shedding of transmembrane proteins, expanding their functional repertoire beyond matrix proteolysis.

MMP-2 (Gelatinase) was shown to be up-regulated in resected colorectal tumours, where drives aberrant shedding of β1 integrins, resulting in decreased adhesion to collagen and fibronectin, and enhancing invasion [119]. In this context, MMP-3 (Stromelysin) and MMP-7 (Matrilysin) has been shown to shed E-cadherin, thus augmented expression of these MMPs increments release of E-cadherin, impacting on epithelial barrier integrity allowing tumour cell detachment [120,121]. In the context of inflammation, MMP-mediated cleavage of chemokines or their receptors can alter leukocyte recruitment and local cytokine gradients, as for example MMP-12 (Macrophage-specific Metalloelastase) shedding of mCXCL2 (macrophage-inflammatory protein-2 [MIP-2]) and mCXCL3 (dendritic cell inflammatory protein-1 [DCIP-1]) suppresses the acute inflammatory response by terminating leukocyte recruitment [122].

Although secreted, many of these MMPs exhibit their sheddase activity directly at the cell surface, prompting a key question of how they localize to and remain in proximity to their membrane-anchored substrates. One mechanism involves heparan sulfate proteoglycans (HSPGs), such as syndecans and glypicans, that bind MMP at their HPX domain, acting as docking platforms on the cell surface [123]. In fact, MMP-7 is known to bind syndecan-1 on epithelial cells, thus enabling the shedding of both syndecan-1 itself and other nearby proteins [124].

1.2.1.8 Legumain (δ-secretase)

Legumain (LGMN) is an asparagyl endopeptidase (AEP) localized mainly into the endo-lysosomal compartment, where activation occurs through autocatalytic cleavage of its pro-domain at low pH (<5) [19,20]. Active site of LGMN contains a cysteine (C189), a histidine (H148), and an asparagine (N42), which specifically bind and cut after asparagine or aspartic acid residues [125]. Due to its lysosomal localization, it participates in protein degradation and lysosomal homeostasis [20].

In pathological conditions, such as in Alzheimer's disease (AD), legumain translocates from the endo-lysosome to other (extra-)cellular compartments, functioning as a "part-time"

sheddase. Indeed, LGMN was demonstrated to act as APP δ-secretase, shedding in proximity of BACE1 cleavage site and enhancing production of β-amyloid plaques [126]. Legumain can be also secreted, participating in ECM remodelling [19].

1.2.1.9 Cathepsins S and L

Cysteine cathepsins belong to a family of cysteine proteases normally confined to the endo-lysosomal system, as well as legumain. In particular, protocathepsins S and L are enzymatically processed by legumain, allowing their maturation and functioning role [127–129]. For instance, their activation is critical for adaptive immunity responses, as antigen-presenting cells (APCs) mostly expresses cathepsin S, playing a key role in processing invariant chains of major histocompatibility complex II (MHC-II), therefore facilitating antigen presentation to $CD4^+$ T cells [130,131].

Cathepsin S – differently from other members of this family that require an acidic pH for being activated – exhibits a proteolytic potential also at neutral pH, enabling its extracellular activity[132]. Shedding of the neuronal chemokine fractalkine (CX3CL1) mediated by Cathepsin S has been shown to drive neuroinflammation, through microglial activation and leukocyte recruitment [133].

Cathepsin L can also be secreted, remaining proteolytically active in the ECM, preferentially in acidic environments, such as those found in tumours and remodeling tissues [134].

In light of these, both cathepsins emerged as significant contributors in cancer progression [135]. Acting as "part-time" sheddases, extracellular cathepsins were shown to promote *in vivo* shedding of ALCAM and CD44; in particular cathepsin S-deficient mouse pancreatic cancers not only showed a reduction in shedding of these substrates, but also impacted intracellular signalling mediated by aberrant Ras GTPase activity, thus leading to a putative connection either extracellular and intracellular activity of cathepsins in ECM remodelling and improving tumour invasiveness [21].

1.2.2 Non-canonical sheddases

1.2.2.1 Rhomboids

Rhomboid proteases are multi-pass intramembrane serine proteases [136], firstly discovered in *Drosophila melanogaster* [137–139]. Rhomboids are present in most prokaryotes and eukaryotes, sharing the characteristic feature of six conserved transmembrane helices (TMH) embebbed in the lipid bilayer [140], with a catalytic core of serine (S) and histidine (H) within a GxSx motif within TMH-4 and TMH-6 – that distinguish them from classical soluble serine proteases [141,142]. Although three-dimensional structure is highly similar, their amino acid sequences diverge [22]. Rhomboids usually shed within substrates' TM domain, leading the release of the ectodomain to the extracellular/luminal part of the membrane [139].

In mammals, the rhomboid-like superfamily comprises five rhomboid proteases (RHBDL1, RHBDL2, RHBDL3, RHBDL4, and PARL), but only RHBDL2, RHBDL4, and PARL a role in shedding has been demonstrated [143,144].

RHBDL2 is localised at the plasma membrane and regulates cell migration and proliferation by cleaving thrombomodulin (TM) and ephrins, implicating a role in wound healing [145–147]. In *Drosophila*, RHBDL2 is the major regulator of EGFR signalling pathway, shedding the EGFR ligand Spitz [138], whereas in mammals, members of ADAM proteases (ADAM10 and ADAM17) represent the main sheddases [7]. Nevertheless, upon ADAM metalloprotease inhibition, only RHBDL2 can shed proEGF [148].

On the other hand, RHBDL4 resides in endoplasmic reticulum (ER) and it is implicated in ER-associated degradation (ERAD) by cleaving off unstable and misfolded proteins [149]. Interestingly, RHBDL4 expression correlates positively with tumour growth in hepatocellular carcinoma [150], glioblastoma [151] and colorectal carcinoma [152] cell lines. As non-canonical sheddase, this rhomboid protease was showed to have a role in APP shedding in ER, suggesting an alternative cleavage mechanism lacking γ-secretase [153].

PARL, the mitochondrial rhomboid protease, is located in the inner mitochondrial membrane[154], whose primary function is to maintain mitochondrial homeostasis, by controlling the stability of PTEN-induced kinase (PINK1) , a kinase essential for mitochondrial quality control, through clevage [144]. It has been linked to Parkinson's disease (PD) [155], in that, impaired shedding of the PTEN-induced kinase (PINK1) in damaged mitochondria, leads to PINK1 accumulation on the outer mitochondrial membrane and consequently the activation of parkin and mitophagy, compromising proper turnover [155,156].

1.2.2.2 SPP/SPPL family

Signal peptide protease (SPP) and signal peptide proteases-like (SPPLs) are part of a large family of intramembrane-cleaving proteases (I-CLiPs) [157,158]. As the name suggests, SPP main role is to remove signal peptides from nascent secretory proteins in ER [159], although it was also demonstrated a role as "part-time" non-canonical sheddase in ER-associated degradation (ERAD) [160]. First, SPP forms a homo-tetramer, then associates with Derlin1 and ERAD E3 ubiquitin ligases TRC8 to shed hemeoxigenase-1 and XBP1u, which target rapidly to proteasome degradation [161,162].

Regarding SPPLs, four members of this group have been identified in mammals (SPPL2a, SPPL2b, SPPL2c, and SPPL3), located in distinct cellular compartments and with a broad range of substrates[157].

SPPL2a and SPPL2b mainly perform RIPping on type II transmembrane proteins, immediately after a canonical sheddase cleavage [163,164]. Noteworthy, SPPL2a plays a crucial role in immune regulation by cleaving CD74, the invariant chain of MHC class II molecules. Following initial ectodomain shedding—typically by ADAM proteases—SPPL2a processes the remaining membrane-bound N-terminal fragment in late endosomes and lysosomes. Loss of SPPL2a activity leads to CD74 fragment accumulation, disrupted B cell maturation, and immunodeficiency [165].

SPPL3 is a Golgi-resident intramembrane-cleaving protease capable of directly cleaving full-length, membrane-bound glycosyltransferases and other type II transmembrane enzymes within the transmembrane domain. By using SPECS (see 1.2.1.2), SPPL3 was found to have role as non-canonical sheddase, by cleaving several glycosyltransferases, such as MGAT5 and B4GALT1, involved in protein N-glycosilation [166,167]. Through a similar proteomic approach, SPPL3 shed also the O-glycosylation enzyme GALNT2 [168]. Releasing of these ectodomains results in inactivation of the glycan-modifying enzymes [167].

1.2.2.3 Presenilin/ɣ-secretase

The multi-subunit aspartyl protease ɣ-secretase comprises four core proteins (presenilin-1 or -2 as catalytic subunit, nicastrin, APH-1, and PEN-2) and it is known as the critical enzyme involved in the production of Aβ peptide in Alzheimer's disease (AD) [169,170].

Other than APP, more than 90 substrates have been identified for ɣ-secretase, which can act as sheddase occasionally [171]. Proteolytic regulation of ɣ-secretase is mediated by nicastrin, which induces conformational changes rearranging the overall complex structure enabling the exposure of the catalytic subunit presenilin [172].

Fulfilling this role, ɣ-secretase shed directly the APP-homolog APLP1, in addition to ADAM10 and BACE1, which are major sheddases [173]. APLP1 long ectodomain might be processed by another protease prior ɣ-secretase cleavage, although it is still not clear mechanistically [173].

1.3 ADAM17 and its co-factors iRhom1 and iRhom2

ADAM17 is a member of the ADAM family, first discovered over 30 years ago as the protease responsible for the release of tumour necrosis factor alpha (TNF) [174,175]. Since then, ADAM17 has been shown to mediate the shedding of over 80 different transmembrane proteins, thereby participating in numerous biological processes ranging from cell communication to cell adhesion. ADAM17 function is tightly regulated by its essential co-factors, called iRhoms. Two iRhoms are expressed in mammals, iRhom1 and iRhom2. These proteins are inactive cognates of rhomboid proteases, that originated from catalytically active ancestors but acquired evolutionary mutations that disrupted their catalytic activity, while preserving their overall structure [176]. Notably, iRhoms are evolutionary conserved across all metazoans, indicating that despite the loss of proteolytic activity, they have acquired distinct, yet essential functions [140].

As it will be extensively discussed below, *in vitro* and *in vivo* studies indicate that the main function of iRhoms in mammals is to regulate the maturation, the trafficking and the activity of ADAM17, forming an integrated proteolytic complex composed of a regulatory subunit (iRhom) and a catalytic component (ADAM17) [177]. For this reason, structure and function of ADAM17 and iRhoms will be described not separately, but rather as components of a composite complex (Figure 2).

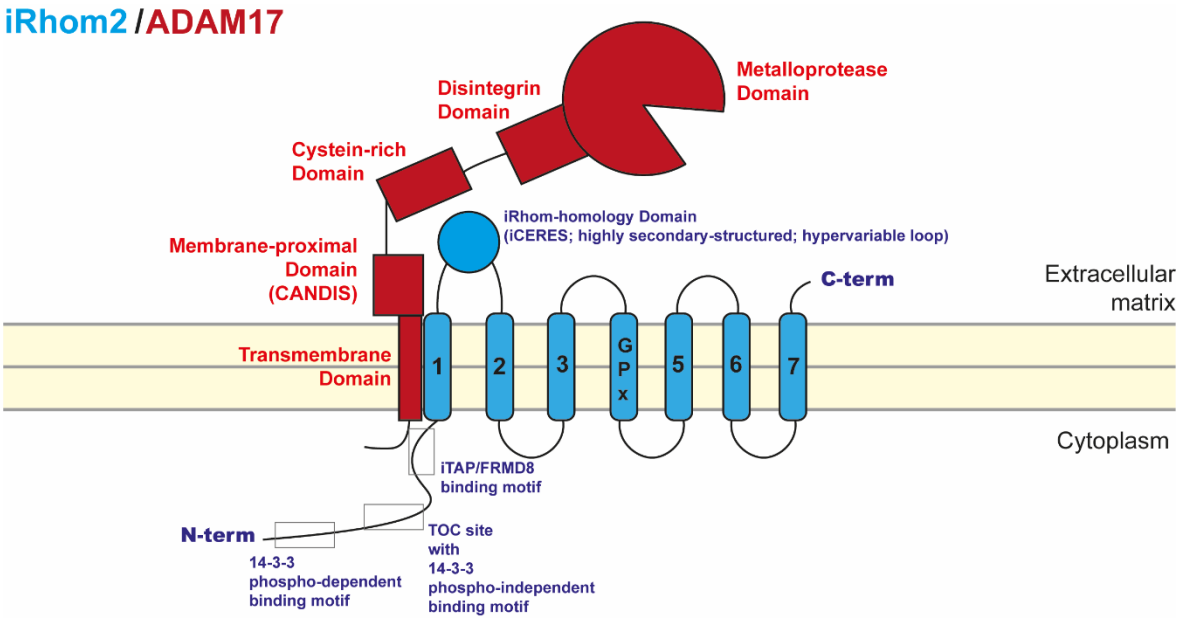

Figure 2: Schematic representation of the structure of iRhom2/ADAM17 complex. ADAM17 (in red) comprises six domains: a cytoplasmic domain, subjected to post-translational modifications, such as phosphorylation; a transmembrane domain; a membrane proximal domain, which is present the Conserved Adam seventeeN Dynamic Interaction Sequence (CANDIS); a cysteine-rich domain; a disintegrin domain and a metalloprotease domain. The seven-membrane spanning pseudoprotease iRhom2 (in light blue) presents a long N-terminal (N-term) cytoplasmic tail, with binding motif for iTAP/FRMD8, for 14-3-3 phospho-dependent and 14-3-3 phospho-independent proteins (the latter in the TOC site), to ensure stability and proper activation of the iRhom2/ADAM17 complex; TMD1 which interacts with ADAM17 TMD; iRhom-homology domain (IRHD) between the TMD1 and TMD2 contains three subdomains: a highly-structured

subdomain for iRhom-ADAM17 interaction (not shown), iCERES for trafficking from ER-to-Golgi, and hypervariable loop; the GPx motif in TMD4 replace the catalytic GxS of rhomboids leading to a lack of protease property; TMD7 is pivotal for specific substrate interaction.

1.3.1 Structure

Like other proteolytically active ADAMs, ADAM17 possesses a multidomain structure and is synthetized as an inactive zymogen, in which the pro-domain has a dual function in limiting its proteolytic activity throughout the secretory pathway and ensuring its proper folding and trafficking[178]. Following the pro-domain, the metalloprotease includes the catalytic domain comprising the conserved catalytic motif **HEXGHXXGXXHD** [7,26], the disintegrin domain, the cysteine rich domain, the transmembrane domain and the intracellular tail (Figure 2). After its synthesis in the ER, ADAM17 functions as a chaperone for iRhom2 [179]. In the absence of ADAM17, iRhom2 does not fold properly, does not proceed to the Golgi for further maturation, and is instead targeted to the ERAD. This process involves a prior cleavage by SPPL2c, which probably prevents toxic accumulation of misfolded iRhom2 before degradation [180].

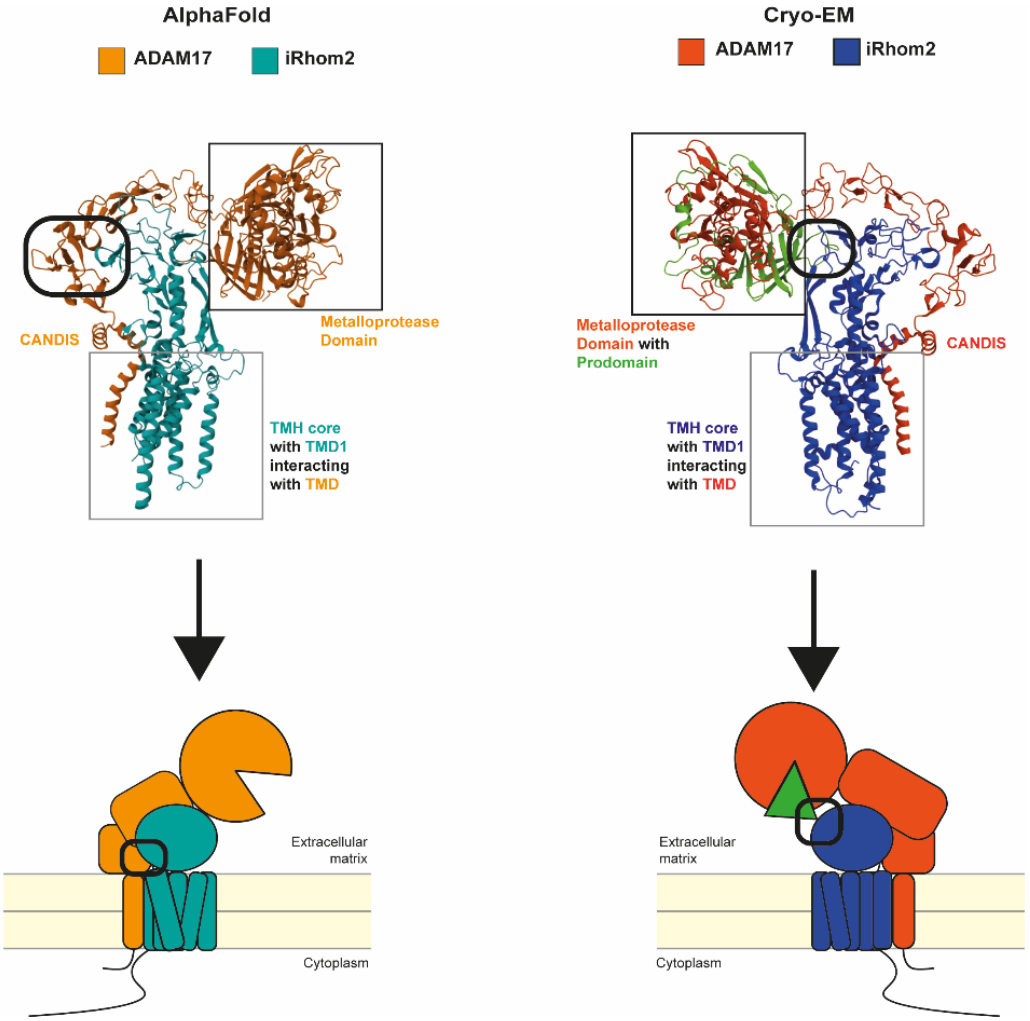

Figure 3: Cartoon representations of iRhom2/ADAM17 mature complex. AlphaFold structure (Kahveci-Türköz S, Bläsius K, Wozniak J, et al. Cell Mol Life Sci. 2023 [181]) and Cryo-EM structure (RCSB PDB: 8SNL, structure data from Lu F, et

al. Mol Cell 2024 [182]) represented ADAM17 and iRhom2 with different colours. Visualizations are created with Mol* Viewer [183]. Both representations highlighted a TMH core (dark grey squares) comprising all seven iRhom2 TMDs and ADAM17 TMD, which interacts with iRhom2 TMD1. Then, ADAM17 binds in a C-shape around the IRHD, with multiple contacts with its MPD, Disintegrin domain, Metalloprotease domain, and in addiction with Pro-domain in the Cryo-EM structure (black squares). According to AlphaFold model, the binding between MPD-IRHD is pivotal for conformational rearrangement associated with ADAM17 activation (bold black circle), whereas Cryo-EM evidenced pro-domain-IRHD essential in restraining ADAM17 flexibility and activity in non-stimulating condition (bold black circle).

Interestingly, despite 69% similarity to iRhom2 [184], iRhom1 does not require ADAM17 for proper folding and is not degraded when the protease is absent. Structurally, iRhom1 and iRhom2 have seven transmembrane domains (TMDs) and, unlike rhomboids, lack catalytic activity due to a substitution of the conserved catalytic serine with proline (GxS < GxP) [140]. Compared to rhomboids, through evolution iRhoms have acquired two additional structural features: a long N-terminal cytoplasmic tail and a large disordered loop between TMD1 and TMD2, also known as the iRhom homology domain (IRHD).

Two recent seminal studies used cryo-EM to characterize the overall structure of the iRhom2/ADAM17 complex, confirming earlier findings and providing deeper insights into their interaction [182,185] (Figure 3). The transmembrane domain of ADAM17 interacts with TM1 of iRhom2, in line with previous observations in the mouse bearing the iRhom2 *sinecure* mutation. This is a single amino acid substitution at position 186 (I186T), within TM1 of iRhom2, which prevents ADAM17 from binding and impairs its maturation [186].

Furthermore, these studies highlighted the crucial role of the IRHD in interacting with ADAM17. Structurally, the IRHD comprises a highly ordered core, a conserved loop containing the iCERES motif (iRhom Conserved ER-to-Golgi Export Sequence), and a highly flexible hypervariable loop. These subdomains collectively endow the IRHD with the capacity to mediate both trafficking and conformational regulation of the sheddase complex [181,187]. The IRHD facilitates the formation of a stable complex with the immature form of ADAM17 in the endoplasmic reticulum (ER). This interaction is essential for the proper folding, stabilization, and subsequent export of ADAM17 to the Golgi apparatus, where its inhibitory pro-domain is cleaved.

Notably, the study by Lu et al. described an interaction between the pro-domain of ADAM17 and IRHD residue D475, which keeps the pro-domain in place even after the furin cleavage in the Golgi. This non-covalent interaction constrains ADAM17 activity even at the cell surface and is disrupted upon activation of the proteolytic complex (e.g. by PMA stimulation), when the pro-domain is released, allowing greater flexibility of the catalytic domain and enabling substrate cleavage [182]. Importantly, this mechanism was not confirmed by Maciag et al, who predicted a similar overall Cryo-EM structure but did not observe persistent pro-domain binding after furin cleavage. This discrepancy may be due to

methodological differences: Lu et al. used overexpressed pro-ADAM17 carrying an upstream furin-site mutant, while Maciag et al. used an anti-ADAM17 pro-domain antibody to show that no pro-domain can be detected on the cell surface of wild type cells expressing endogenous ADAM17.

Moreover, structural modelling from Kahveci-Türköz et al. revealed that the IRHD interacts extensively with several extracellular regions of ADAM17, including its membrane-proximal domain, disintegrin-like domain, and catalytic domain. These contact points help stabilize ADAM17 in a conformation that is non-permissive for substrate cleavage, adding an additional layer of inhibitory regulation. The iCERES motif, though not directly involved in binding ADAM17, is indispensable for the ER-to-Golgi trafficking of the complex. Mutations in this motif disrupt the forward transport and consequently impede the maturation and activity of ADAM17 [181] (Figure 3).

Beyond the domains directly involved in the iRhom2/ADAM17 interaction, TM2-TM5 of iRhom2 are supposed to form the interaction surface for ADAM17 substrates, which are transiently bound to the TM7 [188].

1.3.2 Regulation of iRhom/ADAM17 proteolytic complex

Some of the unique structural features of iRhoms have emerged to play a role in regulating the activity of ADAM17 (Figure 4).

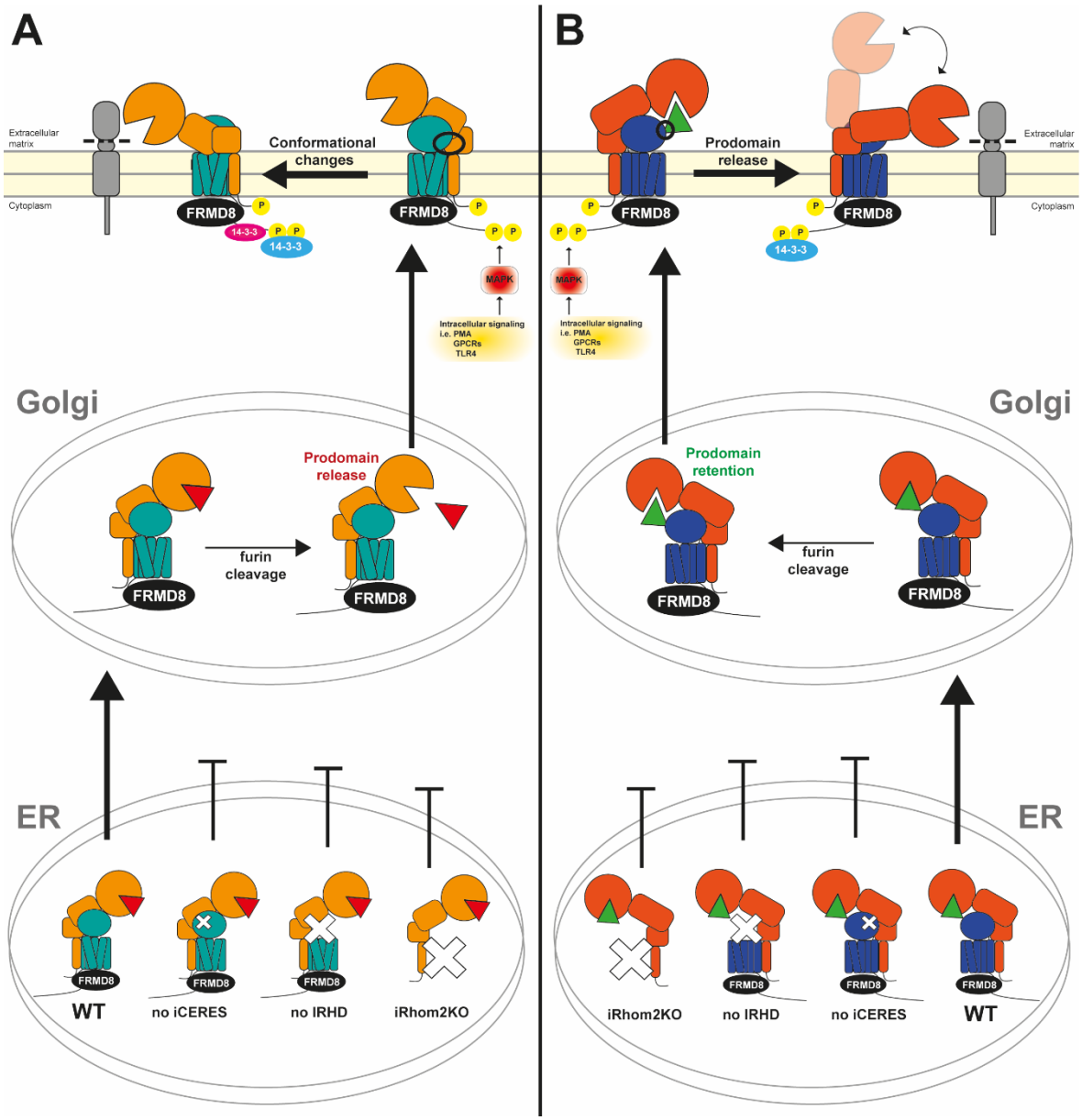

Figure 4: Models created using Adobe Illustrator (Adobe Inc., San Jose, CA) for iRhom2 functional role on trafficking, maturation and activation of ADAM17 as complex iRhom2/ADAM17. In the ER, the presence of WT iRhom2 promotes the trafficking of proADAM17 to the Golgi Apparatus, which is regulated by iCERES in the IRHD. Without iCERES or IRHD or iRhom2, proADAM17 remains stuck in the ER (A and B). The presence of FRMD8 since the ER ensure stability to the iRhom2/ADAM17 complex (A and B). In the Golgi, furin-mediated cleavage removes ADAM17 pro-domain (A and B). In the Model A, ADAM17 pro-domain is removed after furin cleavage, allowing the mature complex iRhom2/ADAM17 to traffic to the plasma membrane. Then, in response to intracellular signaling (i.e. activation of GPCRs, TLR4) or upon PMA stimulation, MAPK cascade phosphorylation of ADAM17 cytotail and phosphorylation of iRhom2 residues on N-term cytoplasmic tail recruits 14-3-3-phospho-dependent proteins (in blue) and 14-3-3-phospho-independent proteins (in pink). These engagements cause conformational changes in the iRhom2/ADAM17 complex, in that MPD-IRHD interaction (bold black circle) becomes weak and allows ADAM17 to shed its substrates. In Model B, ADAM17 pro-domain is retained in Golgi and plasma membrane by interacting with IRHD. Then, similar to model A, ADAM17 cytotail and iRhom2 N-term cytoplasmic tail are phosphorylated by activation of MAPK cascade in response to intracellular signaling (i.e. activation of GPCRs, TLR4) or upon PMA stimulation. iRhom2 phosphorylated residues allowing 14-3-3 proteins recruitment. These post-translational modifications weaken the interaction between the pro-domain and IRHD (bold black circle), resulting in pro-domain release and a more flexible ADAM17 conformation able to perform ectodomain shedding.

1.3.2.1 N-terminal cytoplasmic tail

The N-terminal cytoplasmic domain of iRhoms is a disordered region of approximately 400 amino acids, which pivotal for regulating the functional role of the iRhom/ADAM17 complex. Although this domain has been quite extensively investigated for protein interactors that bind iRhom2 at this site, using both unbiased proteomics approaches and machine learning, the general view is that these interactions have not yet been fully characterised. Similarly, studies have mainly focused on iRhom2 and therefore specific interactors of iRhom1 have not been investigated. Many more interactors of iRhom cytoplasmic tail are likely to be discovered in the coming years, which will help explain the complexity of ADAM17 regulation by iRhom1 and iRhom2.

Activation of iRhom2/ADAM17 complex. By using a mass spectrometry-based interatomic approach, two separate groups found that a number of 14-3-3 proteins interact with iRhom2 cytotail, and this interaction modulates the rapid activation of ADAM17. Indeed, mature ADAM17 is known to reside on the cell surface in an inactivated state, until specific stimuli activate its proteolytic function, including stimulation through G-protein coupled receptors (GPCRs). Upon stimulation by GPCRs, TLR4 signalling or treatment with phorbol 12-myristate 13-acetate (PMA, a synthetic compound widely used for ADAM17 activation), iRhom2 cytoplasmic domain gets phosphorylated at three different residues (S60, S83, and S359). This drives the recruitment of multiple 14-3-3 proteins, which induce a conformational change in the iRhom2/ADAM17 complex leading to ADAM17 activation and shedding of its substrates [189,190]. Moreover, recent findings identified an additive non-canonical, phosphorylation-independent 14-3-3 binding motif in the iRhom2 cytotail region called TOC site (I186, P189, D189, D188, R197), which harbors mutations observed in tylosis with oesophageal cancer [191]. In particular, *in silico* and *in vitro* experiments showed 14-3-3σ/stratifin (SFN) interacts with I186, D188, and R197, that mimic phosphoserine residues, thus facilitating its binding. This novel interaction gave insights into the molecular biology of constitutive and stimulated ADAM17 shedding activity, in that it appeared phosphorylation-independent 14-3-3 proteins alone restrain basal ADAM17 activity, which is impaired by pathological TOC mutations [191].

Stability of iRhom2/ADAM17. A similar mass spectrometry-based approach as the one described above identified protein interactors of iRhom2 cytotail that contribute to stabilize the iRhom2/ADAM17 complex. One such proteins is FERM domain-containing protein 8 (FRMD8), also referred to as iRhom Tail-Associated Protein (iTAP), which binds the

iRhom2 cytotail in its 200–300 amino acid region. This binding stabilizes the complex of iRhom2/ADAM17 in the late secretory pathway, preventing its lysosomal degradation [189,190]. Loss of FRMD8 had similar effects as iRhom deficiency in cells, leading to a reduction in the level of mature ADAM17. Similarly, the murine spontaneous iRhom2 mutation called curly-bare (cub) lacking the N-term residues 1–268 (corresponding to residues 1-298 in human) disrupts the interaction site of FRMD8, and so it implies a role to the complex molecular defects observed in the cub phenotype [192,193].

Cytoplasmic tail as a transcriptional regulator. iRhom2 N-terminal cytoplasmic domain contains a nuclear localization signal (NLS) motif, that allows a shorter fragment of about 50 kDa to translocate from ER-to-nucleus [194]. This fragment is the product of two sequential cleavages by the signal peptidase complex (SPC) in the luminal juxtamembrane region of TMD1, which releases the whole cytotail, and by an unknown cytoplasmic protease that results in the production of the 50 kDa fragment. Then, this fragment translocates into the nucleus and binds to the nuclear repressors CtBP1 and CtBP2, thus modulating gene expression. Overexpression of this iRhom2 fragment promoted cellular keratinocyte proliferation by upregulating Keratin 16, a protein commonly associated with hyperproliferative states, such as inflammation, wound healing and cancer.
It is important to mention that these experiments were also conducted on iRhom1, and comparable results were observed [195].

1.3.2.2 ADAM17 membrane proximal domain (MPD)

A distinctive hallmark in ADAM17 structure is the membrane proximal domain (MPD). It is involved in tuning shedding activity [196], through two different conformational changes: open – more flexible –, and closed – more rigid. In 2013, this mechanism was initially explained by the interaction between the Protein-disulfide Isomerase (PDI) and MPD [197], in which NMR and mass spectrometry-based analysis showed PDI catalysed an isomerization of disulfide bridges within the thioredoxin motif C600-XX-C603 (more likely belonging to the cysteine-rich domain) switching from an open-to-closed and inactive conformation. However, another possible regulatory mechanism of conformational changes still resides within the membrane proximal domain, where it is presents a short juxtamembrane segment of 17 amino acids called CANDIS (Conserved Adam seventeeN Dynamic Interaction Sequence). By forming electrostatic interactions with the cell membrane, three positively charged residues (R625-K626-G627-K628) bind to the phosphatidyl-serine flipped to the outer-layer of the plasma membrane, upon phorbol ester stimulation, thus allowing the

switch into an open and active [198,199]. Although, current evidence suggests that iRhoms, in particular iRhom2, through IRHD, interfaces with the disintegrin domain, metalloprotease domain, the MPD mainly serves as the primary regulatory machinery of ADAM17 different conformational changes. This does not exclude the contribution of alternative pathways but emphasizes the central role of the iRhom2/ADAM17 complex in controlling shedding activity.

1.3.3 Function

ADAM17 is also known as TNFα-converting enzyme (TACE), since it was firstly discovered as the sheddase responsible of tumour necrosis factor α (TNFα) release [174,175]. Since then, more than a hundred ADAM17 substrates have been identified *in vitro* and *in vivo*, showing its involvement in several biological processes (Table 2).

ADAM17 is ubiquitously expressed in mammals and its constitutive ablation leads to perinatal death in mouse [200]. iRhom1 and iRhom2 show some redundancy in regulating ADAM17 activity mostly to the same extent, since they act in different cell types based on their relative expression [184]. This implies that all ADAM17 functions – from the release of TNFα, EGFR-ligands to several other substrates, depend on iRhoms. Ablation of either iRhom1 or iRhom2 in mice showed no differences compared to wild-type (WT), suggesting a compensatory role of the two forms in regulating ADAM17 activity. On the other hand, iRhom1/2 ablation phenocopied Adam17-/- in mice, in that they died shortly after birth with open eyes, misshapen heart valves, and growth plate defects [201].

Among all functions that have been described for ADAM17, in this PhD thesis, I will focus on those validated *in vivo*, especially in the context of cancer. This is in accordance with my PhD project "Proteomic-based approach to investigate the role of iRhoms in cancer" funded by PON R&I 2014/2020 per lo sviluppo delle Azioni IV.4 "Dottorati e contratti di ricerca su tematiche dell'innovazione".

Table 2: List of validated ADAM17 substrates.
Adapted from Cuffaro, D. et al. Chapter 3.5 - A disintegrin and metalloproteinases (ADAMs) and tumor necrosis factor-alpha-converting enzyme (TACE). in Metalloenzymes 2024.

Cytokine	Cell-to-Cell Communication	Signalling receptor	Cell Adhesion	Cellular Transport	Enzyme	Others
CSF-1 [202]	Amphiregulin [53,203]	Axl [204]	ALCAM [205]	IGF-2R [206]	ACE-2 [207,208]	APLP-2 [209]
CX3CL1 [210]	DLL-1 [211]	CD16 [212]	CD44 [205]	LDL-R [57]	Carbonic Hydrolase 9 [213]	APP [214,215]
IL-8 [216]	Epigen [217]	CD163 [218]	Collagen XVII [219]	LRP-1 [220]	Klotho [221]	Pre-adypocyte factor [222]
KL-1 [223]	Epiregulin [53]	CD30 (TNFRSF8) [224]	Desmoglein-2 [205]	SORCS-1 [225]	NPR-1 [226]	PMEL-17 [227]
KL-2 [223]	HB-EGF [53,228]	CD40 (TNFRSF5) [229]	EpCam [205]	SORCS-3 [225]		PrP [230]
Lymphotoxin-α [231]	ICOS-L [232]	CD89 [233]	GP-1ba [234]	SORL-A [225]		Syndecan-1 [235]
RANKL [236]	IL-15R [237]	EPCR [238]	GP-5 [234]	SORT-1 [225]		Syndecan-4 [235]
TNF-α [174,175]	IL-1R2 [239]	ErbB4 [240,241]	GP-6 [234]	TREM-2 [242]		Vasorin [243]
	IL-6R [244]	GHRH receptor [245,246]	ICAM-1 [247]			
	Jagged [248]	M-CSFR [249]	JAM-A [250]			
	LAG-3 [251]	Notch-1 [248]	L1-CAM [252]			
	MHC-I [253]	NRP-1 [254]	L-selectin [200]			
	MIC-A [255]	NTRK1 [256]	LYPD3 [257]			
	MIC-B [255]	PTK7 [258]	MUC-1 [259]			
	NRG-1 [260]	PTPRF [261]	NCAM [262]			
	PD-L1 [263]	PTPRZ [261]	Nectin-4 [264]			
	TGFα [53,200,265–267]	SEMA-4D [268]	SynCAM-1 [269]			
	TIM-1 [270]	TNF-R1 [271]	Thrombospondin-1 [272]			
	TIM-4 [270]	TNF-R2 [271]	VACM-1 [273,274]			
		VEGF-R2 [254]				

1.3.3.1 iRhom/ADAM17 in immunity and cancer

The role of ADAM17 in immune responses [275] was recognized since its discovery of being the key regulator of the pro-inflammatory cytokine TNFα, as previously mentioned.

The pro-inflammatory effects of TNFα are primarily mediated by its soluble form, which signals in a paracrine or autocrine manner through TNFα receptor 1 (TNFR1). In contrast, TNFα receptor 2 (TNFR2) is preferentially activated by membrane-bound TNFα and is generally associated to anti-inflammatory and protective properties [276].

Monocyte/macrophages represent main source of TNFα, although it is almost undetectable under healthy conditions [277]. In response to TLR4 activation by LPS (e.g. bacterial infection) [278,279], effector cells become activated releasing increased amount of TNFα, whose binding with TNFRs trigger pro-inflammatory cascade (NF-κB and AP-1) [280]. Interestingly, ADAM17 also shed TNFR1 and TNFR2, generating soluble TNFR ectodomains that bind TNFα and reduce its availability, thus regulating downstream signalling of inflammatory [281].

Considering its pivotal role in TNFα release, ADAM17 conditional inactivation in myeloid cells provides protection from endotoxin shock lethality [282], even broadly ADAM17-deficient leukocytes (neutrophils, monocytes, and lymphocytes) have impaired shedding L-selectin, resulting in less neutrophil infiltration, reduced inflammation and TNFα release and longer survival after peritoneal sepsis [283,284].

ADAM17 has also been reported to shed the IL-6 receptor (IL-6R) [244]. The cytokine IL-6 can drive both pro-inflammatory and anti-inflammatory responses. Binding to the membrane-tethered IL-6R on the cell surface of hepatocytes and lymphocytes activates the so-called IL-6 classic signalling pathway, leading to the activation of anti-inflammatory cascade. In contrast, ADAM17 shedding of IL-6R results in the formation of IL-6/sIL-6R complex, that trigger IL-6-trans-signalling pathway through activation of all cells due to the uniform expression of gp130, resulting in pro-inflammation associated with the development of several inflammatory diseases, including rheumatoid arthritis [285,286].

As highlighted previously, iRhom2 plays a crucial role in tuning ADAM17 and its substrates in immune system [287], especially TNFα [279,288] and IL-6R [285].

Upregulation of iRhom2 expression was shown to be pivotal in inflammatory diseases, such as in synovial macrophages from rheumatoid arthritis (RA) [289], in damaged murine and human kidney from systemic lupus erythematosus (SLE) [290], and in Kupffer cells from hepatic steatosis, metabolic syndrome and dyslipidaemia [291].

Given its ability to shed pro-inflammatory molecules, pro-tumorigenic substrates, and adhesion molecules, ADAM17 plays a key role in tumours across different cancer stages and types. Historically, ADAM17 has been linked to cancer as the sheddase of EGFR ligands [7]. As previously mentioned, ADAM17 is the principal sheddase of EGFR ligands, driving EGFR signalling during embryonic development. In fact, mice lacking ADAM17 die perinatally and show developmental abnormalities — such as defective heart valve formation, compromised epidermal barrier, and open eyelids at birth — that phenocopy EGFR-null mice [200,292]. Dysregulated shedding of EGFR ligands positively correlates with poor cancer prognosis [293]. In particular, ablation of ADAM17 reduced amphiregulin and TGFα shedding, resulting in diminished progression of colon and breast cancer [266,294]. In addition, inhibition of IL-6 trans-signalling was also sufficient to inhibit ADAM17-mediated tumorigenesis, further suggesting that anti-IL-6 therapeutic approach might be promising for colorectal cancer resistant to EGFR-targeted therapies [294]. ADAM17 involvement in cancer is broader than EGFR regulation. It has been demonstrated that aberrant shedding of TNFR1 leads to endothelial cell necroptosis, that leads to tumour extravasation and metastasis [295].

To the same extent, ADAM17 has a role in gastric tumour formation by modulating EGFR and TNFα signalling pathways [296], in metastasis via Notch and Wnt [297], and via TGFβ signalling pathways promoting epithelial-mesenchymal transition (EMT) [298].

ADAM17 has also been shown to facilitate immune evasion by mediating the shedding of programmed death-ligand 1 (PD-L1) [263], a signalling receptor expressed at high levels in several human cancers that suppress adaptive immune responses of $CD8^+$ T cells and $CD4^+$ T helper cells [299,300]. For its role in immune escaping, several immunotherapy strategies have been studied to target PD-L1 and trigger an immune response in poorly immunogenic cancers, referred to as cold tumours [301]. Curiously, increased levels of ADAM17 and soluble PD-L1 are considered prognostic biomarkers.

Conversely, both iRhoms are implicated in cancer at different stages and in different tumour cell types, because of their involvement in TNFα/EGFR/IL-6R signalling pathways [302]. Even though iRhom1 is still less investigated, the first evidence for a role of iRhom1 in tumorigenesis showed it highly expressed in early-stage breast cancer and a positive correlation between its expression and metastasis, resistance to chemotherapy and poor prognosis [303,304]. Through deregulation of EGFR signalling in complex with ADAM17, iRhom1 has a role in growth, proliferation and invasion of head and neck squamous cancer cell lines and xenograft tumour [305]. For these reasons, targeting iRhom1 in combination with chemotherapeutic approach could be a promising strategy for several resistant tumours [306].

The previously mentioned mutations in the iRhom2 cytotail (I186, P189L, D189N, D188Y) cause the rare disease Tylosis with Oesophageal Cancer (TOC), characterized by palmo-plantar hyperkeratosis and a high risk of developing oesophageal cancer in middle age [307–309]. These gain-of-function mutations lead to an exacerbated shedding of the EGFR-ligand amphiregulin (AREG), resulting in proliferation and migration of tylotic keratinocytes [310]. The four amino acid region carrying mutations in TOC patients has been shown to affect iRhom2/ADAM17 substrate selectivity mechanism [311]. Interestingly, partial deletion of the N-terminal cytoplasmic domain – the murine curly bare (*cub*) mutation – impairs stabilization of mature ADAM17 at the plasma membrane [192].

1.4 Mass spectrometry-based analysis for proteomics

In 1994, Marc Wilkins coined for the first time the term *proteome*, defining it as "PROTEin complement expressed by a genOME", and *proteomics* as the technology to identify proteins in large scale [312].

Despite a plethora of definitions, proteome is best described as the comprehensive set of proteins produced and modified by a cell, a tissue, an organ, or an organism at a specific time and defined spatial environment. Differently from the genome, the proteome is highly dynamic and reflects the functional state of a biological system.

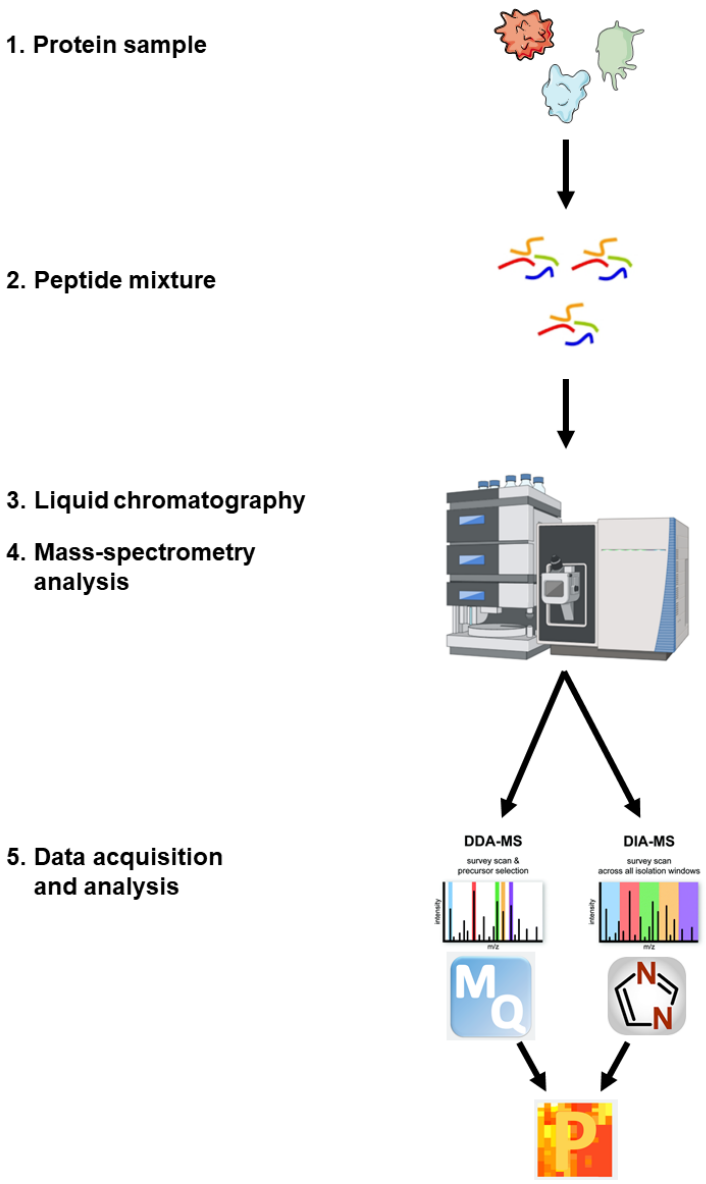

Figure 5: Schematic mass spectrometry-based proteomics workflow. **1.** Proteins are extracted from a biological sample and **2.** enzymatically digested into peptides. **3. 4.** Then, peptides are separated by liquid chromatography and analysed by tandem mass spectrometry (LC-MS/MS). **5.** Data acquisition is performed using either data-dependent acquisition (DDA-MS) or data-independent acquisition (DIA-MS) strategies [313]. Subsequent data analysis is conducted using dedicated software (e.g. MaxQuant for DDA [314] or DIA-NN for DIA [315]) to identify and quantify peptides and proteins, and to perform bioinformatic analysis (e.g. Perseus [316])

Proteomics is the technology applied to study proteomes in a large scale, and has evolved into a multifaceted discipline addressing different subfields of protein biology. Quantitative proteomics focuses on measuring protein abundance across conditions, by using labelling or label-free mass spectrometry techniques. Structural proteomics aims to determine protein conformations, complexes, and interactions, by using approaches such as cross-linking MS or cryo-EM. Functional proteomics explores the roles and activities of proteins, including post-translational modifications and enzymatic functions. Proteomics found in mass spectrometry (MS)-based analysis a powerful tool, in directly and accurately identifying and quantifying amino acid sequences for a systematic analyses of protein expression, modifications and interactions across various conditions [317].

Quantitative proteomics is still a milestone in proteomic-based research and it is widely used both for structural and functional studies, depending on the investigative approach. In particular, two strategies can be applied, bottom-up and top-down. Bottom-up proteomics is a quantitative proteomics approach that allows the identification and quantification of proteins by proteolytic digestion prior to mass spectrometry (MS) analysis, whereas top-down proteomics analyses intact proteins directly by MS without prior digestion to preserve full protein information [318].

Bottom-up proteomics allows deeper high-throughput data analysis of a complex protein mixture, and it is primarily applied in investigating sheddomes [319]. For this reason, the following paragraphs will focus on bottom-up proteomics. This method requires three fundamental steps: sample preparation (proteins extraction and digestion), separation of peptides by liquid chromatography and tandem mass spectrometry analysis (Figure 5).

1.4.1 Sample preparation

Depending on biological samples and experimental needs, several methodologies are currently used to prepare samples for MS analysis, depending on specific experimental needs.

Protein extraction is the first critical step. Detergent- (e.g SDS, Triton X-100, NP-40) or organic solvent-based extractions (e.g. TCA/acetone precipitation), are mostly used for less complex matrices to efficiently solubilize proteins and remove contaminants, or they could be combined to mechanical disruption to improve protein recovery from organ or tissue types.

Proteins are then unfolded and digested into smaller peptides that can be ionized and analysed by MS. Breaking disulphide bridges leads to disruption of proteins three-dimension conformation and subsequent linearization, allowing enzymatic digestion and peptide

generation. For this purpose, proteins are reduced and alkylated by sequential treatments with dithiothreitol (DTT) and iodoacetamide (IAA).

Trypsin is the gold standard protease used for peptide generation, as it specifically cleaves at the carboxyl side of lysine (K) and arginine (R), creating a manageable and predictable cleavage pattern and a charge distribution that enhance ionization efficiency and fragmentation reproducibility.

For the latter, other stepwise proteases could be coupled to tryptic digestion, such as Lys-C (C-terminal cleavage at lysine (K) residues only) or chymotrypsin (C-terminal cleavage at phenylalanine (F), tyrosine (Y), tryptophan (W), to improve individual protein sequence coverage.

All together these treatments are crucial for proper protein identity, since peptides are mapped to the primary amino acid sequences of a given proteome.

Noteworthy, Filter-Aided Sample Preparation (FASP) is a widely adopted method for protein digestion in bottom-up proteomics. It is an on-filter processing method suitable for retaining proteins on the molecular weight cut-off (MWCO) filter unit and for efficient removal of contaminants from detergent- or organic solvent-degradation steps [320].

1.4.2 Liquid Chromatography

Liquid chromatography (LC) is the core separation technique used in proteomics to reduce sample complexity and improve the resolution of peptide mixtures derived from protein digestion. The rationale behind LC is on the differential interaction of analytes with a stationary phase and a mobile phase, allowing peptides separation according to their physicochemical properties such as hydrophobicity, charge, polarity, or size (Reversed-Phase Chromatography, Ion-Exchange Chromatography, Hydrophilic Interaction Liquid Chromatography, or Size-Exclusion Chromatography, respectively) [317]. The most common LC method is the Reversed-Phase Chromatography (RP-LC), in which the mobile phase comprises water, an organic solvent (e.g. acetonitrile), and a strong (e.g. formic acid) for their combined properties of polarity modifier allow a better resolution, whereas the stationary phase uses non-polar C18 groups bonded to silica gel. Peptides are retained based on hydrophobic interactions; the more hydrophobic molecules interact the more strongly and elute later. In proteomics, high performance LC (HPLC) is the most commonly used, providing high-speed, high-resolution and high-sensitivity separation of analytes.

Flow regime also influences analytes separation outcomes. For this reason, flow regime is the nano-flow rate, typically less than 1000 nanoliters per minute (nL/min). This ultra-low flow rate is specifically optimized for high-sensitivity analysis of complex peptide mixtures.

Combination of the small diameter of nano-LC columns (commonly 75 μm) and low flow rates enhance ionization efficiency during electrospray ionization (ESI), improving detection sensitivity for low-abundance peptides [321].

1.4.3 Mass spectrometer

Mass spectrometer is the central analytical instrument in proteomics, which performs the detection, identification, and quantification of peptides based on their mass-to-charge ratio (m/z).

In proteomics, the m/z values are used to determine protein identity, whereas the relative abundance indicate protein levels across different samples. A mass spectrometer comprises three main components: ion source, analyser and detector.

1.4.3.1 Ion source

As the mass spectrometer works exclusively with ions, generated peptides must be converted into charged species, prior being analysed. This is an essential in any MS-based workflow.

In bottom-up proteomics, electrospray ionization (ESI) is the most widely used ionization method due to its compatibility with liquid chromatography (LC) and its ability to generate multiply charged peptide ions. In ESI, the peptide-containing solution is passed through a needle held at a high voltage (around 3 kV), creating charged droplets. By heat and gas flow, the solvent evaporates and these droplets undergo Coulomb fission, producing gas-phase ions that are directed into the mass spectrometer [322].

1.4.3.2 Analyzer and Detector

After ionization, the charged peptides enter the analyzer, which separates them according to their m/z values. There are several types of mass analyzers, each with unique characteristics in terms of resolution, mass range, and speed. Modern mass spectrometers often incorporate multiple analyzers (hybrid instruments) to increase the robustness of different analysis.

In this paragraph, I am focusing on the most common analyzers for bottom-up proteomics, that are Quadrupole, Orbitrap and the Quadrupole-Orbitrap hybrid system, since the latter is the analyzer incorporate in the two mass-spectrometers that I used for my proteomics analysis (Q-Exactive and Orbital Exploris, Thermo Fisher Scientific).

The Quadrupole mass analyzer consists of four parallel metal rods to which different voltage frequencies are applied. This configuration creates an oscillating electric field that

selectively stabilizes the trajectory of ions within a specific m/z window, allowing only those ions to pass through to the detector, which is typically electron multipliers. This makes the quadrupole mass analyzer most suitable for targeted quantification method. In contrast, the Orbitrap is a high-resolution mass analyzer based on electrostatic ion trapping and Fourier transform detection. It consists of a vacuum chamber with an inner spindle-shaped electrode and a coaxial outer electrode. Ions are injected tangentially and are "trapped" in orbital motion around the central electrode, whose frequency depends exclusively on m/z of each ion. Then, orbital motions are detected and transformed via Fourier transform, resulting in a frequency spectrum and subsequently in a mass spectrum. The longer the ions are trapped, the more oscillations are recorded, leading to increased resolution. For this reason, the Orbitrap technology allows high-resolution and high-mass accuracy measurements, making it highly suitable for discovery proteomics [317,323].

Combining the Quadrupole and Orbitrap technologies develops the hybrid system Quadrupole-Orbitrap, in which the selective electric field applied for each precursor ion is coupled with the ions' trapping system in orbital motion. Moreover, the presence of a fragmentation chamber with Higher-Energy Collisional Dissociation method, in which precursor ions are accelerated by an electric field and collided with inert gas molecules (typically N_2), enables the generation of smaller products, thus allowing more oscillations, more mass spectra and increased resolution and accuracy. This mechanism called tandem mass-spectrometry (MS/MS) is a critical step in bottom-up proteomics, since the amino acid sequence of the original peptide is analyzed in a second stage of mass spectrometry [324].

1.4.4 Data acquisition

A specific application of the bottom-up strategy is shotgun proteomics, which is an unbiased and investigative proteomics approach [317].

In shotgun proteomics, raw data acquired from tandem mass-spectrometry analysis can be analysed through two different methods: data-dependent analysis (DDA) and data-independent analysis (DIA).

In DDA mode, a continuous full-scan MS (MS^1) quantifies all the precursors within a specific m/z range. Then, the mass spectrometer selects the most intense precursors (typically top 10 or 20) for the fragmentation and the MS^2 analysis. DDA is considered a stochastic method, as the precursors selected for fragmentation can vary from run to run, depending on their abundance and signal intensity at a specific time [325].

In DIA mode, the instrument systematically fragments all ions across a predefined m/z range, regardless of their intensity or abundance. DIA divides the full MS^1 m/z range (e.g.,

400–1200 m/z) into sequential isolation windows (typically 5–25 Da m/z ranges). Within each window, all precursors are fragmented simultaneously, and the resulting MS^2 spectra contain fragments from multiple co-isolated peptides. Fragment ions in overlapping spectra are deconvoluted and assigned to their respective precursors using advanced data processing tools designed for DIA workflows, such as Sequential Windowed Acquisition of all THeoretical fragment ions (SWATH) [326] and DIA-NN [315].

DDA is particularly well suited for discovery proteomics and targeted proteomics, for obtaining detailed sequence information with high confidence. Its ability to generate high-quality MS/MS spectra makes it valuable for identifying novel peptides and localizing modifications. On the other hand, DIA is better adapted to quantitative and large-scale proteomic studies, offering superior reproducibility and comprehensive peptide coverage across diverse and complex sample sets. The decision to employ DDA or DIA should be based on experimental goals, sample complexity, and desired analytical outcomes.

Chapter Two:
Materials and Methods

2.1 Secretome analysis of mEFs

2.1.1 Cell culture

WT, iR1KO, iR2KO or iR1/2 dKO mouse embryonic fibroblasts (mEFs), kindly provided by Dr. Carl P. Blobel, were isolated as described previously [327]. Cells were grown until confluence in 6-well plates in high glucose Dulbecco's Modified Eagle's Medium (DMEM) (Biowest, Riverside, Newry and Mourne, UK) supplemented with 1% L-Glutamine, 1% Penicillin and Streptomycin (Pen-Strep), 1% Sodium Pyruvate and 10% Fetal Bovine Serum (FBS) at 37 °C, 5% CO_2. Then, cells were thoroughly washed with PBS to remove remnants of serum, and incubated 3 h with serum-free DMEM, either in the presence or absence of 25 ng/mL phorbol 12-myristate 13-acetate (PMA - Sigma-Aldrich, St. Louis, MO, US).

For rescue experiments, iR1/2 dKO mEFs were seeded at 70% confluency in 6-well plates, then media was replaced with OptiMEM (Gibco, Thermo Fisher Scientific, Waltham, MA, USA). Recombinant murine iRhom1 and/or recombinant murine iRhom2 were cloned into a pcDNA3.1/Zeo (+) plasmid, in frame with the CD5 signal peptide for efficient secretion and a 3xFLAG-tag sequence at their C-term. 500 ng of iRhom1-FLAG and iRhom2-FLAG were used either alone or in combination (iR1, iR2, iR1/2), mixed with 5 µL of Lipofectamine 3000 (Invitrogen, Thermo Fisher Scientific, Waltham, MA, US) and added to cells. After 5 h, OptiMEM was replaced with DMEM containing 10% serum and grown for 48 h. After washing, cells were incubated 3 h with or without 25 ng/mL PMA in serum-free conditions.

2.1.2 Sample processing

Conditioned media were harvested and centrifuged at 14,000 x g for 10 min to remove cell debris, and then applied to filter-aided sample preparation (FASP) [320] by using Vivaspin protein concentrator spin columns with a 10 kDa molecular weight cut-off (Sartorius, Göttingen, Germany). First, proteins were reduced (1M Dithiothreitol (DTT) in 100 mM Tris/HCl, 8 M urea pH 8.5) for 30 min at 37° C, then alkylated in 50 mM iodoacetamide (IAA) for 5 min at room temperature and washed twice in 100 mM Tris/HCl, 8 M urea pH 8.0 at 14,000 x g for 30 min. 10 µg of proteins per sample were digested with 0.2 µg LysC (Promega, Madison, WI, US) in 25 mM Tris/HCl, 2 M urea pH 8.0 overnight (enzyme to protein ratio 1:50) and with 0.1 µg trypsin (Promega, Madison, WI, USA) in 50 mM ammonium bicarbonate for 4 h (enzyme to protein ratio 1:100). Resulting peptides were desalted by stop-and-go extraction (STAGE) method on reverse phase C18 (Supelco Analytical Products, part of Sigma-Aldrich, Bellefonte, PA, USA) [328]. The C18 resin was activated with 100 µL of methanol and then washed twice with 0.1% formic acid. Samples

were forced through the tip and washed four times with the same formic acid solution, and then eluted in 40 µL of 60% acetonitrile in 0.1% formic acid. The volume was reduced in a SpeedVac (Thermo Fisher Scientific, Waltham, MA, US) and the peptides were resuspended in 20 µL of 0.1% formic acid, ready to be analysed by LC-MS/MS.

2.1.3 LC-MS/MS analysis

An Ultimate 3000 nanoLC system (Thermo Scientific) was coupled online with an Acclaim PEPMap C18 column (50 cm × 75 µm ID, Thermo Fisher Scientific) to Q-Exactive Plus mass spectrometer (Thermo Fischer Scientific). 1 µg peptides were separated with 250 nL/min flow using a 220 min binary gradient of water and acetonitrile (from 2% to 95% acetonitrile in water), injected into the mass spectrometer, and their intensities quantified by using label-free quantification (LFQ) and data-dependent acquisition (DDA). Full MS scans were acquired at a resolution of 70,000 (m/z range: 300–1400; automatic gain control (AGC) target: 1×10^6; max injection time 50 ms). The DDA was used on the 10 most intense peptide ions per full MS scan for peptide fragmentation. A dynamic exclusion of 120 s was used for peptide fragmentation.

To achieve more sensitivity for iRhom-rescued mEFs analysis, the LC-MS/MS analysis was performed using a nanoLC system (Vanquish Neo UHPLC - part of Thermo Scientific) connected to Acclaim PEPMap C18 column (25 cm × 75 µm ID, Thermo Scientific, Waltham, MA, USA) for peptide separation to an Exploris 480 mass spectrometer (Thermo Fisher Scientific). 1 µg peptides were separated at a flow rate of 250 nL/min using a 130 min binary gradient of water and acetonitrile containing 0.1% formic acid at fixed column temperature of 50°C. Data-independent acquisition (DIA) was used for identification of proteins and their label free quantification (LFQ). The mass spectrometer was set in positive ion mode to acquire a full MS^1 scan at a resolution of 120,000 across a mass-to-charge (m/z) scan range of 400 to 1000, followed by 60 consecutive DIA windows with a 1 m/z overlap and optimized window placement. The automatic gain control (AGC) target was set to 3 x 10^6 ions to enter the mass analyser within 50 ms as maximum injection time. Then, 60 isolation windows were acquired at a resolution of 30,000, an AGC target of 8 x 10^5, and the maximum injection time was automatically adjusted to optimise cycle time. Collision-induced fragmentation was set to 30% of the normalized higher-energy collisional dissociation (HCD).

2.1.4 Proteomic data analysis

For analysis with DDA method, data were normalized and analysed using Maxquant software (maxquant.org, Max-Planck Institute Munich, version 2.0.1.0 [329]) and searched against a reviewed canonical FASTA database of *mus musculus*. The Perseus software platform (http://www.perseus-framework.org (accessed on 7 July 2022); copyright of Max Planck Institute of Biochemistry- Martinsried- Munich; Germany) was used to perform statistical analysis. For DIA analysis, data were elaborated with the software DIA-NN (version 1.8.1), and matched with a reviewed canonical FASTA database of *mus musculus*. The Perseus software platform (http://www.perseus-framework.org (accessed on 9 May 2024); copyright of Max Planck Institute of Biochemistry- Martinsried- Munich; Germany) was used to perform statistical analysis. LFQ values were log2 transformed and a two-sided Student's t-test was used for the statistical analysis of stimulated versus control mEFs. Up to three biological replicates were used for these analyses.

2.2 Secretome analysis of HTB94 cells

2.2.1 Generation of iR1KO, iR2KO and A17KO HTB94 cells

Fibroblast-like HTB94 cells were cultured in high glucose Dulbecco's Modified Eagle's Medium (DMEM) (Biowest, Riverside, Newry and Mourne, UK) supplemented with 1% L-Glutamine, 1% Penicillin and Streptomycin (Pen-Strep), 1% Sodium Pyruvate and 10% Fetal Bovine Serum (FBS) at 37 °C, 5% CO_2. CRISPR-Cas9 was used to generate iR1KO, iR2KO and A17KO cell lines. CRISPR guide for iRhom1 (5'-GGGAATGTCCAGCTTTAGCC-3', targeting exon 2), iRhom2 (5'-GCATGCTGTCCTGCTCGCCA-3', targeting exon 3), ADAM17 (5'-GGTCGCGGCGCCAGCACGAA-3', targeting exon 1) and not targeting control sequences (NTC, 5'-TCCGGAGCTTCTTTCAGTCAA-3' – referred as WT) were cloned into vector lentiCRISPRv2 (Addgene, cat. No. 52961) as previously described [330]. HEK293T packaging cells were used for CRISPR/Cas9 lentiviral particle production. Cells were seeded on 10 cm culture dish and incubated overnight at normal growth condition (37°C, 5% CO2, DMEM with 10% FBS, P/S, 1% L-Glutamine and 10mM sodium pyruvate). 1 mL of OptiMEM was supplemented with 37 µL of Lipofectamine 3000 and mixed. In a second tube, 1 mL of OptiMEM was mixed with 13.3 µg of the packaging plasmid pxPAX2, 9 µg pcDNA3.1-VSVG and with 18 µg of lentiCRISPRv2-iRhom1, lentiCRISPRv2-iRhom2, lentiCRISPRv2-ADAM17 or lentiCRISPRv2-NTC. Lipofectamine and plasmid were mixed and incubated for 20 minutes at 37°C. HEK293T were washed with PBS and medium was changed with OptiMEM 10% FBS prior to cell transfection. The transfection mix was added

to the cells and incubated overnight Then, the medium was changed with DMEM supplemented with 2% FBS, 1% P/S, 10mM sodium butyrate and after 24 hours the conditioned medium containing viral particles was collected, centrifuged to remove cell debris and used for lentiviral transduction. 500 µL of medium containing lentiviral particles were added to 500 µL HTB94 cell suspension, in the presence of 5 µg/mL polybrene. Cells were transferred onto a 6-well plate and spinfected by centrifuging cells at 1800 rpm for 2 hours at 33°C. After an overnight incubation with the viral suspension, cells were collected, washed twice and incubated with growth media supplemented with 1µg/mL of puromycin for selection of transduced cells. After selection, the generation of iR1KO, iR2KO and A17KO cell lines was evaluated by Western blotting.

2.2.2 Cell culture

WT, iR1KO, iR2KO and A17KO HTB94 cells grown until confluency in 6-well plates with high glucose Dulbecco's Modified Eagle's Medium (DMEM) (Biowest, Riverside, Newry and Mourne, UK) supplemented with 1% L-Glutamine, 1% Penicillin and Streptomycin (Pen-Strep), 1% Sodium Pyruvate and 10% Fetal Bovine Serum (FBS) at 37 °C, 5% CO2. Then, cells were thoroughly washed with PBS to remove remnants of serum, and incubated 3 h or 1 h with serum-free DMEM, either in the presence or absence of 25 ng/mL phorbol 12-myristate 13-acetate (PMA - Sigma-Aldrich, St. Louis, MO, US).

2.2.3 Mass spectrometry-based analysis

WT, iR1KO, iR2KO, A17KO HTB94 conditioned media were collected, applied to FASP and STAGE-tips, and analysed by LC-MS/MS as described above. Peptide intensities were quantified by using label-free quantification (LFQ) and data-dependent acquisition (DDA), and then searched against a reviewed canonical FASTA database of Homo sapiens by using MaxQuant software. LFQ values were log2 transformed and a two-sided Student's t-test was used for the statistical analysis of stimulated WT, iR1KO or iR2KO versus A17KO cells. In addition, one-way Anova with Dunnett's multiple comparisons test was used to statistically compare levels of specific proteins in the conditioned media of iR1KO, iR2KO or A17KO cells versus that of WT cells. Three biological replicates were used for this analysis.

2.3 Western Blotting

2.3.1 Evaluation of ectodomain shedding on endogenous proteins

mEFs or HTB94 cells were grown in 6-well plates in DMEM supplemented with 10% serum until confluence. Then, cells were washed in PBS, and incubated 3 h with serum free DMEM, with or without 25 ng/mL PMA (Sigma-Aldrich, St. Louis, MO, US) and 10 µM

Marimastat (Sigma-Aldrich). Conditioned media were harvested and proteins precipitated with 5% v/v trichloroacetic acid (Sigma-Aldrich, St. Louis, MO, US) before being resuspended in Laemmli sample buffer (Bio-Rad, Hercules, CA, US). Cells were collected with STET lysis buffer (50 mM Tris, pH 7,5, 150 mM NaCl, 2 mM EDTA, 1% Triton), containing protease inhibitor cocktail (1:25, Roche Life Science, Merck, Mannheim, Germany). Protein concentration was measured by using a colorimetric 562 nm BCA assay (T-Pro Biotechnology, Taiwan, China). Proteins from conditioned media and lysates were reduced with 2-Mercaptoethanol (Sigma-Aldrich, St. Louis, MO, USA) and denatured at 95 °C for 5 min before being loaded onto an acrylamide gel and analysed using SDS-PAGE electrophoresis, then by immunoblotting with the following antibodies used: anti-PTK7 (R&D Systems, Minnesota, US), anti-APP (Millipore, Burlington, Massachusetts, US), anti-EPHB3 (Abcam, Cambridge, United Kingdom), anti-LAMP1 (Abcam, Cambridge, United Kingdom). Anti-calnexin (ENZO lifescience, Farmingdale, NY, US) was used for protein loading control. A donkey anti-goat, a goat anti-rabbit and an anti-mouse HRP-conjugated secondary antibody were used (Promega, Madison, Wisconsin, US). Bands corresponding to specific proteins were quantified using Image Lab software (Bio-Rad, Hercules, CA, US). A two-sided Student's t-test was used to evaluate proteins statistically significantly regulated. A p-value less than 0.05 was set as the significance threshold.

2.3.2 Evaluation of ectodomain shedding on recombinant proteins

Recombinant human matrix associated remodelling 8 (MXRA8), mouse H2-D1, human signal regulatory protein α (SIRPα) or seizure protein 6 (SEZ6) was cloned into a pcDNA3.1/Zeo (+) plasmid, in frame with the CD5 signal peptide for efficient secretion and a FLAG tag sequence. APP was cloned into pEAK12 as previously reported [331]. mEFs or HTB94 cells were grown in 6-well plates until 70% confluence, then media was replaced with OptiMEM (Gibco, Thermo Fisher Scientific, Waltham, MA, USA). 1 µg of plasmid was mixed with 5 µL of Lipofectamine 3000 (Invitrogen, Thermo Fisher Scientific, Waltham, MA, US) and added to cells. After 5 h, OptiMEM was replaced with DMEM containing 10% serum and grown for 48 h. After washing, cells were incubated with or without 25 ng/mL PMA and 10 µM marimastat and treated as described above. Anti-FLAG [M2] (Sigma-Aldrich, St. Louis, MO, US) was used to detect MXRA8 in the conditioned media and lysates of MEFs and HTB94 cells. Anti-FLAG was also used to detect H2-D1 and SIRPα; anti-HA [HA7] (Sigma-Aldrich, St. Louis, MO, US), to detect recombinant APP and SEZ6 in the lysate of the different mEFs. An anti-mouse HRP-conjugated secondary

antibody was used to develop immunoblots. An anti-β actin (Santa Cruz, Dallas, Texas, US) and a goat anti-mouse were used to detect actin as a protein loading control.

2.3.3 Evaluation of protein stability

WT, iR1KO, iR2KO and iR1/2 dKO MEFs were plated onto 12-well plates and transfected with FLAG-H2D1 as described above. Cells were incubated for 1 h in serum-free DMEM supplemented with 10 µM MG132 (Sigma-Aldrich, St. Louis, MO, USA) or 100 µM Chloroquine biphosphate (Sigma-Aldrich, St. Louis, MO, USA) and then stimulated for 3 h with 25 ng/mL PMA. Equal volume of DMSO was used for negative controls. Cell lysates were collected in STET, and 20 µg proteins were loaded into a polyacrylamide gel for SDS-PAGE analysis and subsequent immunoblotting. The following antibodies were used: anti-FLAG [M2] (Sigma-Aldrich, St. Louis, MO, US), anti-LC3 (Novus Biologicals, Cambridge, UK); anti-ubiquitin [P4G7] (Covance, Princeton, New Jersey, US), anti-calnexin (ENZO LifeScience, Farmingdale, NY, US).

2.4 RNA extraction and RT-qPCR analysis

H2-D1 transfected iR1KO, iR2KO, iR1/2 dKO and WT mEFs were grown to confluence in 12-well plates and stimulated or not with 25 ng/ml PMA for 3 h. Then, cells were washed twice with PBS and lysed with 700 µL of QIAzol (QIAGEN, Hilden, Germany). Total RNA was extracted with the miRNeasy Mini Kit (QIAGEN, Hilden, Germany) according to the manufacturer's instructions. Genomic DNA was removed by DNase treatment for 30 min. 1 µg of mRNA was retrotranscribed to cDNA using Retro High-Capacity kit (Applied Biosystems, Thermo Fisher Scientific). SybrGreen was used to detect amplified target mRNAs and their expression levels were evaluated using ΔΔCT calculation method with H2D1 (qMmuCEP0043536, Bio-Rad, Hercules, CA, US) as target and GAPDH (qMmuCEP0039581, Bio-Rad, Hercules, CA, US) as reference mRNA. SsoAdvanced™ Universal SYBR® Green Supermix from Bio-Rad was used according to the manufacturer's instruction.

2.5 Analysis on MHC-I trafficking

2.5.1 Flow cytometry analysis

Cells plated in 6-well plates were grown in DMEM supplemented with 10% serum until confluence. Then, cells were washed in PBS, and incubated 3 h with serum free DMEM, with or without 25 ng/mL PMA (Sigma-Aldrich, St. Louis, MO, US) and 10 µM Marimastat (Sigma-Aldrich). were harvested with TryPLE reagent (Gibco, Thermo Fisher Scientific,

Waltham, MA, USA). Then, cells were harvested and processed to flow cytometry analysis. Briefly, mEFs, HTB-94 and THP-1 were stained with FITC anti-HLA Class I [W6/32], isotype IgG2a (Abcam, Cambridge, UK) or PE anti-HLA Class I [W6/32], isotype IgG2a (BioLegend, San Diego, CA) at room temperature for 15 minutes according to the manufacturer's instruction, washed with PBS and then resuspended in 300 µL PBS. Cells were analysed with FACS Celesta SORP flow cytometer and FACS Diva software version 9.0 (BD Biosciences, CA, US).

2.5.2 Evaluation of ER-to-Golgi transport

iRhom2KO HTB94 cells and its WT counterparts were grown in 6–well plates and then treated with 10 µg/ml brefeldin A (Sigma-Aldrich, US) or monensin (BD GolgiStop™ Protein Transport Inhibitor containing monensin, BD Biosciences, US) for 3 h. Then, cells were harvested with TryPLE reagent (Gibco, part of Thermo Fisher Scientific) and processed for flow cytometry analysis. Briefly, HTB94 were stained with FITC anti-HLA Class I [W6/32], isotype IgG2a (Abcam, Cambridge, UK) or PE

anti-HLA Class I [W6/32], isotype IgG2a (BioLegend, San Diego, CA) at room temperature for 15 min according to the manufacturer's instruction, washed with PBS and then resuspended in 300 µl PBS. Cells were analysed with FACS Celesta SORP flow cytometer and FACS Diva software version 9.0 (BD Biosciences, CA, US).

2.5.3 Co-immunoprecipitation

For the co-immunoprecipitation of iRhom2 and HLA, 2.2×10^6 cells were seeded in a 10 cm dish. Then, 10 µg of pcDNA3.1 plasmid containing HA tagged iRhom2, HA tagged inactive signal peptide peptidase-like 2 protease b (Sppl2b-D/A) or empty plasmid were transfected with 30 µl of Lipofectamine 3000 (Invitrogen). After 48 h, cells were lysed in 1 ml of lysis buffer (50 mm Hepes pH 7.4, 150 mm NaCl, 5 mm EGTA, 1% Glycerol, 1% Triton X100, 1.5 mm MgCl2, 10 mm 1,10-Phenanthroline) supplemented with complete protease inhibitor (Roche, Basel, CH). Cell lysates were cleared by centrifugation at 16,000g for 20 min at 4 °C. 500 µl of cleared lysates were applied to agarose beads coupled with anti-HA antibodies (A2095, Sigma–Aldrich, US) and incubated o/n at 4 °C. Then, beads were washed 6 times in lysis buffer and incubated with 20 µl of Laemmli buffer at 65 °C for 20 min. Eluted proteins were loaded onto an acrylamide gel, separated by SDS-PAGE electrophoresis and then analysed by Western blotting using following antibodies: anti-ADAM17 (ab39162, Abcam, Cambridge, UK), anti-HA [HA7] (Sigma-Aldrich, St. Louis,

MO, US), anti-HLA,ABC [EMR8-5] (ab70328, Abcam, Cambridge, UK) and anti-GAPDH (Code 5174, Cell Signaling, Danvers, Massachusetts, US).

Chapter Three:
Characterization of iRhom-mediated substrate selectivity of stimulated ADAM17 by high-resolution proteomics

3.1 Introduction

The membrane-bound metalloprotease ADAM17 was first discovered as the enzyme responsible for release of tumour necrosis factor α (TNFα), and therefore it is also known as TNFα converting enzyme (TACE) [174,175]. In addition, ADAM17 plays a pivotal role in activation of the EGFR as it mediates the release of several EGFR ligands [53,200]. For this reason, since its discovery ADAM17 has been considered of pharmaceutical interest, especially in the context of autoimmune diseases characterized by excess release of soluble TNFα, such as rheumatoid arthritis [289], and malignancies in which EGFR signalling is aberrantly activated [332]. However, therapeutic inhibition of ADAM17 has been difficult to achieve for its broad list of substrates and the lack of selectivity of small molecule inhibitors and potential related mechanism-based toxicity arising from the inhibition of TGFα/EGFR-dependent protection of the skin and intestinal barrier [333–335]. Nowadays, the list of ADAM17 substrates includes over 80 different transmembrane proteins, spanning from proteins playing a role in inflammation, such as TNFα, its receptors TNFR1 and TNFR2, and IL-6R, to growth factors, endocytic receptors and adhesion molecules [177,200,336].

ADAM17 maturation and activity is strictly regulated by its essential co-factors iRhom1 and iRhom2, seven-transmembrane-spanning proteins belonging to the family of inactive rhomboid proteases [184,201,279,288]. After forming a tight complex with ADAM17, iRhoms mediate its maturation and trafficking from the ER to the cell surface. iRhom1 and iRhom2 are both expressed in most tissues and they are somewhat redundant in supporting ADAM17 maturation [184,201,289]. At the cell surface, iRhoms can integrate the stimuli leading to ADAM17 activation, functioning as the regulatory subunit of an iRhom/ADAM17 catalytic complex [337,338]. Finally, iRhoms have been reported to address the proteolytic activity of ADAM17 toward specific substrates [188,327]. iRhom-mediated selectivity for some ADAM17 substrates has been tested on a limited number of substrates so far, including the EGFR ligands. Interestingly, while the stimulated shedding of all substrates was supported by iRhom2, iRhom1 was able to compensate for iRhom2 loss only in few cases [327].

Clearly, a systematic identification of ADAM17 substrates and elucidating the involvement of either iRhom in their cleavage is of general relevance to understanding the contribution of these molecules to the pathogenesis of diseases states as diverse as autoimmune diseases and cancer.

To address this, I employed a mass spectrometry–based proteomic approach aimed at identifying substrates cleaved by ADAM17 in an iRhom1- or iRhom2-dependent manner. This analysis was conducted in mouse embryonic fibroblasts (mEFs) and in the human

chondrosarcoma-derived fibroblast-like cell line HTB94, both of which endogenously express iRhom1 and iRhom2. By comparing the proteomic profiles of these cell systems under conditions of specific iRhom depletion or modulation, in this chapter I aim to define the molecular specificity of ADAM17-mediated shedding and its regulation by individual iRhom isoforms.

3.2 Mass spectrometry-based characterization of iRhom-mediated substrate selectivity of stimulated ADAM17 in mEFs

To explore the contribution of iRhom1 or iRhom2 to the substrate selectivity of stimulated ADAM17, I treated WT, iRhom1KO (iR1KO), iRhom2KO (iR2KO) or iRhom1/2dKO (iR1/2dKO) mEFs with PMA (phorbol 12-myristate 13-acetate) - a commonly used ADAM17 activator [53,202,327], and applied their conditioned media to a systematic mass spectrometry-based secretome analysis. Label-free quantification (LFQ) was used to quantitatively compare abundance of proteins detected in each MEF line versus their abundance in the same line upon PMA-stimulation (Figure 6).

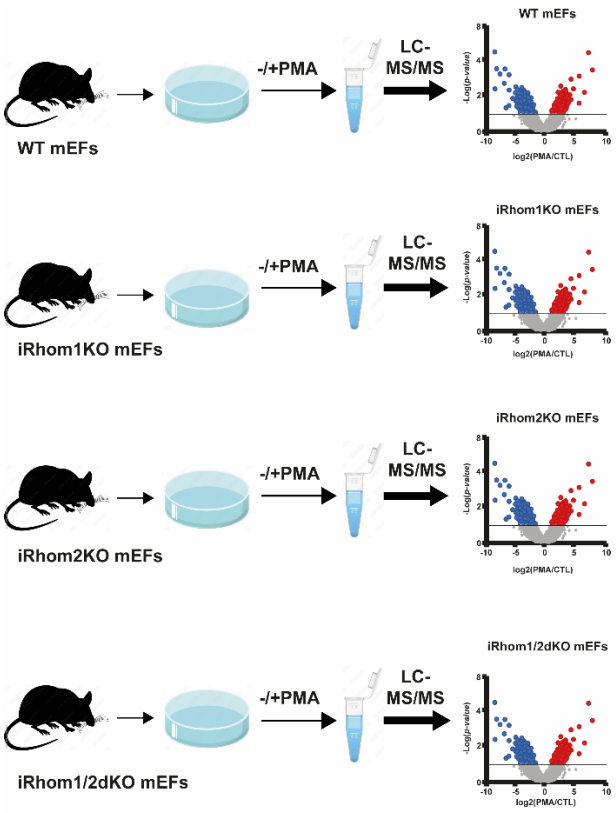

Figure 6: Schematic representation of the mass spectrometry-based approach used to identify ADAM17 substrates and investigate their iRhom-mediated selectivity in mEFs. Mouse embryonic fibroblasts (mEFs) were isolated from iRhom1KO, iRhom2KO, iRhom1/2 double KO (dKO) and WT control mice, grown until confluence in 6-well plates and stimulated with PMA in serum-free media. Conditioned media of PMA-stimulated cells and their untreated controls were subjected to mass spectrometry analysis and label-free quantification. For each cell line (WT, iR1KO, iR2KO or iR1/2dKO)

the relative abundance of proteins in the conditioned media of PMA stimulated cells was quantified versus its untreated controls.

To note, mEF cultures consist of a heterogeneous population of cells that are isolated from different mouse embryos (i.e. iR1KO, iR2KO, iR1/2 dKO or WT mouse), rather than a clonal cell line in which iR1 or iR2 were ablated. This limits the possibility to investigate the contribution of either iRhom to ADAM17-mediated shedding by comparing the secretome of different mEF lines (for instance, to compare abundance of proteins in the secretome of stimulated iR1KO or iR2KO mEFs with that of iR1/2 dKO mEFs). Indeed, LFQ of proteins in the secretome of different mEF lines could conceivably also recognize alterations in protein levels that reflect differences in their genetic background or in the cell types present in different cultures, rather than protein alterations due to the ablation of iRhom1 or iRhom2.

LFQ found 871 proteins in the secretome of stimulated and control WT mEFs; 813 in stimulated and control iRhom1KO mEFs; 669 in stimulated and control iRhom2KO mEFs; and 846 in the secretome of stimulated and control iRhom1/2dKO mEFs (Figure 7A). Once stimulated, ADAM17 mostly mediates ectodomain shedding (i.e. the proteolytic release of transmembrane proteins) of single-pass transmembrane (either type 1 and type 2) and GPI-anchored proteins [339]. The ectodomain of these shed proteins accumulate in the conditioned media and can systematically be detected by mass spectrometry (sheddome) [340]. Thus, I focused my analysis on proteins with this topology. The sheddome of PMA-stimulated WT mEFs comprised 82 proteins (68 type 1, 6 type 2 and 8 GPI-anchored proteins, according to Uniprot annotation), of iRhom1KO mEFs 72 proteins (62 type 1, 7 type 2 and 3 GPI-anchored proteins), of iRhom2KO mEFs 57 proteins (48 type 1, 5 type 2 and 4 GPI-anchored proteins) and of iRhom1/2dKO 60 proteins (50 type 1, 4 type 2 and 6 GPI-anchored proteins) (Figure 7B). 38 proteins were detected in the sheddome of WT, iRhom1KO and iRhom2KO mEF lines (Figure 7C). 55 proteins were present in the sheddome of both WT and iRhom1KO mEFs, accounting for about 60% of total proteins in their sheddomes, and 45 proteins were detected in the sheddome of both WT and iRhom2KO mEFs (about 49% of total proteins).

Sheddome analysis of WT MEFs by mass spectrometry and LFQ revealed that 32 single-pass/GPI-anchored proteins increased upon PMA stimulation (proteins were arbitrarily considered as altered upon PMA stimulation when the p-value of their change, measured with a two-sided Student t-test without correction for multiple hypothesis testing, was below 0.05, and when their levels changed by at least 30%) (Figure 7D, Table 3). As expected, the ectodomain of most of these proteins did not increase in the conditioned media of stimulated iR1/2 dKO mEFs, in which ADAM17 is inactive due to lack of both iRhoms [184,201] (Figure

7E). Only four transmembrane proteins increased in iR1/2 dKO MEFs upon PMA stimulation, and among them COLEC12 and LAMP2 also increased in WT MEFs, suggesting that these are not ADAM17 substrates and their regulation involves mechanisms unrelated to ADAM17-dependent shedding (Figure 7D, 7E). Within the group of proteins whose shedding was increased in stimulated WT MEFs versus untreated controls, and unchanged in iR1/2 dKO MEFs, 14 are known ADAM17 substrates (e.g. VASN, AXL and ALCAM), and 16 proteins are putative novel substrates of the protease, including matrix remodeling associated 8 (MXRA8) that emerged among the most highly stimulated proteins upon activation of ADAM17 (Figure 7D, Table 3).

Table 3: List of ADAM17 substrates in mEFs. In bold, putative novel substrates. The table contains a list of 30 single-pass transmembrane proteins that were significantly increased in the secretome of WT MEFs upon PMA stimulation. Indicated are the protein IDs, names of the proteins, the gene names, the number of peptides detected by MS for each protein, the mean of the ratio between PMA-stimulated mEFs and untreated controls of 3 biological replicates, the p-value calculated with a two-sided, heteroscedastic t-test based on the intensity ratios for PMA-stimulated and control MEFs, and the reference, when available, to the protein validation as an ADAM17 substrate.

Protein ID	Protein name	Gene name	Peptides	Ratio	Difference	*p*-value	-LOG(P-value)	Ref
Q8BKG3	Inactive tyrosine-protein kinase 7	Ptk7	64	6,782522	2,76	6,97E-07	6,16	258
P35951	Low-density lipoprotein receptor	Ldlr	33	12,25401	3,62	1,61E-06	5,79	57
Q9DBV4	**Matrix-remodeling-associated protein 8**	**Mxra8**	**27**	**8,149036**	**3,03**	**1,87E-06**	**5,73**	***Putative novel***
Q64449	C-type mannose receptor 2	Mrc2	72	30,34769	4,92	5,07E-05	4,29	341
Q9QUR8	Semaphorin-7A	Sema7a	18	4,595394	2,2	1,22E-04	3,92	342
P29533	Vascular cell adhesion protein 1	Vcam1	44	5,912116	2,56	1,83E-04	3,74	274
Q61490	CD166 antigen	Alcam	16	3,91777	1,97	2,11E-04	3,68	205
Q8C351	**Layilin**	**Layn**	**2**	**2,819482**	**1,5**	**2,66E-04**	**3,58**	***Putative novel***
O08747	**Netrin receptor UNC5C**	**Unc5c**	**17**	**3,51239117**	**1,81**	**1,16E-03**	**2,94**	***Putative novel***
P97798	Neogenin	Neo1	36	5,796026	2,54	1,69E-03	2,77	343,344
Q9DC11	**Plexin domain-containing protein 2**	**Plxdc2**	**16**	**3,137656**	**1,65**	**3,53E-03**	**2,45**	***Putative novel***
Q8BH27	**Multiple epidermal growth factor-like domains protein 9**	**Megf9**	**4**	**3,888195**	**1,96**	**3,77E-03**	**2,42**	***Putative novel***
Q00993	Tyrosine-protein kinase receptor UFO	Axl	12	2,055221	1,04	4,05E-03	2,39	204

P54754	**Ephrin type-B receptor 3**	**Ephb3**	**30**	**2,499191**	**1,32**	**5,73E-03**	**2,24**	***Putative novel***
P25118	Tumor necrosis factor receptor superfamily member 1A	Tnfrsf1a	9	2,846855	1,51	6,40E-03	2,19	271
P25119	Tumor necrosis factor receptor superfamily member 1B	Tnfrsf1b	5	2,746208	1,46	7,38E-03	2,13	271
O35598	**Disintegrin and metalloproteinase domain-containing protein 10**	**Adam10**	**19**	**2,408665**	**1,27**	**8,09E-03**	**2,09**	***Putative novel***
Q05909	**Receptor-type tyrosine-protein phosphatase gamma**	**Ptprg**	**12**	**3,533848**	**1,82**	**1,18E-02**	**1,93**	***Putative novel***
Q8R2Y2	**Cell surface glycoprotein MUC18**	**Mcam**	**25**	**1,796482**	**0,85**	**1,25E-02**	**1,9**	***Putative novel***
P59222	**Scavenger receptor class F member 2**	**Scarf2**	**13**	**2,412781**	**1,27**	**1,34E-02**	**1,87**	***Putative novel***
Q9DBH5	**Vesicular integral-membrane protein VIP36**	**Lman2**	**24**	**3,62164**	**1,86**	**1,37E-02**	**1,86**	***Putative novel***
O35188	Fractalkine	Cx3cl1	11	3,044432	1,61	1,82E-02	1,74	210
Q9CZT5	Vasorin	Vasn	17	3,031875	1,6	1,87E-02	1,73	243
P12023	Amyloid beta A4 protein	App	21	3,829073	1,94	2,24E-02	1,65	214,215
P15379	CD44 antigen	Cd44	3	1,835225	0,88	2,66E-02	1,57	205
B0V2N1	**Receptor-type tyrosine-protein phosphatase S**	**Ptprs**	**48**	**9,411166**	**3,23**	**2,78E-02**	**1,56**	***Putative novel***
O89026	**Roundabout homolog 1**	**Robo1**	**34**	**6,068036**	**2,6**	**3,07E-02**	**1,51**	***Putative novel***
O70458	**Oncostatin-M-specific receptor subunit beta**	**Osmr**	**15**	**1,641915**	**0,72**	**3,72E-02**	**1,43**	***Putative novel***
Q8VCF1	**Soluble calcium-activated nucleotidase 1**	**Cant1**	**8**	**1,66544886**	**0,74**	**4,30E-02**	**1,37**	***Putative novel***

By using a similar approach, I found that levels of 28 single-pass transmembrane/GPI-anchored proteins increased in the conditioned media of iR1KO cells upon PMA stimulation (Figure 7F). Within this group of proteins, which included several known ADAM17 substrates,15 proteins were also found more abundant in the sheddome of PMA-stimulated

WT mEFs (Figure 7F, 7G), suggesting that iRhom1 could be dispensable for the cleavage of these known and putative ADAM17 substrates. Conversely, levels of 7 proteins that were increased in the sheddome of PMA-stimulated WT mEFs, including the known ADAM17 substrates ALCAM and APP, that were not altered in the sheddome of iR1KO mEFs (Figure 7G). 13 proteins increased in the sheddome of PMA-stimulated iR1KO mEFs and were not detected in the conditioned media of WT mEFs. For these proteins, a similar cross-evaluation of their secretome alteration in WT and iR1KO MEFs could not be performed. This group of proteins comprised a number of known ADAM17 substrates (e.g. CSF1, LRP1 and SORCS1), whose shedding still occurs in the absence of iRhom1 (Figure 7G).

16 single-pass transmembrane/GPI-anchored proteins increased upon PMA stimulation in the sheddome of iR2KO mEFs (Figure 7G). 11 of these proteins, which include several known ADAM17 substrates (e.g. PTK7, LDLR, MRC2, NEO1, AXL, VCAM1, VASN, APP, CX3CL1) were also found more abundant in the conditioned media of PMA-stimulated WT mEFs, suggesting that iRhom2 is not essential for their shedding (Figure 7G). On the other hand, 9 proteins that were more abundant in the sheddome of WT mEFs upon PMA stimulation, were not altered in stimulated iR2KO mEFs, suggesting that release of these proteins could specifically be regulated by iRhom2. The remaining 5 proteins increased in the sheddome of PMA-stimulated iR2KO mEFs were not identified in the conditioned media of WT mEFs. This group of proteins comprised known (CSF1, GPC1, SDC4) and putative novel (SIRPα, PTPRK) ADAM17 substrates, shedding of which can also occur when iRhom2 is ablated (Figure 7G).

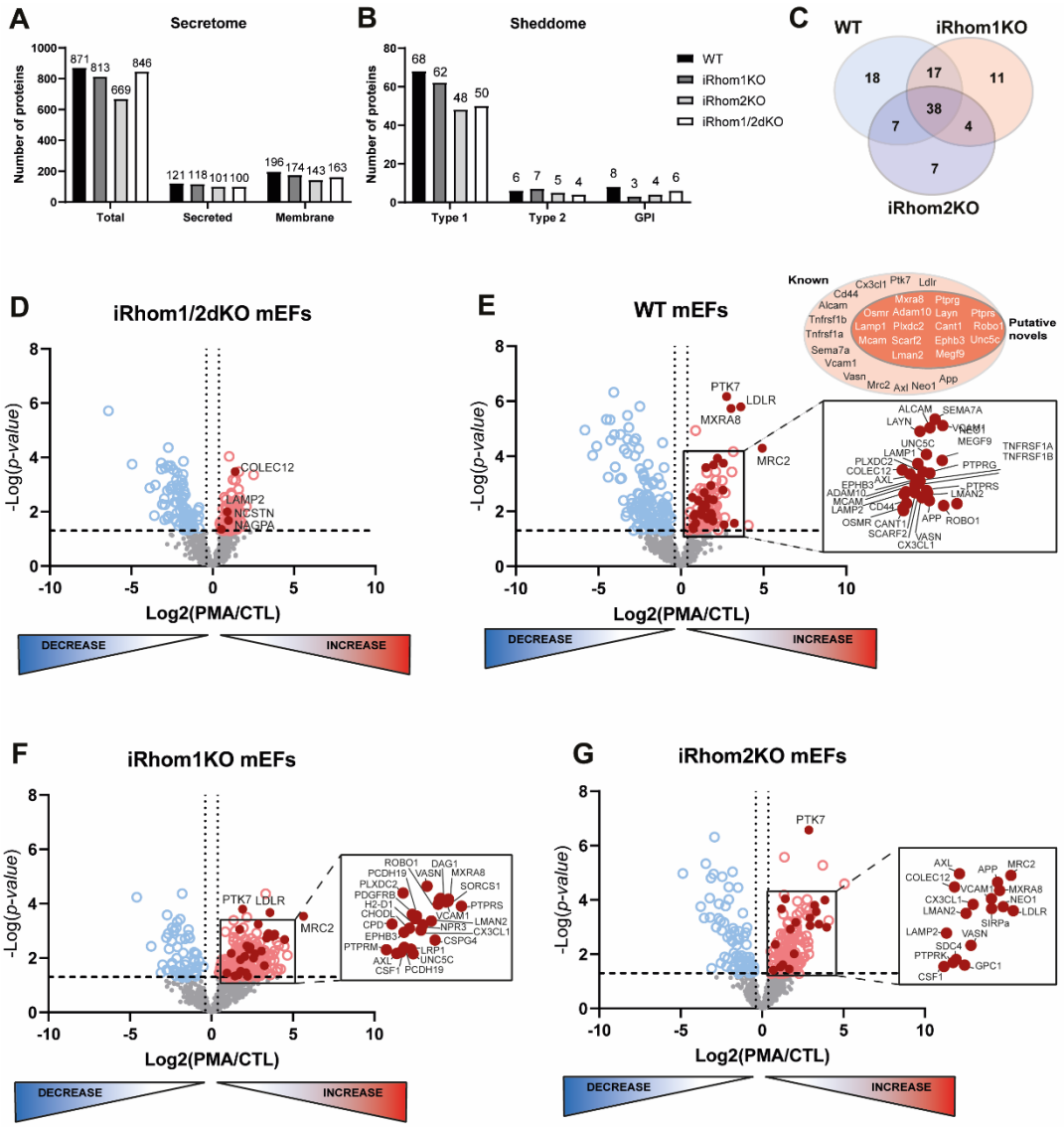

Figure 7: Unbiased high-resolution proteomics identified novel ADAM17 substrates in mEFs and the iRhom-dependency of their cleavage. A) Number of proteins detected in the secretome of WT, iR1KO, iR2KO and iR1/2dKO. In WT, 871 total proteins were identified in the secretome, of which 121 were secreted and 196 membrane-associated; in iR1KO, 813 total proteins were identified in the secretome, of which 118 were secreted and 174 membrane-associated; in iR2KO, 669 total proteins were identified in the secretome, of which 101 were secreted and 143 membrane-associated; in iR1/2dKO, 846 total proteins were identified in the secretome, of which 100 were secreted and 163 membrane-associated, based on annotations in the reviewed canonical FASTA database of Mus musculus from UniProt. B) Number and topology of proteins detected in the sheddome of WT, iR1KO, iR2KO and iR1/2dKO mEFs. Among the transmembrane proteins identified in the WT sheddome, 68 proteins were type 1, 6 were type 2 and 8 were GPI-anchored; in iR1KO sheddome, 62 transmembrane proteins were type 1, 7 were type 2 and 3 were GPI-anchored; in iR2KO sheddome, 48 transmembrane proteins were type 1, 5 were type 2 and 4 were GPI-anchored; in iR1/2dKO sheddome, 50 transmembrane proteins were type 1, 4 were type 2 and 6 were GPI-anchored, based on annotations in the reviewed canonical FASTA database of Mus musculus from UniProt. C) Venn diagram showing the overlapping sheddome of WT, iR1KO, iR2KO and iR1/2dKO. 38 proteins were detected in the sheddome of WT, iRhom1KO and iRhom2KO mEF lines, 18 were detected exclusively in WT, 11 exclusively iR1KO and 7 exclusively in iR2KO. 17 proteins were detected both in WT and iR1KO sheddome, while 7 were detected in WT and iR2KO sheddome. Only 4 proteins were detected both in iR1KO and iR2KO sheddome. D) Volcano plot showing the relative abundance in log2 of 871 proteins detected in the secretome of PMA-stimulated versus control secretome of WT mEFs (n=6). Proteins with a p-value below 0.05 (black dashed horizontal line) were highlighted as blue (log2 PMA/CTL < 0.30; black dotted vertical line) and red (log2 PMA/CTL > 0.30; black dotted vertical line) open circle dots. Transmembrane proteins increased in PMA-treated secretome were represented as red filled dots with their protein names. Moreover, putative novel ADAM17 substrates with a reduction (p-value < 0.05) in PMA-stimulated proteins are highlighted in white (16), while known ADAM17 substrates are highlighted in black (14). E) Volcano plot showing the relative abundance in log2 of 846 proteins detected in the secretome of PMA-stimulated versus control secretome of iRhom1/2dKO mEFs (n=6). Proteins with a p-value below 0.05 (black dashed horizontal line) were highlighted as blue (log2 PMA/CTL < 0.30; black dotted vertical line) and red (log2 PMA/CTL > 0.30; black dotted vertical

line) open circle dots. Transmembrane proteins increased in PMA-treated secretome were represented as red filled dots with their protein names. F) Volcano plot showing the relative abundance in log2 of 813 proteins detected in the secretome of PMA-stimulated versus control secretome of iRhom1KO mEFs (n=6). Proteins with a p-value below 0.05 (black dashed horizontal line) were highlighted as blue (log2 PMA/CTL < 0.30; black dotted vertical line) and red (log2 PMA/CTL > 0.30; black dotted vertical line) open circle dots. Transmembrane proteins increased in PMA-treated secretome were represented as red filled dots with their protein names. G) Volcano plot showing the relative abundance in log2 of 871 proteins detected in the secretome of PMA-stimulated versus control secretome of iRhom2KO mEFs (n=6). Proteins with a p-value below 0.05 (black dashed horizontal line) were highlighted as blue (log2 PMA/CTL < 0.30; black dotted vertical line) and red (log2 PMA/CTL > 0.30; black dotted vertical line) open circle dots. Transmembrane proteins increased in PMA-treated secretome were represented as red filled dots with their protein names.

In order to study iRhom1 or iRhom2 contribution to the shedding of ADAM17 substrates identified by proteomics, I analysed proteins whose release upon PMA stimulation was increased in WT, iR1KO or iR2KO MEFs. Out of the 47 proteins whose release was stimulated by PMA and detected in at least one of the three mEF lines, only 23 were detected in the secretome of all three different mEF lines and for which a cross-evaluation could be performed (Figure 8A, 8B). From this list I additionally removed EPHB3 and LAMP1, as 'quantitative analysis of regulated intramembrane proteolysis' (QARIP), which allows mapping identified peptides to the protein transmembrane topology, revealed that the identified peptides not only match with their ectodomains, but also with their intracellular domains (Figure 8C).

In addition, I confirmed by Western blotting that both proteins are present in the secretome in their full-length form, perhaps tethered to extracellular vesicles (Figure 8D and 8E). On the contrary, I did not remove the ADAM17 substrate PTK7 from this list, for which QARIP also matched peptides with its intracellular domain, as I proved by Western that the majority of PTK7 in the conditioned media is indeed a shed form of the protein, and only a minor fraction of the protein is full-length (Figure 8F).

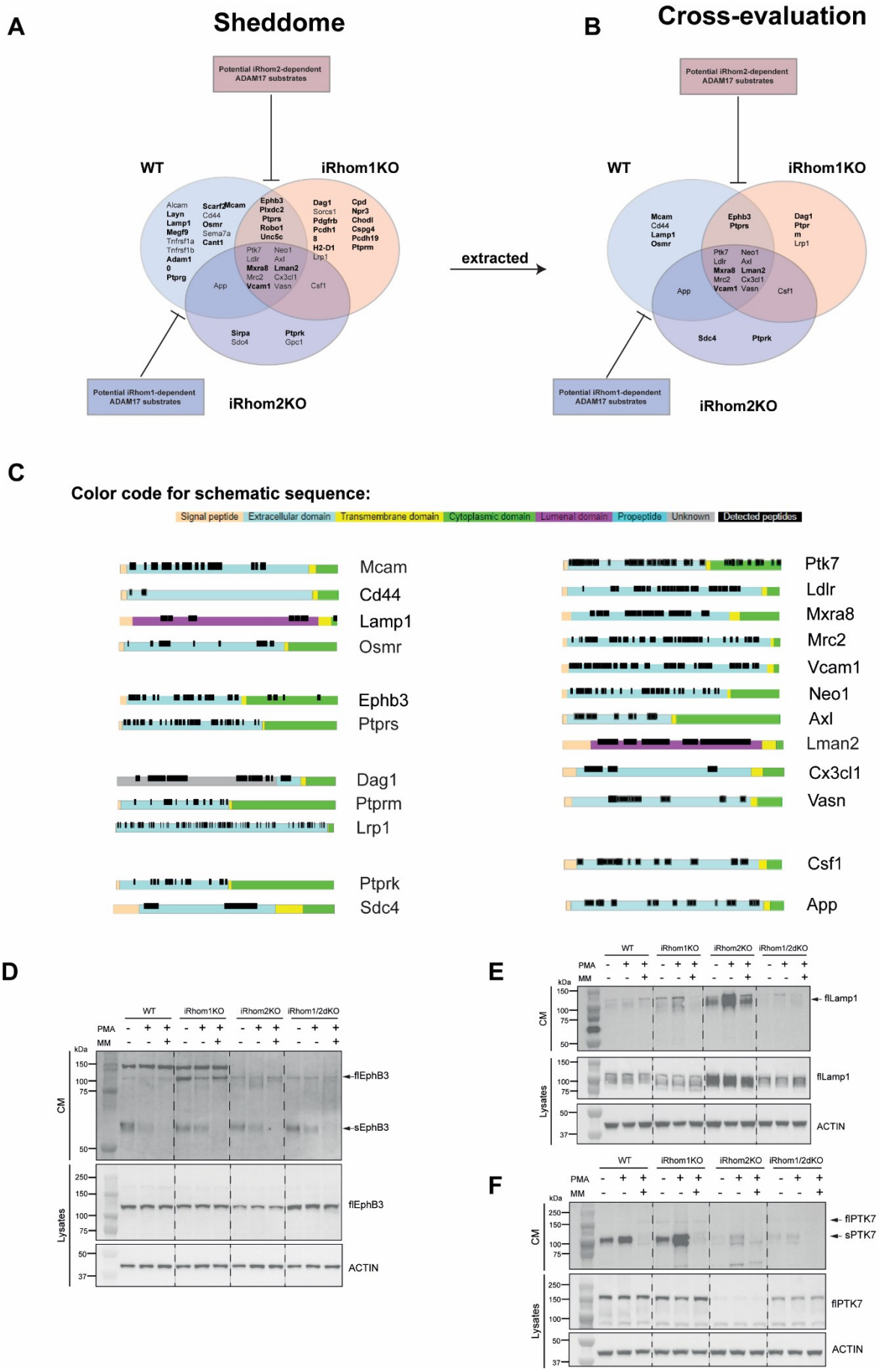

Figure 8: Sheddome analysis revealed that shedding of most ADAM17 substrates can be supported by either iRhom. A) Venn diagrams showing the entire sheddome and B) cross-evaluation of proteins detected in the secretome of mEF lines.

Among the 47 proteins identified, only 23 were extracted since they were detected in at least one of the three mEF lines. In bold, we highlighted putative novel ADAM17 substrates. C) Quantitative analysis of regulated intramembrane proteolysis (QARIP) showed the peptide distribution of 23 proteins extracted from the three secretome analysis' cross-evaluation (orange: signal peptide, blue: extracellular domain, yellow: transmembrane domain, green: cytoplasmic domain, purple: luminal domain, grey: unknown, black: detected peptide). Identified peptides of 20 out of 23 proteins derived from extracellular domains; EphB3, Lamp1 and Ptk7 peptides derived also from their cytoplasmic domains. D) Immunoblots on WT, iRhom1KO, iRhom2KO and iRhom1/2dKO mEFs treated with or without 25 ng/mL PMA and/or 10 μM marimastat (MM) showing soluble and full-length levels of EphB3 in TCA precipitated conditioned media (CM) and cell lysates (Lysates). In CM, full-length EphB3 (flEphB3) protein was detected according with QARIP analysis showed in Figure 8C. Actin was used as a loading control. E) Immunoblots on WT, iRhom1KO, iRhom2KO and iRhom1/2dKO mEFs treated with or without 25 ng/mL PMA and/or 10 μM marimastat (MM) showing soluble and full-length levels of Lamp1 in TCA precipitated conditioned media (CM) and cell lysates (Lysates). In CM, full-length Lamp1 (flLamp1) protein was detected according with QARIP analysis showed in Figure 8C. Actin was used as a loading control. F) Immunoblots on WT, iRhom1KO, iRhom2KO and iRhom1/2dKO mEFs treated with or without 25 ng/mL PMA and/or 10 μM marimastat (MM) showing soluble and full-length levels of Ptk7 in TCA precipitated conditioned media (CM) and cell lysates (Lysates). In CM, full-length Ptk7 (flPtk7) protein was detected according with QARIP analysis showed in Figure 8C. Actin was used as a loading control.

From the mass spectrometry-based cross-evaluation of proteins released in WT, iR1KO and iR2KO MEFs emerged that 10 proteins out of 21 were released in each mEF line upon PMA stimulation: 7 known ADAM17 substrates - PTK7, LDLR, MRC2, VCAM1, AXL, CX3CL1 and VASN - and 3 putative novel substrates - MXRA8, NEO1 and LMAN2. These proteins could be shed by activated ADAM17 in the presence of either iRhom (Figure 7D-7G, 8A). Similarly, CSF1 could be released by either iR1KO or iR2KO MEFs upon PMA stimulation (its increase in WT MEFs did not reach statistical significance). Extracellular levels of PTPRS increased in PMA stimulated iRhom1 KO or WT MEFs, but they were not altered in stimulated iRhom2KO mEFs, suggesting that this protein could be an ADAM17 substrate whose shedding is dependent on iRhom2. Conversely, the ADAM17 substrate APP was shed in iRhom2KO and WT mEFs, while unaltered in iRhom1KO mEFs upon PMA stimulation, suggesting it as an ADAM17 substrate whose cleavage could depend on iRhom1. The remaining 10 proteins were augmented by PMA stimulation only in the secretome of WT, iR1KO or iR2KO mEFs, and unaltered in the others. Of note, *p*-value and ratio of change for proteins belonging to this group were slightly above the threshold of significance that I applied for the analysis, and none of these proteins reached the more stringent significance criterion when using false-discovery rate (FDR) correction for multiple hypothesis testing (1%). This could be due to the fact that proteins within this group, including the ADAM17 substrates SDC4, LRP1 and CD44, can also be shed by a number of other proteinases (i.e. ADAM10, ADAM12 and membrane-type matrix metalloproteinases [12,345,346]). Conversely, the increase of the 10 proteins that were shed in iR1KO, iR2KO and WT MEFs was highly above the significance threshold in all three different cell lines.

To dissect the contribution of iRhom1 and iRhom2, I performed hierarchical clustering on the 21 secreted proteins that were reliably detected across all genotypes—WT, iR1KO, and iR2KO—following 3-hour PMA stimulation. While the cross-evaluation of proteins shed by individual mEFs provided a general overview, this targeted analysis aimed to resolve whether distinct subsets of ADAM17 substrates display differential reliance on either iRhom1 or iRhom2 for their shedding.

The resulting clustered heatmap revealed three major protein groups with distinct shedding patterns. The first cluster included OSMR and LRP1, which were shed by WT cells, but not by iR1KO or iR2KO mEFs, and only minimally by iR1/2 dKO mEFs. The second cluster comprised 6 ADAM17 substrates – APP, SDC4, PTPRK, PTPRM, MCAM, AND CD44 – whose shedding was strongly increased in iR2KO mEFs and, to a lesser extent, in WT and iR1KO cells, compared to iR1/2 dKO cells [187].

The third and the larger cluster included 12 proteins – DAG1, VASN, CSF1, CX3CL1, LMAN2, PTPRS, AXL, VCAM1, MXRA8, LDLR, NEO1, AND MRC2 – which displayed relatively consistent release across all three mEF genotypes. These proteins likely represent substrates whose shedding is supported by either iRhom.

Overall, this analysis did not reveal distinct groups of ADAM17 substrates that are selectively shed when the protease is in complex with iRhom2 or iRhom1, in contrast with the study by Maretzky et al. [327].

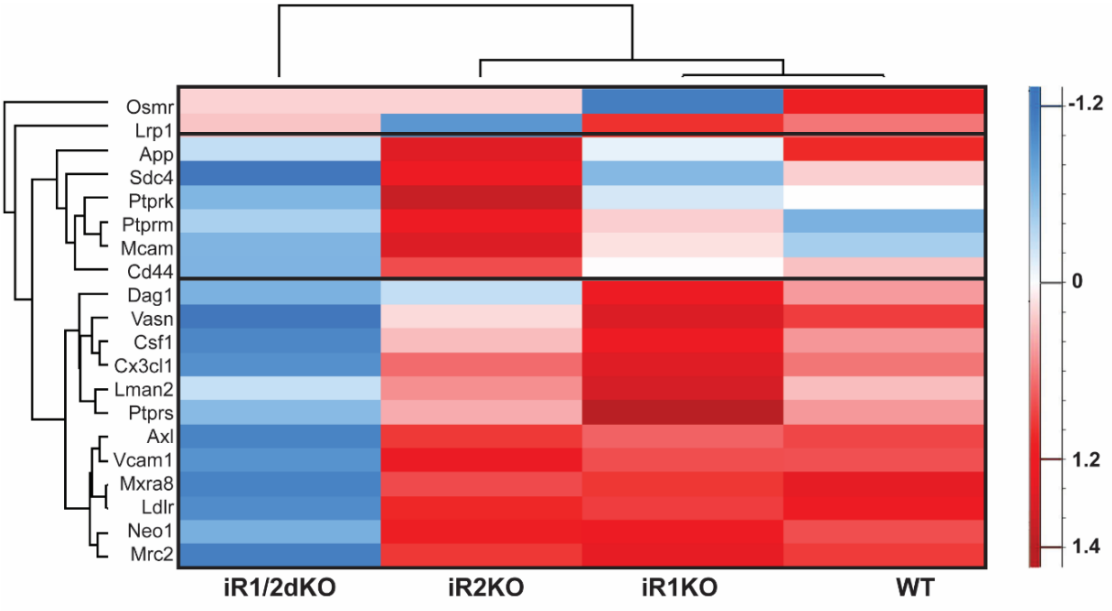

Figure 9: Clustering Analysis of ADAM17 substrates revealed a non-selective dependency on iRhom1 or iRhom2 in mEFs. Clustered heatmap of PMA-induced secreted proteins in WT, iR1KO, iR2KO and iR1/2dKO mEFs. The heatmap shows 21 proteins consistently detected across all three genotypes following 3h PMA stimulation. Rows represent individual proteins, and columns correspond to genotypes. Protein abundance was scaled (Z-score), and hierarchical clustering using Euclidean distance was applied to both proteins and samples. Three main clusters emerged: (1) proteins modestly released in iR1/2dKO; (2) proteins enriched in WT and iR2KO cells, indicating an iRhom1 preferentiality; and (3) proteins similarly secreted across all genotypes, suggesting that either iRhoms are involved in ADAM17-mediated shedding. Color intensity reflects relative secretion levels, with red indicating higher and blue lower abundance.

3.3 Secretome analysis on rescued iRhom1 and iRhom2 in knockout mEFs

To address the limitations posed by the heterogeneous genetic background of mEF cultures, a rescue experiment was performed in iRhom1/2 double knockout (dKO) mEFs. Either iRhom1 or iRhom2 was reintroduced into the same genetic background—that of iR1/2 dKO mEFs—by transient transfection. Secretome profiling was then performed following PMA stimulation (3h), under the same biological conditions used in the initial comparison. However, it is important to note that the proteomic method employed in this analysis differed: while the previous proteomic analysis on knockout mEFs relied on data-dependent acquisition (DDA), the rescue experiment was performed using data-independent acquisition (DIA). This methodological shift is significant, as DIA allows for more comprehensive and reproducible peptide detection by fragmenting all precursor ions within defined mass-to-charge windows, hereby minimizing the sampling bias inherent to DDA, which selectively fragments only the most abundant peptides [347], thus allowing me to have a more

comprehensive and comparable analysis on iRhom1/ADAM17 and iRhom2/ADAM17 sheddome.

Secretome analysis in PMA-stimulated iR1/2dKO mEFs rescued with either iRhom1, iRhom2 or both iRhoms, identified a total of 3609 proteins across all conditions. Among these, proteins annotated as single-pass transmembrane or GPI-anchored (according to UniProt topology classification) were prioritized for downstream analysis, given their potential to be ADAM17 substrates.

When iR1/2 dKO mEFs were transfected with a combination of iRhom1 and iRhom2, 68 putative ADAM17 substrates (including type I and II transmembrane as well as GPI-anchored proteins) increased in abundance in the conditioned media following PMA stimulation (Figure 10A), confirming functional restoration of the ADAM17 shedding machinery.

Single reintroduction of iR1 into iR1/2 dKO mEFs led to an increase of 88 single-pass or GPI-anchored proteins upon PMA stimulation, compared to mock-transfected cells (Figure 10B). Among these proteins, there were numerous known ADAM17 substrates, including AXL, VCAM1, SDC4 and MHC-I molecules, thus confirming that reintroduction of iRhom1 alone is sufficient to restore ADAM17 function.

Similarly, transfection of iRhom2 into iR1/2 dKO mEFs led to an increase in 91 putative ADAM17 substrates upon PMA stimulation, compared to mock-transfected cells (Figure 10C).

Interestingly, the majority of these putative substrates were shed upon reintroduction of either iRhom1, iRhom2, or both into iR1/2 dKO cells (Figure 10B and 10C), indicating that the same set of proteins can be shed regardless of which iRhom is present. The full list of these proteins is provided in Table 4. 23 of these proteins were indeed referenced as ADAM17 substrates (VCAM1, TNFRSF1A, SDC4, AXL, PTK7, NEO1, CX3CL1, MRC2, HBEGF, CSF1, SDC1, APP, VASN, LDLR, APLP2, LRP1, PNP, CD44, KITLG, L1CAM, GPC1, NCAM1, ALCAM), 17 of which were detected in all three secretomes (Table 4), 5 were detected both in iR1 and iR2 rescue secretomes (CD44, KITLG, L1CAM, GPC1, NCAM1) (Figure 10B, 10C), and only 1 (ALCAM) exclusively found in the iR1 secretome (Figure 10B).

Notably, the known ADAM17 substrates HBEGF and KITLG (isoform Kit Ligand 2), which were previously shown to be iRhom2-dependent in a different experimental context [327], were, under the conditions used in this study, effectively shed in the presence of either iRhom1 or iRhom2. This suggests that, unlike in the previous setting, both iRhoms can support their shedding in our system.

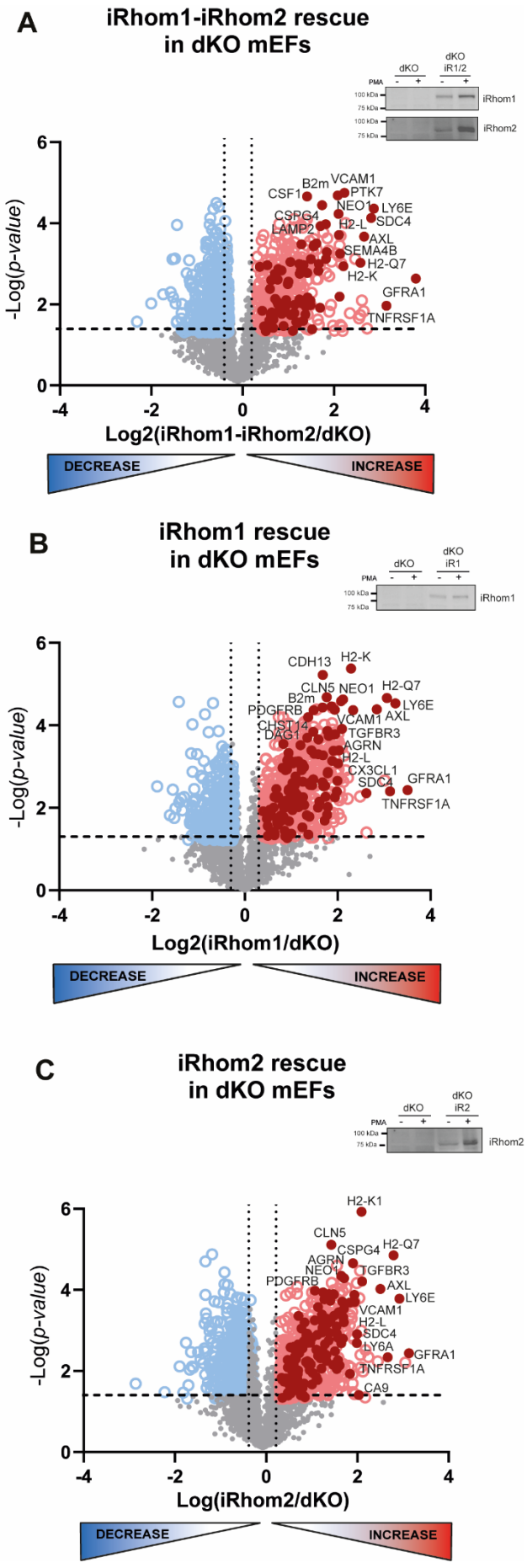

Figure 10: Unbiased high-resolution proteomics on iR1/2dKO mEFs with iR1 and/or iR2 confirmed most ADAM17 substrates can be supported by either iRhom. A) Volcano plot showing the relative abundance in log2 of 3609 proteins detected in the PMA-stimulated secretome of iR1 and iR2-rescue versus secretome of iR1/2dKO mEFs (n=3). Western blots of iRhom1 and iRhom2 are shown both in iR1/2dKO (dKO) and rescued iRhoms (dKO iR1/2). Proteins with a p-value below 0.05 (black dashed horizontal line) were highlighted as blue (log2 iRhom1-iRhom2/dKO < 0.30; black dotted vertical line) and red (log2 iRhom1-iRhom2/dKO > 0.30; black dotted vertical line) open circle dots. Transmembrane proteins increased in the secretome of iRhom1-iRhom2 rescued were represented as red filled dots with their protein names. Moreover, putative novel ADAM17 substrates with a reduction (p-value < 0.05) in iR1/2-rescue secretome are highlighted in white, while known ADAM17 substrates are highlighted in black. B) Volcano plot showing the relative abundance in log2 of 3609 proteins detected in the PMA-stimulated secretome of iR1-rescue versus secretome of iR1/2dKO mEFs (n=3). Western blot of iRhom1 is shown both in iR1/2dKO (dKO) and rescued iRhom1 (dKO iR1). Proteins with a p-value below 0.05 (black dashed horizontal line) were highlighted as blue (log2 iRhom1/dKO < 0.30; black dotted vertical line) and red (log2 iRhom1/dKO > 0.30; black dotted vertical line) open circle dots. Transmembrane proteins increased in the secretome of iRhom1 rescued were represented as red filled dots with their protein names. Moreover, putative novel ADAM17 substrates with a reduction (p-value < 0.05) in iR1-rescue secretome are highlighted in white, while known ADAM17 substrates are highlighted in black. C) Volcano plot showing the relative abundance in log2 of 3609 proteins detected in the PMA-stimulated secretome of iR2-rescue versus secretome of iR1/2dKO mEFs (n=3). Western blot of iRhom2 is shown both in iR1/2dKO (dKO) and rescued iRhom2 (dKO iR2). Proteins with a p-value below 0.05 (black dashed horizontal line) were highlighted as blue (log2 iRhom2/dKO < 0.30; black dotted vertical line) and red (log2 iRhom2/dKO > 0.30; black dotted vertical line) open circle dots. Transmembrane proteins increased in the secretome of iRhom2 rescued were represented as red filled dots with their protein names. Moreover, putative novel ADAM17 substrates with a reduction (p-value < 0.05) in iR2-rescue secretome are highlighted in white, while known ADAM17 substrates are highlighted in black.

.

Table 4: List of ADAM17 substrates in rescue mEFs. In bold, putative novel substrates. The table contains a list of 71 single-pass transmembrane proteins that were significantly increased across rescue iR1/iR2, rescue iR1, and rescue iR2 upon 3h PMA stimulation. Indicated are the protein IDs, names of the proteins, the gene names, the mean of the ratio between PMA-stimulated iRhom-rescue mEFs and iR1/2dKO controls of 3 biological replicates, the p-value calculated with a two-sided, heteroscedastic t-test based on the intensity ratios for PMA-stimulated iRhom-rescue mEFs and iR1/2dKO controls, and the reference, when available, to the protein validation as an ADAM17 substrate.

Protein ID	Protein name	Gene name	Ratio	Difference	*p*-value	-LOG(P-value)	Ref
A2ASQ1	**Agrin**	**Agrn**	**11,055867**	**3,47**	**2,43E-02**	**1,61**	***Putative novel***
Q8K4Q8	**Collectin-12**	**Colec12**	**10,779199**	**3,43**	**2,75E-02**	**1,56**	***Putative novel***
Q62351	**Transferrin receptor protein 1**	**Tfrc**	**2,619099**	**1,39**	**2,14E-01**	**0,67**	***Putative novel***
O89051	**Integral membrane protein 2B**	**Itm2b**	**2,684435**	**1,42**	**2,53E-01**	**0,60**	***Putative novel***
Q99J85	**Neuronal pentraxin receptor**	**Nptxr**	**7,428826**	**2,89**	**4,22E-01**	**0,38**	***Putative novel***
Q69ZN7	**Unconventional myosin-Ic**	**Myof**	**8,827677**	**3,14**	**4,75E-01**	**0,32**	***Putative novel***
P29533	Vascular cell adhesion protein 1	Vcam1	25,169530	4,65	8,31E-03	2,08	274
P25118	Tumor necrosis factor receptor superfamily member 1A	Tnfrsf1a	3,821588	1,93	7,08E-04	3,15	271
O35988	Syndecan-4	Sdc4	17,120499	4,10	1,53E-03	2,82	235
Q00993	Tyrosine-protein kinase receptor UFO	Axl	12,460244	3,64	2,18E-03	2,66	204
P14429	**H-2 class I histocompatibility antigen, Q7 alpha chain**	**H2-Q7**	**7,958733**	**2,99**	**2,64E-03**	**2,58**	***Putative novel***
Q8BKG3	Inactive tyrosine-protein kinase 7	Ptk7	26,318345	4,72	5,92E-03	2,23	258
P01901	**H-2 class I histocompatibility antigen, K-B alpha chain**	**H2-K1**	**7,498731**	**2,91**	**6,22E-03**	**2,21**	***Putative novel***
Q62179	**Semaphorin-4B**	**Sema4b**	**9,292230**	**3,22**	**7,32E-03**	**2,14**	***Putative novel***
P01897	**H-2 class I histocompatibility antigen, L-D alpha chain**	**H2-L**	**12,778687**	**3,68**	**7,80E-03**	**2,11**	***Putative novel***
P97798	Neogenin	Neo1	18,317881	4,20	7,97E-03	2,10	343,344
O35188	Fractalkine	Cx3cl1	9,569776	3,26	1,44E-02	1,84	210
Q64449	C-type mannose receptor 2	Mrc2	8,507627	3,09	1,50E-02	1,82	341
Q8VHY0	**Chondroitin sulfate proteoglycan 4**	**Cspg4**	**15,354146**	**3,94**	**1,51E-02**	**1,82**	***Putative novel***
P55144	**Tyrosine-protein kinase receptor TYRO3**	**Tyro3**	**3,693474**	**1,88**	**2,01E-02**	**1,70**	***Putative novel***
O88393	**Transforming growth factor beta receptor type 3**	**Tgfbr3**	**7,782785**	**2,96**	**2,14E-02**	**1,67**	***Putative novel***
Q8BHN0	**Protein phosphatase 1L**	**Ppm1l**	**6,940109**	**2,79**	**2,20E-02**	**1,66**	***Putative novel***

B0V2N1	**Receptor-type tyrosine-protein phosphatase S**	**Ptprs**	**10,550273**	**3,40**	**2,77E-02**	**1,56**	***Putative novel***
Q61495	**Desmoglein-1**	**Dsg1**	**2,555676**	**1,35**	**2,99E-02**	**1,52**	***Putative novel***
Q06186	Proheparin-binding EGF-like growth factor	Hbegf	8,472230	3,08	3,19E-02	1,50	53
Q9EPR5	**VPS10 domain-containing receptor SorCS2**	**Sorcs2**	**3,853908**	**1,95**	**3,27E-02**	**1,49**	***Putative novel***
Q9DBV4	**Matrix remodeling-associated protein 8**	**Mxra8**	**4,176919**	**2,06**	**3,28E-02**	**1,48**	***Putative novel***
Q64695	**Endothelial protein C receptor**	**Procr**	**4,145261**	**2,05**	**3,57E-02**	**1,45**	***Putative novel***
Q8K1E3	**Protein delta homolog 2**	**Dlk2**	**4,402706**	**2,14**	**3,76E-02**	**1,43**	***Putative novel***
O35375	**Neuropilin-2**	**Nrp2**	**6,696546**	**2,74**	**3,84E-02**	**1,42**	***Putative novel***
P07141	Macrophage colony-stimulating factor 1	Csf1	24,696181	4,63	3,87E-02	1,41	282
P18828	Syndecan-1	Sdc1	3,290717	1,72	4,23E-02	1,37	235
P12023	Amyloid-beta A4 protein	App	7,651424	2,94	4,66E-02	1,33	214,215
Q61730	**Interleukin-1 receptor accessory protein**	**Il1rap**	**2,947571**	**1,56**	**4,77E-02**	**1,32**	***Putative novel***
Q9EPL2	**Calsyntenin-1**	**Clstn1**	**10,892017**	**3,45**	**5,19E-02**	**1,28**	***Putative novel***
P05622	**Platelet-derived growth factor receptor beta**	**Pdgfrb**	**6,946851**	**2,80**	**5,31E-02**	**1,27**	***Putative novel***
Q9CZT5	Vasorin	Vasn	4,254572	2,09	5,70E-02	1,24	243
P98156	**Very low-density lipoprotein receptor**	**Vldlr**	**2,825481**	**1,50**	**6,29E-02**	**1,20**	***Putative novel***
Q7TMJ8	**Phosphoinositide-3-kinase-interacting protein 1**	**Pik3ip1**	**2,889211**	**1,53**	**6,70E-02**	**1,17**	***Putative novel***
O88572	**Low-density lipoprotein receptor-related protein 6**	**Lrp6**	**2,482048**	**1,31**	**7,91E-02**	**1,10**	***Putative novel***
Q05909	**Receptor-type tyrosine-protein phosphatase gamma**	**Ptprg**	**3,249811**	**1,70**	**8,77E-02**	**1,06**	***Putative novel***
P35951	Low-density lipoprotein receptor	Ldlr	8,055738	3,01	9,01E-02	1,05	57
P14719	**Interleukin-1 receptor-like 1**	**Il1rl1**	**5,756840**	**2,53**	**1,00E-01**	**1,00**	***Putative novel***
Q924X6	**Low-density lipoprotein receptor-related protein 8**	**Lrp8**	**3,801260**	**1,93**	**1,14E-01**	**0,94**	***Putative novel***
O88792	**Junctional adhesion molecule A**	**F11r**	**3,439883**	**1,78**	**1,15E-01**	**0,94**	***Putative novel***
Q06335	Amyloid-like protein 2	Aplp2	2,702705	1,43	1,28E-01	0,89	209
Q8BTJ4	**Bis(5'-adenosyl)-triphosphatase enpp4**	**Enpp4**	**3,325121**	**1,73**	**1,39E-01**	**0,86**	***Putative novel***
Q8C351	**Layilin**	**Layn**	**6,971745**	**2,80**	**1,41E-01**	**0,85**	***Putative novel***

O35516	**Neurogenic locus notch homolog protein 2**	**Notch2**	**3,625919**	**1,86**	**1,53E-01**	**0,81**	***Putative novel***
P18572	**Basigin**	**Bsg**	**7,151270**	**2,84**	**1,66E-01**	**0,78**	***Putative novel***
Q62470	**Integrin alpha-3**	**Itga3**	**3,930085**	**1,97**	**1,69E-01**	**0,77**	***Putative novel***
B2RXS4	**Plexin-B2**	**Plxnb2**	**4,136589**	**2,05**	**1,78E-01**	**0,75**	***Putative novel***
Q03145	**Ephrin type-A receptor 2**	**Epha2**	**4,293291**	**2,10**	**1,93E-01**	**0,72**	***Putative novel***
Q91ZX7	Prolow-density lipoprotein receptor-related protein 1	Lrp1	3,409321	1,77	2,31E-01	0,64	220
Q91XX1	**Protocadherin gamma C3**	**Pcdhgc3**	**5,907757**	**2,56**	**2,38E-01**	**0,62**	***Putative novel***
P59222	**Scavenger receptor class F member 2**	**Scarf2**	**3,255235**	**1,70**	**2,39E-01**	**0,62**	***Putative novel***
O35598	**Disintegrin and metalloproteinase domain-containing protein 10**	**Adam10**	**2,961059**	**1,57**	**2,60E-01**	**0,58**	***Putative novel***
P15116	**Cadherin-2**	**Cdh2**	**7,644007**	**2,93**	**2,88E-01**	**0,54**	***Putative novel***
O35664	**Interferon alpha/beta receptor 2**	**Ifnar2**	**2,588221**	**1,37**	**3,12E-01**	**0,51**	***Putative novel***
Q80TF3	**Protocadherin-19**	**Pcdh19**	**2,670106**	**1,42**	**3,36E-01**	**0,47**	***Putative novel***
Q62165	**Dystroglycan**	**Dag1**	**2,981320**	**1,58**	**4,02E-01**	**0,40**	***Putative novel***
P97785	**GDNF family receptor alpha-1**	**Gfra1**	**6,076436**	**2,60**	**1,61E-04**	**3,79**	***Putative novel***
Q64253	**Lymphocyte antigen 6E**	**Ly6e**	**20,095369**	**4,33**	**1,33E-03**	**2,88**	***Putative novel***
P05533	**Lymphocyte antigen 6A**	**Ly6a**	**4,460274**	**2,16**	**7,58E-03**	**2,12**	***Putative novel***
P0CW02	**Lymphocyte antigen 6C1**	**Ly6c1**	**3,783190**	**1,92**	**4,19E-02**	**1,38**	***Putative novel***
Q9WTR5	**Cadherin-13**	**Cdh13**	**6,594002**	**2,72**	**5,64E-02**	**1,25**	***Putative novel***
O08542	**Efna4**	**Efna4**	**3,879679**	**1,96**	**7,27E-02**	**1,14**	***Putative novel***
Q61468	**Mesothelin**	**Msln**	**6,932915**	**2,79**	**1,66E-01**	**0,78**	***Putative novel***
P35456	**Urokinase plasminogen activator surface receptor**	**Plaur**	**2,677373**	**1,42**	**3,41E-01**	**0,47**	***Putative novel***
P04925	Major prion protein	Prnp	3,499557	1,81	3,73E-01	0,43	230

To gain further insight into the overall effect of iRhom1 and iRhom2 re-expression on the ADAM17 sheddome, I performed hierarchical clustering on secretome data derived from iRhom1/2 dKO mEFs rescued with either iRhom1, iRhom2, or both, following PMA stimulation for 3h.

Hierarchical cluster analysis revealed that the sheddome of iR1/2 dKO cells transfected with both iRhoms clustered closely with those of cells transfected with either iRhom1 or iRhom2 alone. No proteins were identified as being selectively shed by only one iRhom, further indicating that, under my experimental conditions, either iRhom is sufficient to support the shedding of all detected ADAM17 substrates.

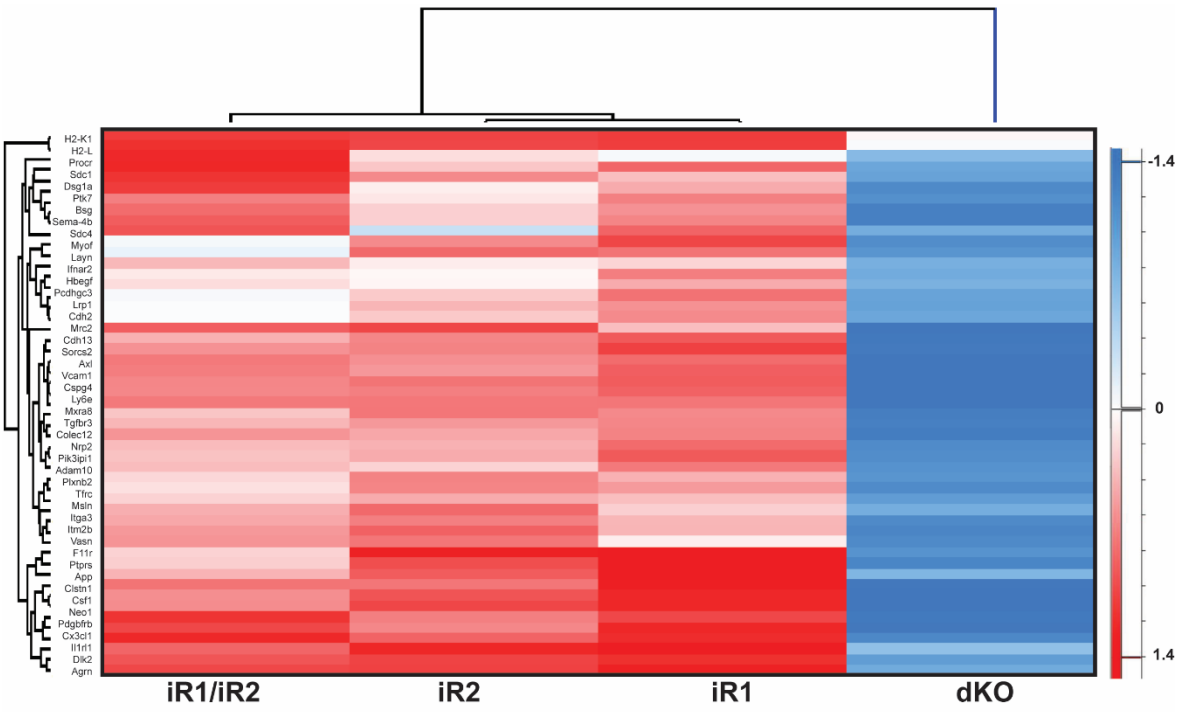

Figure 11: Clustering Analysis of ADAM17 substrates revealed a non-selective dependency on iRhom1 or iRhom2 in rescue mEFs. Clustered heatmap of PMA-induced secreted proteins in rescue iR1/iR2, rescue iR2, rescue iR1 and iR1/2dKO mEFs. The heatmap shows 71 proteins consistently detected across all three genotypes following 3h PMA stimulation. Rows represent individual proteins, and columns correspond to genotypes. Protein abundance was scaled (Z-score), and hierarchical clustering using Euclidean distance was applied to both proteins and samples. One main cluster emerged: proteins similarly secreted across all genotypes, suggesting that either iRhoms are involved in ADAM17-mediated shedding. Color intensity reflects relative secretion levels, with red indicating higher and blue lower abundance.

In conclusion, I used a mass spectrometry-based approach for a systematic identification of ADAM17 substrates in mEFs, and to explore the iRhom-mediated substrate selectivity of stimulated ADAM17 in an unbiased manner. This approach allowed me the identification of putative novel substrates of ADAM17 and, altogether, my results suggested that most substrates could be cleaved by stimulated ADAM17 in the presence of either iRhom.

3.4 Shedding of most ADAM17 substrates is supported by either iRhom1 and iRhom2 in human fibroblast-like cells

iRhom KO mEFs are an established model to investigate iRhom-mediated substrate selectivity of ADAM17 [327,348]. However, since these are immortalized cell lines that potentially originate from different embryonic cell types, a direct mass spectrometry-based comparison across different MEF lines could not be performed. For this reason, I ablated ADAM17, iRhom1 and iRhom2 in a human fibroblast-like cell line (HTB94) and used the generated ADAM17 KO (A17KO), iR1KO and iR2KO HTB94 cell lines to compare abundance of ADAM17 substrates in their secretome and further investigate iRhom-mediated substrate selectivity of the protease in a more quantitative manner. To this aim, WT, A17KO, iR1KO and iR2KO HTB94 cells were stimulated with PMA for 3 h, then conditioned media were collected and subjected to quantitative secretome analysis (the experimental workflow used is represented in Figure 12).

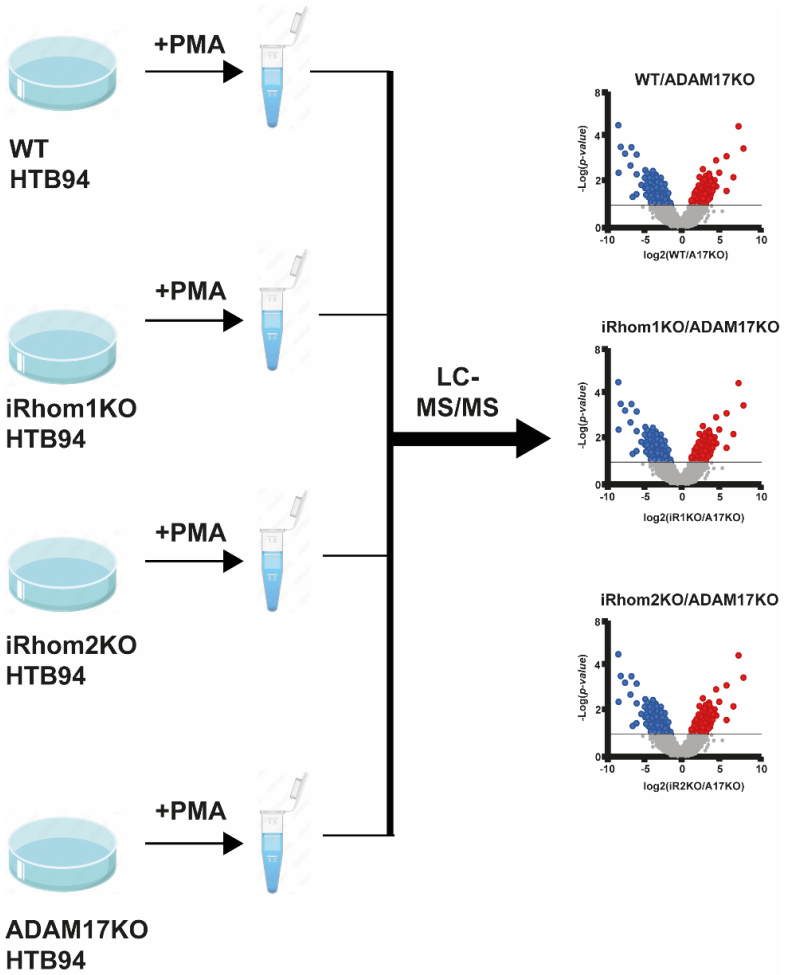

Figure 12: Schematic representation of the mass spectrometry-based approach used to identify ADAM17 substrates and investigate their iRhom-mediated selectivity in human HTB94 cells. ADAM17, iRhom1 or iRhom2 was ablated in fibroblast-like HTB94 cells. Then, iR1KO, iR2KO, A17KO or NTC controls were grown until confluence in 6-well plates, stimulated with PMA in serum-free media and conditioned media subjected to high resolution mass spectrometry analysis. Abundance of proteins in WT, iR1KO or iR2KO cells was measured and relatively quantified versus A17KO cells.

1616 proteins were found in conditioned media of PMA-stimulated A17KO HTB94 cells and WT controls, of which 578 membrane proteins and 275 secreted proteins. 19 single-pass/GPI-anchored proteins were found more abundant in the secretome of the stimulated WT HTB94. Among them, 10 known ADAM17 substrates (SDC4, NRG1, VASN, SEMA4D, PTK7, MRC2, JAG1, PTPRF, APLP2 and APP) and 9 potential novel substrates (MXRA8, PROCR, NTM, PVRL1, NEO1 AMIGO2, PTPRG, CADM1 and MET) (Figure 13A).

To identify ADAM17 substrates preferentially shed when the proteinase is in complex with iRhom1 and/or iRhom2, I compared abundance of single-pass/GPI-anchored proteins in the secretome of iR1KO or iR2KO cells with that of proteins in A17KO cells. 20 single-pass/GPI proteins were significantly increased in the secretome of iR1KO compared to A17KO cells (Figure 13B), and 19 were increased in the iR2KO compared to A17KO (Figure 13C).

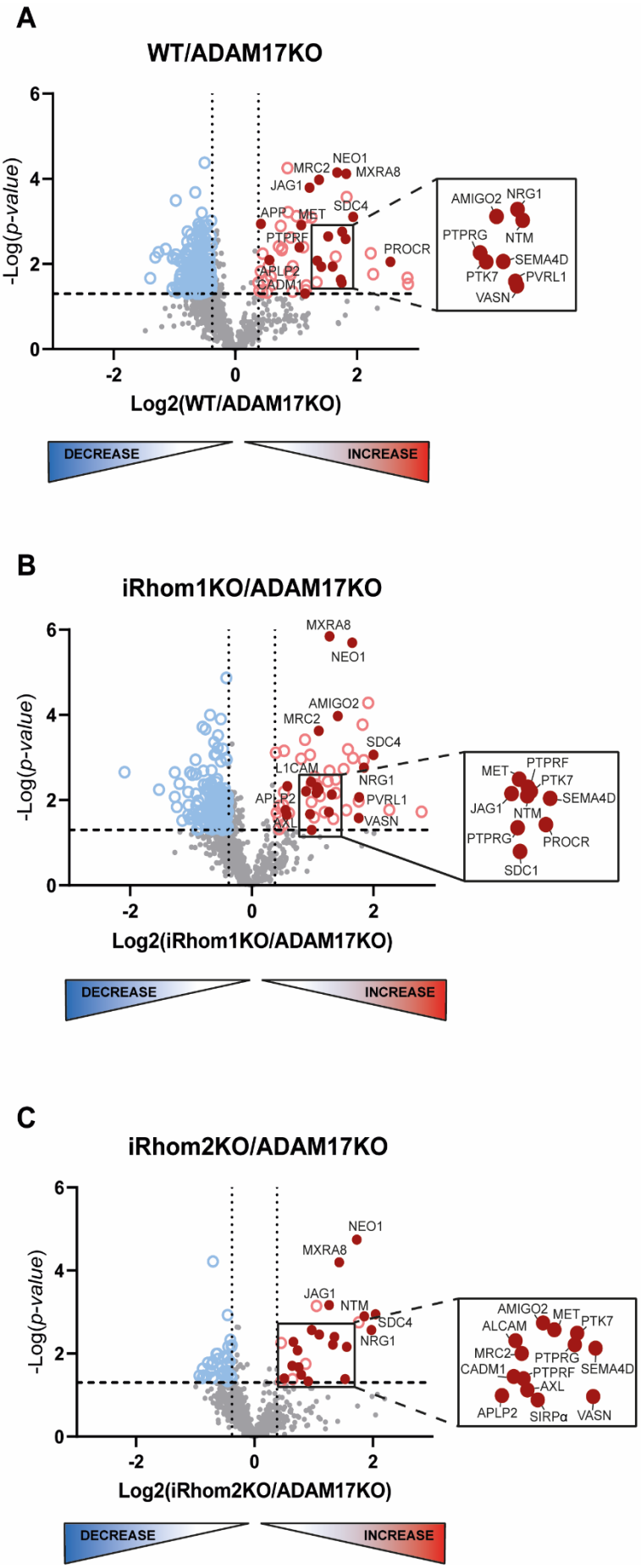

Figure 13: Unbiased high-resolution proteomics identified novel ADAM17 substrates in genetically ablated HTB94 and iRhom-dependency of their cleavage. A) Volcano plot showing the relative abundance in log2 of proteins detected in the secretome of WT versus ADAM17KO secretome of HTB94 stimulated for 3h with PMA (n=3). Proteins with a p-value below 0.05 (black dashed horizontal line) were highlighted as blue (log2 PMA/CTL < 0.30; black dotted vertical line) and red (log2 PMA/CTL > 0.30; black dotted vertical line) open circle dots. Transmembrane proteins increased in WT secretome were represented as red filled dots with their protein names. B) Volcano plot showing the relative abundance in log2 of proteins detected in the secretome of iRhom1KO versus ADAM17KO secretome of HTB94 (n=3). Proteins with a p-value below 0.05 (black dashed horizontal line) were highlighted as blue (log2 PMA/CTL < 0.30; black dotted vertical line) and red (log2 PMA/CTL > 0.30; black dotted vertical line) open circle dots. Transmembrane proteins increased in iRhom1KO secretome were represented as red filled dots with their protein names. C) Volcano plot showing the relative abundance in log2 of proteins detected in the secretome of iRhom2KO versus ADAM17KO secretome of HTB94 (n=3). Proteins with a p-value below 0.05 (black dashed horizontal line) were highlighted as blue (log2 PMA/CTL < 0.30; black dotted vertical line) and red (log2 PMA/CTL > 0.30; black dotted vertical line) open circle dots. Transmembrane proteins increased in iRhom2KO secretome were represented as red filled dots with their protein names.

Table 5: List of ADAM17 substrates detected in WT, iR1KO, iR2KO HTB94 (3h PMA stimulation). In bold, putative novel substrates. The table contains a list of 24 single-pass transmembrane proteins that were significantly increased across WT, iR1KO, iR2KO HTB94 upon 3h PMA stimulation. Indicated are the protein IDs, names of the proteins, the gene names, the mean of the ratio between PMA-stimulated WT and ADAM17KO controls of 3 biological replicates, the p-value calculated with a two-sided, heteroscedastic t-test based on the intensity ratios for PMA-stimulated WT and ADAM17KO controls, and the reference, when available, to the protein validation as an ADAM17 substrate.

Protein ID	Protein name	Gene name	Ratio	Difference	*p*-value	-LOG(P-value)	Ref
P05067	Amyloid beta A4 protein	APP	1,34	0,427108129	1,14E-03	2,94354629	214,215
Q9UNN8	**Endothelial protein C receptor**	**PROCR**	**5,89**	**2,557636897**	**8,82E-03**	**2,054424342**	***Putative novel***
Q15223	**Nectin-1**	**PVRL1**	**3,35**	**1,7425855**	**2,34E-02**	**1,630398071**	***Putative novel***
P18827	Syndecan-1	SDC1	1,73	0,789938609	9,66E-02	1,015070695	235
P32004	Neural cell adhesion molecule L1	L1CAM	1,47	0,555720011	7,57E-02	1,120640972	252
Q9BY67	**Cell adhesion molecule 1**	**CADM1**	**2,23**	**1,154051463**	**4,95E-02**	**1,30575307**	***Putative novel***
P78324	**Tyrosine-protein phosphatase non-receptor type substrate 1**	**SIRPA**	**1,84**	**0,88205719**	**2,21E-01**	**0,655107098**	***Putative novel***
Q13740	**CD166 antigen**	ALCAM	1,78	0,828751246	1,60E-01	0,796618069	205
P30530	Tyrosine-protein kinase receptor UFO	AXL	2,14	1,09725825	6,30E-02	1,200965382	204
P31431	Syndecan-4	SDC4	3,85	1,944568634	7,78E-04	3,109117401	235
Q13308	Inactive tyrosine-protein kinase 7	PTK7	2,68	1,422921499	1,16E-02	1,936202239	258
Q9BRK3	**Matrix-remodeling-associated protein 8**	**MXRA8**	**3,56**	**1,831478755**	**7,66E-05**	**4,115877721**	***Putative novel***
Q9UBG0	C-type mannose receptor 2	MRC2	2,61	1,386271159	1,06E-04	3,97629548	341
Q9P121	**Neurotrimin**	**NTM**	**3,54**	**1,823226293**	**2,58E-03**	**2,588059562**	***Putative novel***
P23470	**Receptor-type tyrosine-protein phosphatase gamma**	**PTPRG**	**2,56**	**1,354874293**	**8,38E-03**	**2,076611586**	***Putative novel***
Q02297	Neuregulin-1	NRG1	3,40	1,766304016	1,75E-03	2,757636256	260
P78504	Protein jagged-1	JAG1	2,34	1,228529612	1,62E-04	3,791019921	248
Q6EMK4	Vasorin	VASN	3,38	1,759130478	2,74E-02	1,563040771	243
P08581	**Hepatocyte growth factor receptor**	**MET**	**2,13**	**1,092961629**	**1,22E-03**	**2,91210608**	***Putative novel***
Q92859	Neogenin	NEO1	3,21	1,680378596	7,15E-05	4,145581607	343,344

P10586	Receptor-type tyrosine-protein phosphatase F	PTPRF	2,09	1,061140696	4,03E-03	2,394186404	261
Q86SJ2	**Amphoterin-induced protein 2**	**AMIGO2**	**2,90**	**1,534685771**	**2,25E-03**	**2,648439006**	***Putative novel***
Q06481	Amyloid-like protein 2	APLP2	1,48	0,567075094	8,07E-03	2,093058607	209
Q92854	Semaphorin-4D	SEMA4D	3,05	1,606820424	1,14E-02	1,942294585	268

The proteomic method used to identify ADAM17 substrates that were shed in an iRhom1- or iRhom2-dependent manner was based on the relative quantification of their abundance in the secretome of WT, iR1KO or iR2KO cells versus their abundance in the secretome of A17KO cells. In order to better assess the shedding efficiency by which ADAM17 cleaves its substrates when either iRhom is ablated, I complemented this analysis by comparing the secretome abundance of known/putative ADAM17 substrates across the different WT, iR1KO, iR2KO and A17KO HTB94 cells. Extracellular levels of 10 known ADAM17 substrates (VASN, NRG1, SDC4, PTK7, JAG1, PTPRF, APLP2, SEMA4D, AXL and APP) were diminished in A17KO cells and not altered in the secretome of iR1KO or iR2KO cells compared to WT cells, indicating them as proteins that could be shed by stimulated ADAM17 in an iRhom1- or iRhom2-dependent manner (Figure 14A). I also included into this group the known ADAM17 substrates SDC1, ALCAM and L1CAM. Indeed, extracellular levels of these proteins were lower in A17KO than WT cells, although such an alteration in protein abundance did not reach statistical significance when analysed by 2-way ANOVA, and their levels in the conditioned media of iR1KO and iR2KO were similar to those of WT cells (Figure 13A). Moreover, I included, within this group, 6 putatively novel substrates of ADAM17, whose release was equally supported by iRhom1 or iRhom2, as their levels in the secretome of iR1KO and iR2KO cells were similar to those in WT cells, and their levels in A17KO significantly less (NEO1, PTPRG, MET, CADM1, PROCR, MXRA8) (Figure 13A). I also included SIRPα within this group, although changes in its abundance across the different cell lines did not reach statistical significance when analysed by 2-way ANOVA. Altogether, these data showed that shedding of 20 out of the 24 proteins that I identified as known/novel ADAM17 substrates in HTB94 cells could be supported by either iRhom1 or iRhom2. Extracellular levels of one putative ADAM17 substrate, NTM, were lower in A17KO cells compared to WT and iR2KO cells (Figure 13B). Although it did not reach statistical significance, I found that NTM levels in the secretome of iR1KO cells were less than in WT. This suggests that NTM could be preferentially cleaved by ADAM17

when the proteinase is in complex with iRhom1. On the other hand, the decrease of MRC2 (a known ADAM17 substrate), AMIGO2 and PVRL1 (putative substrates) levels in the secretome of iR2KO cells compared to WT was larger than in iR1KO cells. (Figure 13C). This suggests that ADAM17-dependent shedding of MRC2, AMIGO2 and PVRL1 was mainly supported by iRhom2.

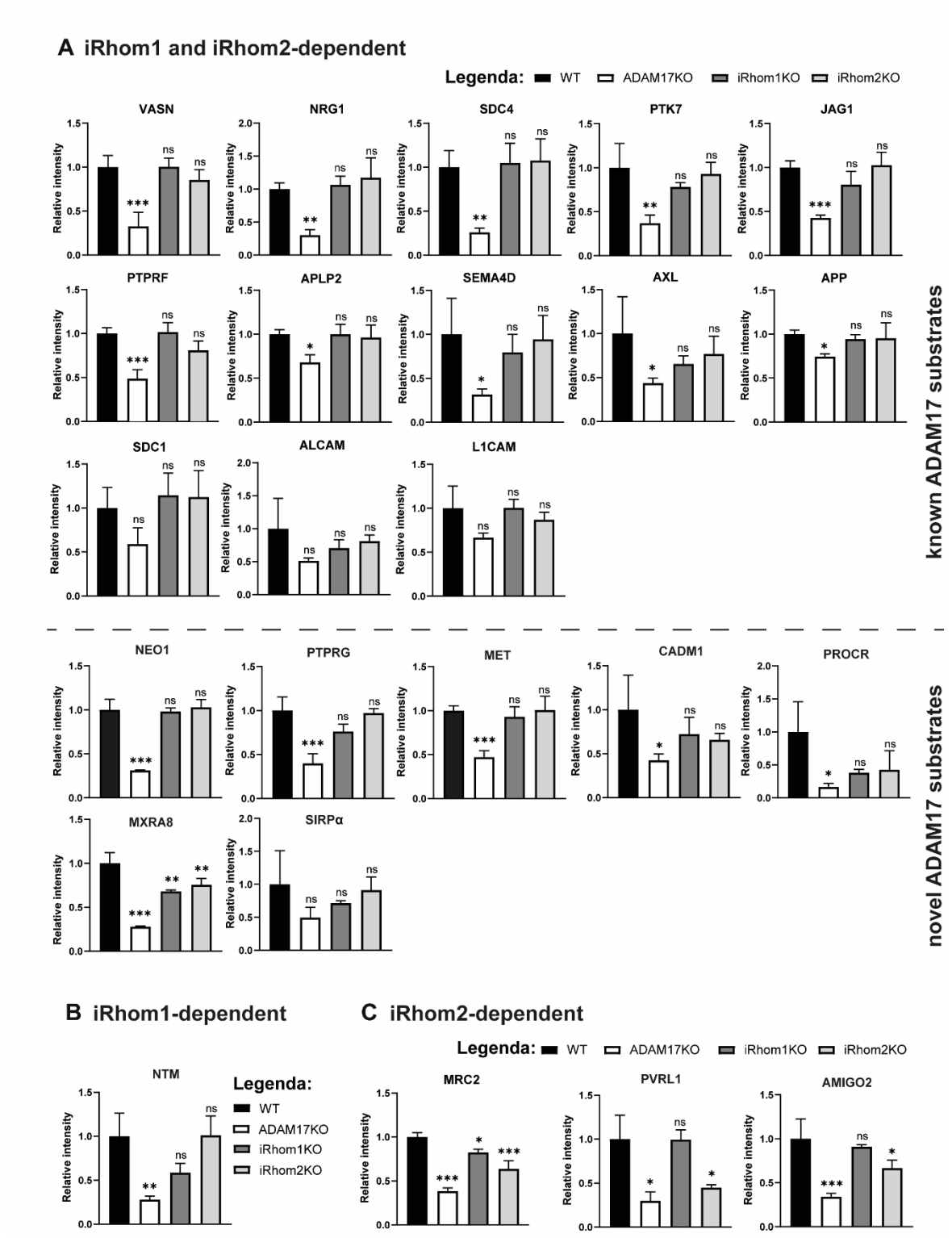

Figure 14: ADAM17 substrates protein intensities showed different shedding efficiency of the complex ADAM17/iRhom1 and ADAM17/iRhom2. A) Quantification of iRhom1/iRhom2-dependent ADAM17 substrates intensities detected in the secretome of stimulated WT, ADAM17KO, iR1KO, and iR2KO HTB94 cells. Additionally, ADAM17 substrates were divided into two groups, known ADAM17 substrates (above black dashed line) and novel ADAM17 substrates (below black dashed line). Statistical analysis was performed by using one-way Anova with Dunnett's multiple comparison tests (mean values ± standard deviation; ns not statistical, ***adjusted p-value<0.001, **adjusted p-value<0.01, *adjusted p-value<0.05; n=3). B) Quantification of iRhom1-dependent ADAM17 substrates intensities detected in the secretome of stimulated WT, ADAM17KO, iR1KO, and iR2KO HTB94 cells. Statistical analysis was performed by using one-way Anova with Dunnett's multiple comparison tests (mean values ± standard deviation; ns not statistical, **adjusted p-value<0.01; n=3). C) Quantification of iRhom2-dependent ADAM17 substrates intensities detected in the secretome of stimulated WT, ADAM17KO, iR1KO, and iR2KO HTB94 cells. Statistical analysis was performed by using one-way Anova with Dunnett's multiple comparison tests (mean values ± standard deviation; ns not statistical, ***adjusted p-value<0.001, *adjusted p-value<0.05; n=3).

Similar to the analysis performed in mEFs, I conducted hierarchical clustering to identify groups of ADAM17 substrates shed in the presence of either iRhom (Figure 14). This approach enables an unbiased classification of putative iRhom1-dependent, iRhom2-dependent, or iRhom1/2-independent ADAM17 substrates.

First, the analysis showed that the sheddomes of iRhom1KO and iRhom2KO cells clustered closely with that of WT cells, and separately from A17KO cells—indicating that loss of either iRhom alone does not fully abrogate ADAM17-mediated shedding.

Second, two major clusters of proteins were identified. The first included L1CAM, PTPRF, AMIGO2, MRC2, and PVRL1, whose ectodomain levels were elevated in WT and iR2KO cells compared to A17KO cells, but not similarly increased in iR1KO cells. This pattern aligns with the two-way ANOVA results and supports the classification of these proteins as putative iRhom2-dependent substrates.

The second cluster comprised the remaining 18 proteins, which—despite some variability—were shed at comparable levels in iRhom1KO, iRhom2KO, and WT cells relative to A17KO cells, suggesting that both iRhoms can support their shedding.

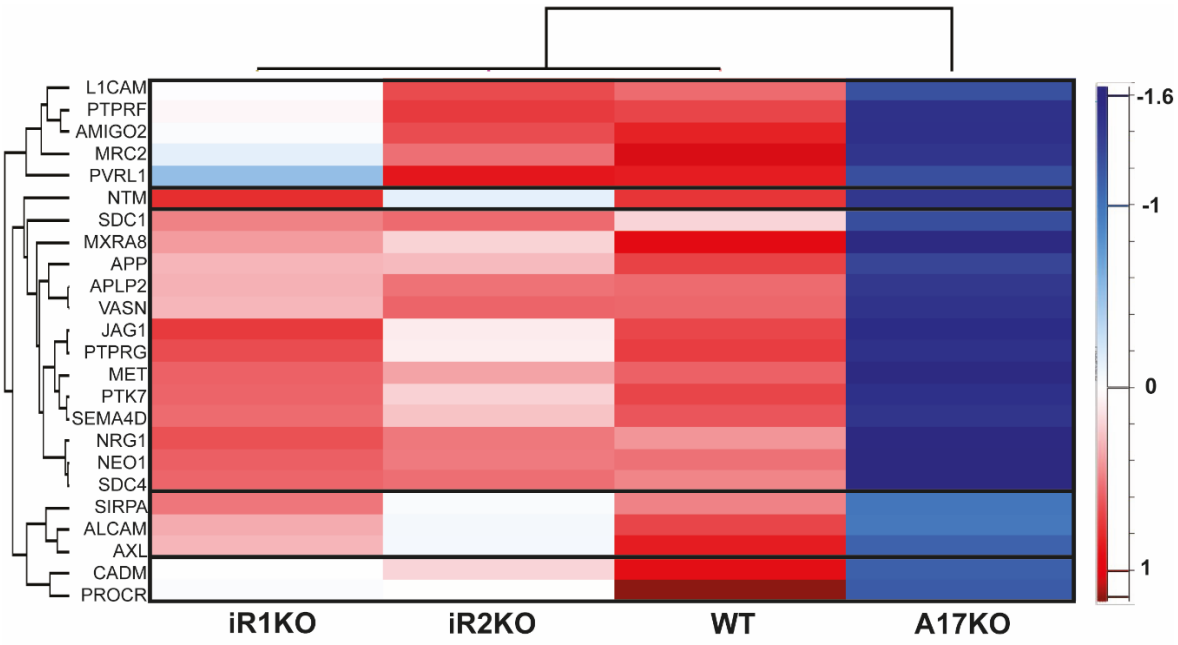

Figure 15: Clustering Analysis of ADAM17 substrates revealed a non-selective dependency on iRhom1 or iRhom2 in WT, iR1KO, iR2KO and A17KO HTB94. Clustered heatmap of PMA-induced secreted proteins in in WT, iR1KO, iR2KO and A17KO HTB94. The heatmap shows 24 proteins consistently detected across all three genotypes following 3h PMA stimulation. Rows represent individual proteins, and columns correspond to genotypes. Protein abundance was scaled (Z-score), and hierarchical clustering using Euclidean distance was applied to both proteins and samples. Color intensity reflects relative secretion levels, with red indicating higher and blue lower abundance.

Altogether, these data indicate that a clear-cut division of ADAM17 substrates into iRhom1-selective or iRhom2-selective groups does not emerge—at least under the experimental conditions used in this study. Therefore, I next explored whether certain substrates might be preferentially, rather than exclusively, shed by either iRhom. To this end, I directly compared the abundance of known and putative ADAM17 substrates in the secretomes of iR1KO and iR2KO cells, aiming to identify substrates more efficiently cleaved when ADAM17 is complexed with iRhom1 or iRhom2 (Figure 16).

Although proteomic analysis did not reveal discrete groups of iRhom1- or iRhom2-dependent substrates, it did highlight a continuum of substrate preference. Some substrates, such as NTM, were more efficiently shed in the presence of iRhom1, while others—including MRC2, AMIGO2, and PVRL1—were preferentially cleaved when ADAM17 was in complex with iRhom2.

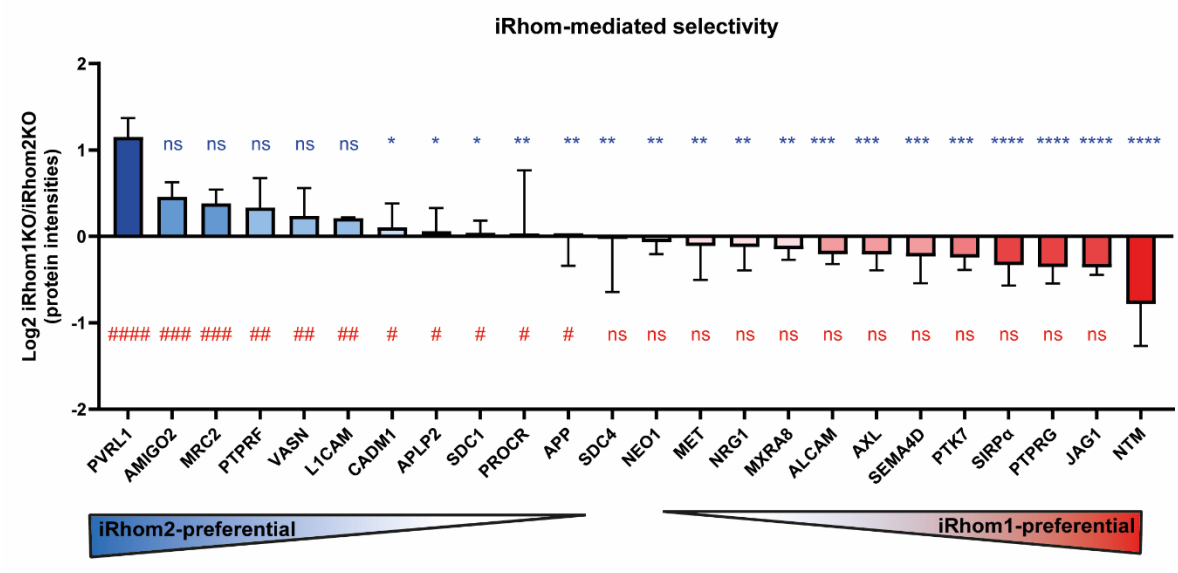

Figure 16: iRhom-mediated selectivity analysis showed a continuum between substrates preferentially shed in the presence of iRhom1 and substrates shed in the presence of iRhom2. Ratio of protein intensities across iRhom1KO and iRhom2KO in logarithmic scale (log2) among ADAM17 putative substrates (n=3). Statistical analysis was performed by using one-way Anova with Dunnett's multiple comparison tests (mean values ± standard deviation; ns not statistical, #### or ****adjusted p-value<0.0001; ### or ***adjusted p-value<0.001, ## or **adjusted p-value<0.01; # or *adjusted p-value<0.05; n=3).

Compared to the seminal study by Maretzky et al. [327], which identified distinct groups of ADAM17 substrates with clear iRhom selectivity, my findings differ significantly. A key distinction between the two studies lies in the duration of ADAM17 stimulation: while

Maretzky et al. used a 1 hour PMA stimulation, my experiments employed a longer stimulation period of 3 hours.

To determine whether prolonged PMA stimulation might introduce secondary effects unrelated to physiological ADAM17 activation—and thereby contribute to the discrepancies between our results—I repeated the secretome analysis using a shorter PMA stimulation time (1 hour instead of 3 hours) in WT, A17KO, iR1KO, and iR2KO HTB94 cells.

As expected, reducing the stimulation time resulted in the identification of fewer proteins in the conditioned media. Specifically, 1519 proteins were identified in PMA-stimulated and non-stimulated WT cells—6% fewer than in cells stimulated for 3 hours (Figure 13). Nevertheless, 1-hour stimulation was sufficient to observe ADAM17 activity in our system: the ectodomains of 18 putative ADAM17 substrates (transmembrane or GPI-anchored proteins) were significantly increased in PMA-stimulated WT cells compared to A17KO cells. These included SEMA7A, ALCAM, CSPG4, and others (Figure 17A, Table 6).

Consistently, in iR1KO and iR2KO HTB94 cells stimulated for 1 hour and compared to A17KO cells, most of these substrates were still efficiently shed, supporting the earlier conclusion that either iRhom can support the shedding of the majority of ADAM17 substrates.

To further explore whether deletion of either iRhom impairs shedding of specific substrate groups, I performed hierarchical clustering of the ADAM17 substrates identified following 1-hour PMA stimulation. This analysis revealed that WT cells clustered with iRhom2KO cells, which were themselves close to iRhom1KO cells, and all were distinct from A17KO cells (Figure 18).

Three main substrate clusters emerged from the analysis. The first cluster—including AGRN, CDH2, and CLSTN1—showed higher abundance in WT and iR2KO cells than in iR1KO and A17KO cells, suggesting these are preferentially shed via iRhom1. The second cluster included PRNP, APLP2, and others, whose levels were elevated in WT and iR1KO cells compared to iR2KO and A17KO cells, indicating preferential reliance on iRhom2. The third cluster comprised numerous substrates that were shed similarly in WT, iR1KO, and iR2KO cells compared to A17KO, implying that either iRhom is sufficient to support their shedding.

Interestingly, and in contrast to previous experiments, these data reveal three distinguishable groups of ADAM17 substrates with a degree of iRhom selectivity: iRhom1-dependent, iRhom2-dependent, and those equally supported by both iRhoms.

Table 6: List of ADAM17 substrates detected in WT, iR1KO, iR2KO HTB94 (1h PMA stimulation). In bold, putative novel substrates. The table contains a list of 18 single-pass transmembrane proteins that were significantly increased across WT, iR1KO, iR2KO HTB94 upon 1h PMA stimulation. Indicated are the protein IDs, names of the proteins, the gene names, the mean of the ratio between PMA-stimulated WT and ADAM17KO controls of 3 biological replicates, the p-value calculated with a two-sided, heteroscedastic t-test based on the intensity ratios for PMA-stimulated WT and ADAM17KO controls, and the reference, when available, to the protein validation as an ADAM17 substrate.

Protein ID	Protein name	Gene name	Ratio	Difference	*p*-value	-LOG(P-value)	Ref
P05067	Amyloid beta A4 protein	APP	2,82	1,680171	1,44E+05	3,278601	214,215
Q9UNN8	**Endothelial protein C receptor**	**PROCR**	16,18	4,022692	7,40E+05	3,863216	***Putative novel***
O94985	Calsyntenin-1	**CLSTN**	0,23	0,475665	4,99E+01	1,478594	***Putative novel***
O00468	Agrin	**AGRN**	0,13	0,358737	1,07E+03	2,008188	***Putative novel***
P26006	Integrin alpha-3	ITGA3	0,29	0,537726	3,70E+01	1,435027	***Putative novel***
Q9BZM5	**NKG2D ligand 2**	**ULBP2**	**2,34**	**1,530799**	**3,69E+03**	**2,273403**	***Putative novel***
O75326	**Semaphorin-7A**	**SEMA7A**	**12,04**	**3,469282**	**8,81E+06**	**4,949001**	***Putative novel***
Q13740	CD166 antigen	ALCAM	6,76	2,599937	1,25E+06	4,070285	205
P30530	Tyrosine-protein kinase receptor UFO	AXL	12,66	3,558235	2,35E+05	3,444789	204
P31431	Syndecan-4	SDC4	7,97	3,469282	2,56E+04	2,759127	235
P35052	Glypican-1	GPC1	12,87	3,587095	9,92E+03	2,509804	349
P04156	Major prion protein	PRNP	0,99	0,992805	2,85E+02	1,76001	230
P55287	**Cadherin-11**	**CDH11**	**1,13**	**1,065071**	**2,66E+04**	**2,770402**	***Putative novel***
Q6UVK1	**Chondroitin sulfate proteoglycan 4**	**CSPG4**	**2,27**	**1,508293**	**4,29E+06**	**4,604696**	***Putative novel***
P16070	CD44 antigen	CD44	0,34	0,582623	9,38E+03	2,49588	205
Q02297	Neuregulin-1	NRG1	16,11	4,014098	1,67E+05	3,329652	260
Q06481	Amyloid-like protein 2	APLP2	2,87	1,694599	9,13E+03	2,489058	209

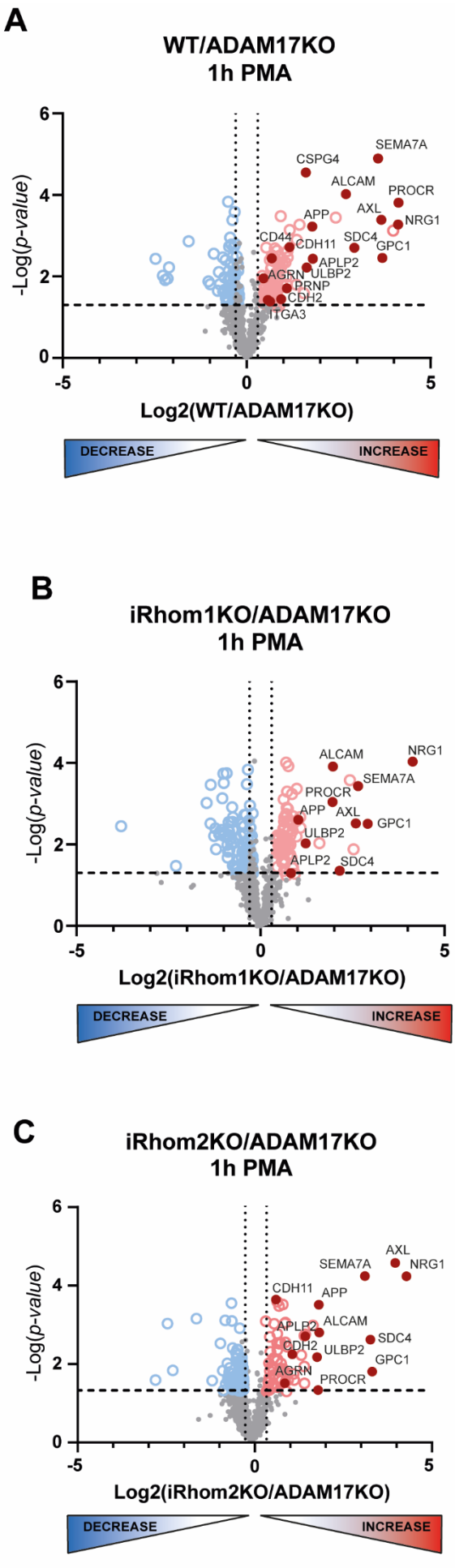

Figure 17: Unbiased high-resolution proteomics identified novel ADAM17 substrates in genetically ablated HTB94 and iRhom-dependency of their cleavage. A) Volcano plot showing the relative abundance in log2 of proteins detected in the secretome of WT versus ADAM17KO secretome of HTB94 stimulated for 3h with PMA (n=3). Proteins with a p-value below 0.05 (black dashed horizontal line) were highlighted as blue (log2 PMA/CTL < 0.30; black dotted vertical line) and red (log2 PMA/CTL > 0.30; black dotted vertical line) open circle dots. Transmembrane proteins increased in WT secretome were represented as red filled dots with their protein names. B) Volcano plot showing the relative abundance in log2 of proteins detected in the secretome of iRhom1KO versus ADAM17KO secretome of HTB94 (n=3). Proteins with a p-value below 0.05 (black dashed horizontal line) were highlighted as blue (log2 PMA/CTL < 0.30; black dotted vertical line) and red (log2 PMA/CTL > 0.30; black dotted vertical line) open circle dots. Transmembrane proteins increased in iRhom1KO secretome were represented as red filled dots with their protein names. C) Volcano plot showing the relative abundance in log2 of proteins detected in the secretome of iRhom2KO versus ADAM17KO secretome of HTB94 (n=3). Proteins with a p-value below 0.05 (black dashed horizontal line) were highlighted as blue (log2 PMA/CTL < 0.30; black dotted vertical line) and red (log2 PMA/CTL > 0.30; black dotted vertical line) open circle dots. Transmembrane proteins increased in iRhom2KO secretome were represented as red filled dots with their protein names.

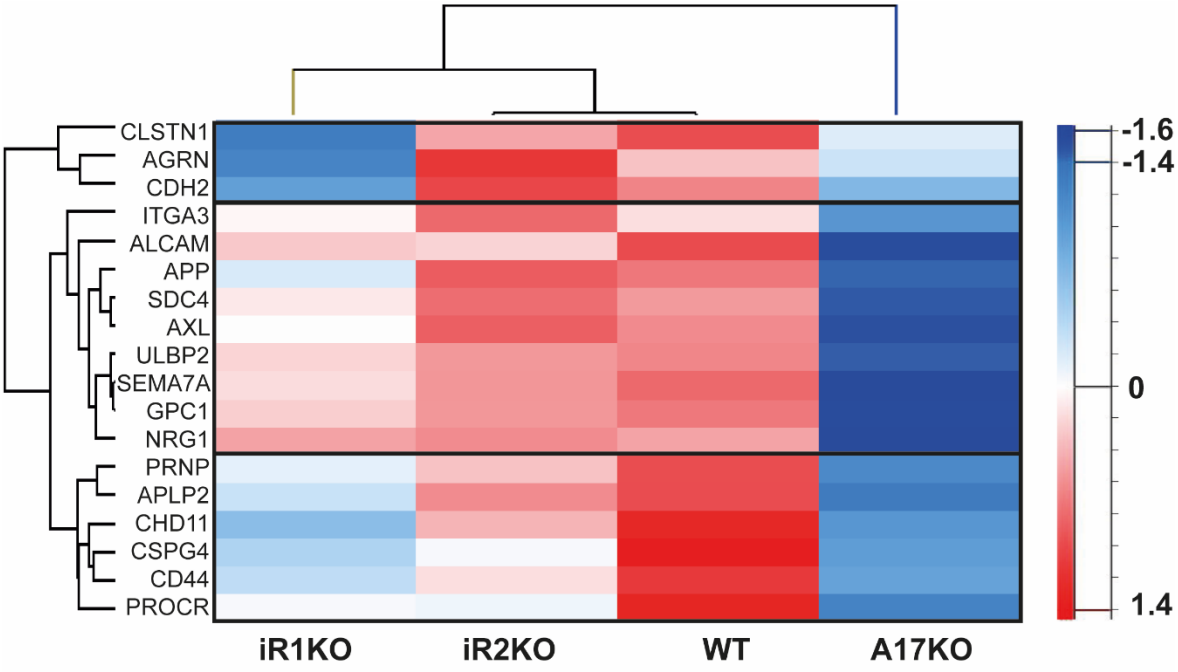

Figure 138: Clustering Analysis of ADAM17 substrates revealed a non-selective dependency on iRhom1 or iRhom2 in WT, iR1KO, iR2KO and A17KO HTB94. Clustered heatmap of PMA-induced secreted proteins in in WT, iR1KO, iR2KO and A17KO HTB94. The heatmap shows 18 proteins consistently detected across all three genotypes following 1h PMA stimulation. Rows represent individual proteins, and columns correspond to genotypes. Protein abundance was scaled (Z-score), and hierarchical clustering using Euclidean distance was applied to both proteins and samples. Color intensity reflects relative secretion levels, with red indicating higher and blue lower abundance.

3.5 Discussion

This study provides a comprehensive analysis of the substrate selectivity of ADAM17 in the context of its regulation by iRhom1 and iRhom2. By integrating mass spectrometry–based secretome profiling with functional validation in both mouse embryonic fibroblasts (mEFs) and human HTB94 fibroblast-like cells, I systematically evaluated how the presence or absence of each iRhom influences ADAM17-mediated shedding. Consistent with previous reports showing partial redundancy between iRhom1 and iRhom2 in promoting ADAM17 maturation and trafficking, my data demonstrated that the majority of ADAM17 substrates can be shed in the presence of either iRhom. This was clearly shown in both mEFs and HTB94 cells, where approximately two-thirds of identified ADAM17 substrates—including known ones such as PTK7, VASN, and APLP2, as well as novel candidates like MXRA8 and SIRPα—were shed efficiently when either iRhom1 or iRhom2 was present. While this supports a model of functional overlap, my data also uncovered cases of substrate preference, albeit not strict selectivity. In particular, APP and NTM exhibited higher dependency on iRhom1 for their release, while MRC2, AMIGO2, and PVRL1 were preferentially shed in an iRhom2-dependent manner. However, these differences appear quantitative rather than absolute, suggesting a continuum of iRhom-mediated regulation rather than distinct, non-overlapping substrate pools.

Importantly, I addressed potential concerns that prolonged PMA stimulation may introduce secondary effects unrelated to physiological ADAM17 activation, potentially explaining discrepancies between my results and those reported by Maretzky et al., which used a 1-hour stimulation protocol [327]. It is well established that most ADAM17-mediated shedding occurs rapidly—within the first 20 to 30 minutes—due to cleavage of a readily available pool of pre-existing membrane-bound substrates. Beyond this window, shedding increasingly reflects the turnover and availability of newly synthesized proteins, the levels of which depend on ongoing biosynthesis, trafficking, and post-translational regulation [202]. Therefore, extended stimulation times risk capturing a mixture of primary and secondary effects, including transcriptional upregulation or compensatory changes in substrate presentation.

To distinguish these contributions and assess the reproducibility of substrate preferences under more acute activation conditions, I performed an additional secretome analysis using a shorter PMA stimulation of 1 hour in WT, A17KO, iR1KO, and iR2KO HTB94 cells. As anticipated, fewer proteins were identified compared to the 3-hour dataset—likely due to reduced cumulative shedding—but 18 transmembrane or GPI-anchored proteins were still

significantly enriched in WT versus A17KO cells, confirming robust ADAM17 activity even at this earlier time point. Hierarchical clustering of these ADAM17 substrates recapitulated trends observed in the 3-hour data, including the emergence of three substrate groups: those preferentially shed via iRhom1 (e.g., AGRN, CDH2), iRhom2 (e.g., PRNP, APLP2), and a numerous one in which substrates were equally supported by both iRhoms.

Previous studies demonstrated that certain ADAM17 substrates, such as EGFR ligands, are more tightly regulated in an iRhom-selective manner. In particular, differential iRhom dependence has been reported for ligands like TGFα and amphiregulin (iR1/iR2-dependent), HB-EGF and epiregulin (iR2-dependent) [327]. Notably, work by Zhao et al. demonstrated that substrate selectivity can also depend on the structural accessibility of the cleavage site, which is influenced by how iRhoms present the substrate to ADAM17. Their findings showed that modifying the transmembrane or juxtamembrane regions of substrates altered their susceptibility to cleavage, suggesting a spatial component to iRhom-mediated regulation [348]. In my study, however, I did not observe significant iRhom-selective differences in EGFR ligand shedding (this is the case of the iRhom-rescue experiment on mEFs. This may indicate that EGFR ligands represent a more specialized subset of ADAM17 substrates where regulatory mechanisms are more stringent, possibly reflecting their potent biological roles in development and disease.

Together, these findings support a model in which activated ADAM17 cleaves a broad yet selectively regulated set of substrates depending on its association with iRhom1 or iRhom2. Rather than enforcing a rigid division of labor, iRhoms appear to act as modulators of substrate accessibility and cleavage efficiency within a shared pool of potential targets. This nuanced view of iRhom function has important implications for therapeutic strategies aiming to fine-tune ADAM17 activity. In particular, selective modulation of iRhom1 or iRhom2—rather than global inhibition of ADAM17—could offer a way to attenuate pathogenic shedding events (e.g., in inflammation or cancer) while preserving beneficial proteolytic functions in the nervous system or epithelial barriers. The ability to discriminate between iRhom-dependent pathways thus opens a path toward more targeted interventions with fewer off-target consequences.

Chapter Four:
Validation of ADAM17 substrates revealed a novel mechanism for iRhom2 in regulating trafficking of MHC-I

4.1 Introduction

ADAM17 is a membrane-anchored metalloprotease that mediates the proteolytic release—or ectodomain shedding—of a wide array of transmembrane proteins, including pro-inflammatory cytokines (e.g., TNFα), receptors, and growth factor precursors. The maturation, trafficking, and activity of ADAM17 are tightly regulated by its obligate co-factors iRhom1 and iRhom2, two catalytically inactive rhomboid proteins that form a complex with ADAM17 and govern its ER exit and cell surface localization. While iRhom1 and iRhom2 are partially redundant in their ability to support ADAM17 maturation, they can also differentially affect the shedding of specific substrates, particularly under stimulated conditions [288,337,338]. Recent studies have started to reveal how the individual iRhoms shape the substrate repertoire of ADAM17, but a comprehensive, experimentally validated map of this regulation has remained limited.

In this context, I performed a series of Western blot–based validation experiments to confirm the identity and regulation of ADAM17 substrates identified through secretome proteomics in both mouse embryonic fibroblasts (mEFs) and human HTB94 fibroblast-like cells. These experiments were conducted under the same stimulation and genetic conditions used for mass spectrometry—namely PMA treatment and targeted ablation of ADAM17, iRhom1, or iRhom2—allowing a direct comparison between proteomic data and biochemical detection of shedding events. Western blotting was used to monitor the release of ectodomains into the culture medium and to evaluate how substrate cleavage depends on ADAM17 activity and the presence of individual iRhoms.

To address limitations related to low endogenous expression or insufficient antibody sensitivity, I additionally employed a substrate overexpression strategy. Full-length constructs of selected single-pass transmembrane proteins were transiently expressed in the same cell lines, and their cleavage was evaluated by detecting soluble fragments in the conditioned media. This complementary approach allowed for more robust validation across genotypes and enhanced sensitivity in detecting quantitative differences in substrate processing.

Among the validated proteins, I identified a novel regulatory connection between iRhom2 and major histocompatibility complex class I (MHC-I) molecules. Prior work from Scilabra's lab had suggested that MHC-I can be cleaved by ADAM17 [253]. I observed a reduction MHC-I levels in the conditioned media of ADAM17-deficient cells. Intriguingly, I also found that iRhom2 plays a role in regulating MHC-I abundance at the cell surface, independent of its effect on ADAM17 maturation. Loss of iRhom2 led to a reduction in both soluble and membrane-associated MHC-I molecules, suggesting that iRhom2 contributes to

MHC-I turnover or trafficking in addition to supporting its shedding. This dual regulation may reflect a broader role for iRhom2 in shaping immune surveillance by controlling antigen presentation pathways—especially in cells of myeloid origin where iRhom2 expression is predominant and where ADAM17 activity is tightly linked to immune function [289].

Together, these validation studies confirm the functional relevance of newly identified ADAM17 substrates and provide new insight into iRhom2-mediated regulation of membrane protein dynamics. In particular, the discovery that iRhom2 influences MHC-I processing highlights a previously underappreciated role for this protein in modulating immune-related functions, expanding its significance beyond classical substrate shedding.

4.2 Validation of ADAM17-mediated shedding supported by either iRhom in mEFs

Thus far, iRhom-mediated selectivity of ADAM17 cleavage has been assessed for 9 substrates. All of them can be effectively cleaved by stimulated ADAM17 when in a complex with iRhom2, while the cleavage of only 3 substrates (TGFα, ICAM, L-selectin) can be stimulated by PMA when iRhom2 is ablated, and the protease is in complex with iRhom1 [327,348]. Interestingly, my mass spectrometry-based analysis identified 10 additional substrates that were shed by activated ADAM17 when in a complex with either iRhom1 or iRhom2. To validate these results, I analysed the contribution of iRhom1 and iRhom2 to PMA-stimulated shedding of PTK7 and APP by Western blotting as an orthogonal method. PTK7 and APP are two known ADAM17 substrates [339], which increased in the conditioned media of WT MEFs with the highest statistical significance upon PMA stimulation (Figure 7, Table 3). Western blotting showed that levels of shed PTK7 and APP highly increased in the conditioned media (CM) of WT MEFs upon PMA stimulation (with a PMA-stimulated/control ratio of about 2 and 3, respectively), in agreement with the proteomic results (Figure 19A, 19B). Cellular PTK7 decreased upon PMA stimulation and in line with its shedding from the cell membrane, while APP levels in the cell lysate did not change. In contrast, PMA stimulation of iR1/2 dKO mEFs did not lead to a similar increase of PTK7 and APP in the extracellular levels, indicating that these two proteins are indeed shed by ADAM17 in response to PMA (Figure 19C, 19D). PMA-stimulation increased their levels in the conditioned media of either iRhom1KO or iRhom2KO mEFs, indicating that either iRhom could support their ADAM17-dependent shedding (Figure 19E-19H).

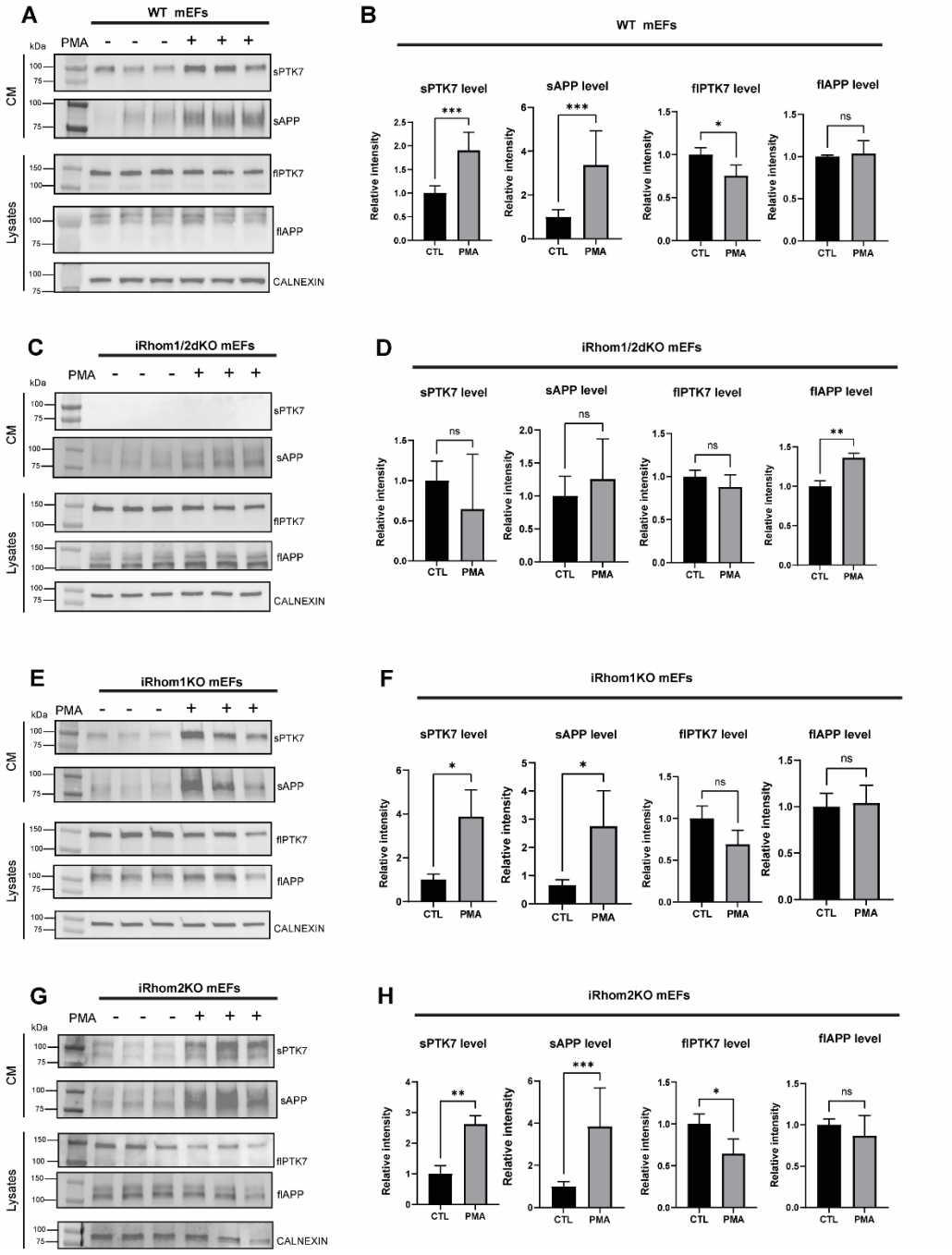

Figure 19: ADAM17 shedding of Ptk7 and APP were supported by either iRhom by validation with western blotting. A) Western blots on WT mEFs treated with or without 25 ng/mL PMA for 3h showing the abundance of soluble Ptk7 (sPtk7) and APP (sAPP) in TCA precipitated conditioned media (CM) and the abundance of full-length Ptk7 (flPtk7) and APP (flAPP) in cell lysates (Lysates). Calnexin was used as loading control. B) Densitometric quantification of levels of sPtk7 and sAPP in CM and flPtk7 and flAPP in Lysates of WT mEFs (mean values ± standard deviation; ns not statistical, * $p<0.05$, *** $p<0.001$; $n>3$). C) Western blots on iRhom1/2dKO mEFs treated with or without 25 ng/mL PMA showing the abundance of soluble Ptk7 (sPtk7) and APP (sAPP) in TCA precipitated conditioned media (CM) and the abundance of full-length Ptk7 (flPtk7) and APP (flAPP) in cell lysates (Lysates). Calnexin was used as loading control. D) Densitometric quantification of levels of sPtk7 and sAPP in CM and flPtk7 and flAPP in Lysates of iRhom1/2dKO mEFs (mean values ± standard deviation; ns not statistical, * $p<0.05$; $n>3$). E) Western blots on iRhom1KO mEFs treated with or without 25 ng/mL PMA showing the abundance of soluble Ptk7 (sPtk7) and APP (sAPP) in TCA precipitated conditioned media (CM) and the abundance of full-length Ptk7 (flPtk7) and APP (flAPP) in cell lysates (Lysates). Calnexin was used as loading control. F) Densitometric quantification of levels of sPtk7 and sAPP in CM and flPtk7 and flAPP in Lysates of iRhom1KO mEFs (mean values ± standard deviation; ns not statistical, ** $p<0.01$, *** $p<0.001$; $n>3$). G) Western blots on iRhom2KO mEFs treated with or without 25 ng/mL PMA showing the abundance of soluble Ptk7 (sPtk7) and APP (sAPP) in TCA precipitated conditioned media (CM) and the abundance of full-length Ptk7 (flPtk7) and APP (flAPP) in cell lysates (Lysates). Calnexin was used as loading control. H) Densitometric quantification of levels of sPtk7 and sAPP in CM and flPtk7 and flAPP in Lysates of iRhom2KO mEFs (mean values ± standard deviation; ns not statistical, * $p<0.05$, ** $p<0.01$, *** $p<0.001$; $n>3$).

4.3 Ectopically expressed proteins are degraded in MEFs lacking iRhom2

Proteomics identified a number of transmembrane proteins whose shedding was increased upon PMA stimulation and therefore potentially novel ADAM17 substrates. Some of these proteins increased in the conditioned media of all three mEFs lines, including MXRA8, which is a type 1 transmembrane protein that has been recently identified as the entry receptor for multiple arthritogenic alphaviruses [350,351]. In order to validate its ADAM17-mediated shedding and further investigate how iRhoms control the process, I planned to exogenously express FLAG-tagged MXRA8 in WT, iR1KO, iR2KO and iR1/2 dKO mEFs. However, I noticed that cellular levels of MXRA8 greatly differed across the different cell lines. MXRA8 was evident in the lysate of WT MEFs, and increased 2-fold in response to 3h of PMA. Such an increase was not dependent on ADAM17 activity since addition of marimastat to the cell culture did not suppress it (Figure 20A and 20B). Similar to WT MEFs, MXRA8 was detected in iR1KO cell lysates and its levels increased in response to PMA. Intriguingly, when transfected in iR2KO or iR1/2 dKO mEFs, MXRA8 was almost negligible (Figure 20A and 20B). In order to clarify whether this mechanism was specific for MXRA8, I transfected the different mEF lines with H2-D1, a murine haplotype of major histocompatibility class I molecules that I have recently identified as an ADAM17 substrate (Calligaris et al. in press), and analysed its levels by Western. H2-D1 band pattern resembled MXRA8 in that the protein was detected in transfected WT and iR1KO mEFs, and its levels increased upon PMA stimulation in these cell lines (Figure 6A and 6C). Yet, cellular H2-D1 was not detected when expressed in iR2KO or iR1/2dKO MEFs. A similar expression pattern was found when mEFs were transfected with SIRPα (a protein that is cleaved by ADAMs [352–354]) and SEZ6 (a BACE1 substrate that is unrelated to ADAM17 [75]) (Figure 20A and 20D-E). Since the plasmid pcDNA3.1 was used to express all these proteins, I additionally transfected the different mEF lines with a construct containing APP cloned into a different expression vector, the pEAK20 [331]. In line with the other overexpressed proteins, APP was clearly detected in the lysate of WT and iR1KO MEFs, where PMA stimulation led to an increment of the protein, and not evident in the lysate of iR2 and iR1/2dKO MEFs (Figure 20A – 20F).

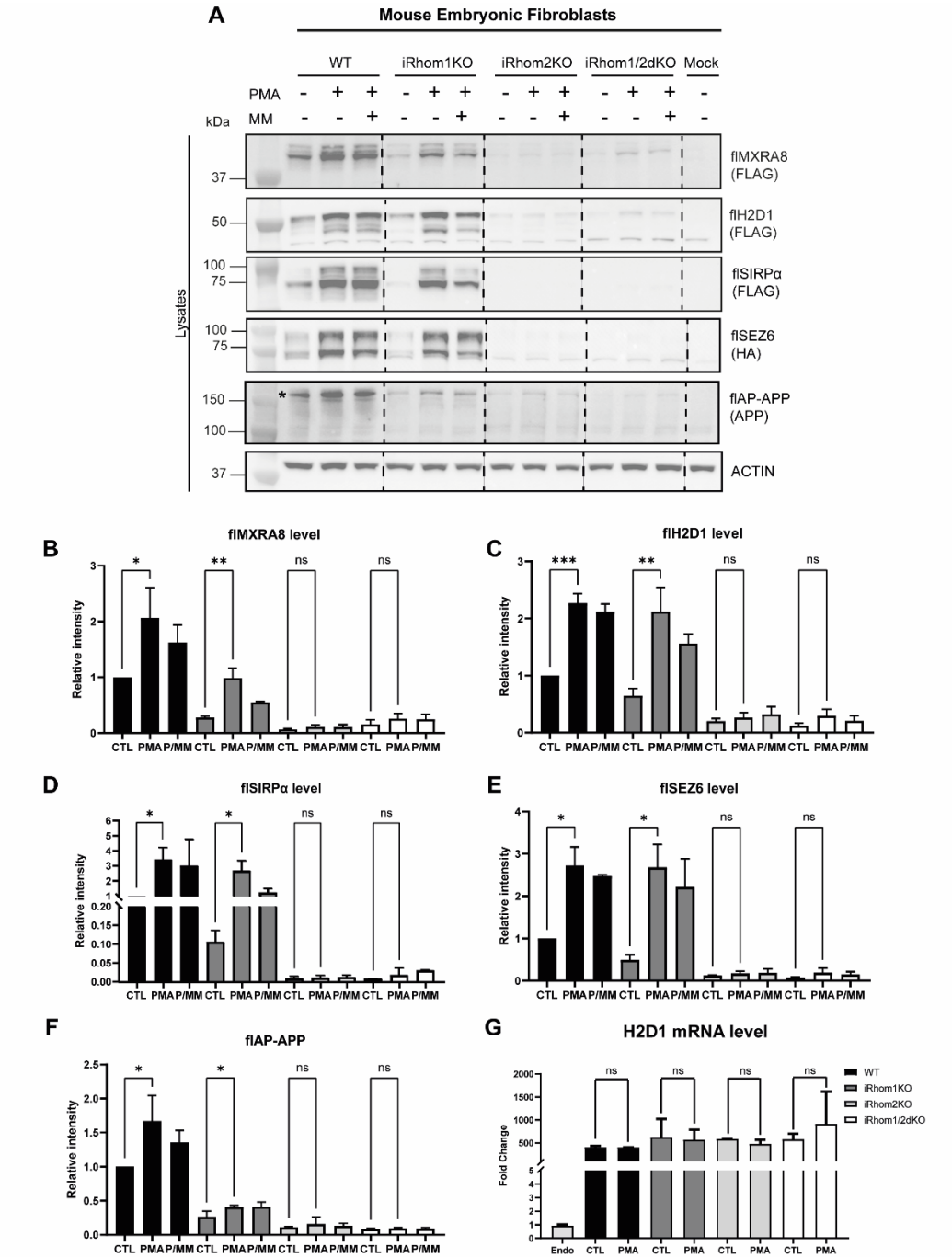

Figure 20: Levels of exogenously expressed proteins decreased in absence of iRhom2. A) Western blots showing Mxra8 FLAG-tagged (flMxra8), H2-D1 FLAG-tagged (flH2D1), Seizure 6 (SEZ6) HA-tagged (fl-SEZ6), Sirpα FLAG-tagged (flSirpα), AP-APP HA-tagged (flAP-APP) protein abundances in cell lysates (Lysates) of WT, iRhom1KO, iRhom2KO, iRhom1/2dKO mEFs treated with PMA and/or MM. Actin was used as a loading control (n>3). B) Densitometric quantification of cell lysates level of full-length Mxra8 (flMxra8) (mean values ± standard deviation; ns not statistical, *p-value<0.05, **p-value<0.01; n=3) C) Densitometric quantification of cell lysates level of full-length H2D1 (flH2D1) (mean values ± standard deviation; *p-value<0.05, **p-value<0.01; n>3). D) Densitometric quantification of cell lysates level of full-length Sirpα (flSirpα) (mean values ± standard deviation; *p-value<0.05; n=3). E) Densitometric quantification of cell lysates level of full-length SEZ6 (flSEZ6) (mean values ± standard deviation; *p-value<0.05; n=2). F) Densitometric quantification of cell lysates level of full-length AP-APP (flAP-APP) (mean values ± standard deviation; *p-value<0.05; n=3). G) Gene expression of H2-D1 by RT-qPCR in WT, iRhom1KO, iRhom2KO, iRhom1/2dKO mEFs treated with or without PMA. Transcript levels were analysed using the $2^{-\Delta\Delta Ct}$ method with GAPDH as reference and H2-D1 as target gene. Data represent mean values ± standard deviation from 2 separate experiments.

Next, to address whether the ablation of iRhom2 could impair efficient transfection and expression of ectopic proteins, I used an established protocol for quantitative PCR to measure the expression of H2-D1 in transfected mEFs. This analysis displayed that, despite the evident difference in protein levels, expression of H2-D1 across WT, iR1KO, iR2KO and iR1/2dKO MEFs was comparable, and PMA did not alter its expression (Figure 20G).

To investigate potential post-transcriptional regulation, I analyzed the effect of the proteasome inhibitor MG132 on H2-D1 protein stability. I found that the proteasome inhibitor MG132 increased flH2-D1 levels in WT MEFs, mirroring the effect of PMA stimulation (Figure 21A and 21B). MG132 also led to an increase in flH2-D1 in iR2KO cells, suggesting that proteasomal degradation contributes to H2-D1 turnover independently of iRhom2. However, the lower basal levels of flH2-D1 in iR2KO cells—despite similar transcript levels—raise the possibility that iRhom2 may modulate protein stability or trafficking in a way that is not fully captured by MG132 treatment alone. Although the increases observed with PMA were not statistically significant in either genotype, the trend suggests a potential role for iRhom2 in stabilizing flH2-D1, particularly under stimulated conditions. In contrast, treatment with the lysosome inhibitor chloroquine did not significantly alter flH2-D1 levels in either WT or iR2KO MEFs (Figure 21C and 21D), supporting the idea that lysosomal degradation is not a major contributor to H2-D1 turnover in this context.

In summary, while the proteasome clearly plays a role in regulating ectopic H2-D1 levels, the contribution of iRhom2 remains suggestive but not definitive in the current dataset. These preliminary findings support a model in which iRhom2 may influence protein stability—possibly by affecting accessibility to the proteasome or modulating post-translational processing—and warrant further investigation with more targeted approaches (e.g. pulse-and-chase with cycloheximide) to clarify its precise role.

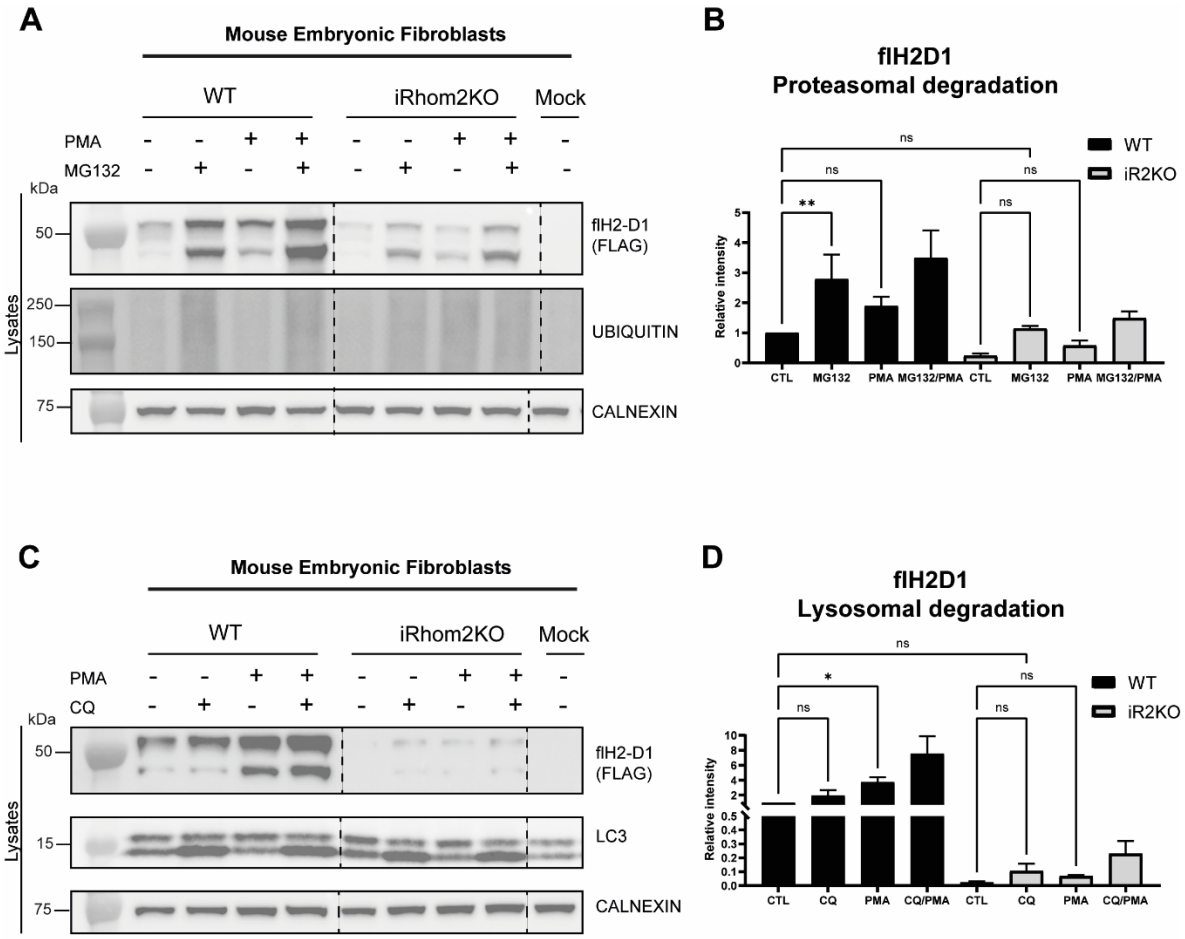

Figure 21: iRhom2 stabilized protein expression impairing proteasomal degradation. A) Immunoblots on WT and iRhom2KO mEFs pre-treated 1h with 10 μM MG132 and 3h with or without 25 ng/mL PMA showing full-length levels of H2D1 in cell lysates (Lysates). Ubiquitin was used as a control for treatment and calnexin was used as a loading control. B) Densitometric quantification of full-length levels of H2D1 (flH2D1) exogenously expressed in WT and iRhom2KO mEFs treated with the proteasomal inhibitor MG132 (mean values ± standard deviation; ns not statistical, *p-value<0.05; n=3). C) Immunoblots on WT and iRhom2KO mEFs pre-treated 1h with 100 μM chloroquine (CQ) and 3h with or without 25 ng/mL PMA showing full-length levels of H2D1 in cell lysates (Lysates). LC3 lipidation was used as a control for treatment and calnexin was used as a loading control. D) Densitometric quantification of full-length levels of H2D1 (flH2D1) exogenously expressed in WT and iRhom2KO mEFs treated with the lysosomal inhibitor chloroquine (CQ) (mean values ± standard deviation; ns not statistical, *p-value<0.05; n=3).

4.4 Validation of ADAM17-mediated shedding supported by either iRhom in HTB94

Next, I validated the results of the mass spectrometry-based analysis that identified a number of novel putative substrates of ADAM17 in murine and human fibroblasts, and provided information about the contribution of either iRhom1 and iRhom2 to their ADAM17-mediated shedding. I started with the validation of two novel substrates: MXRA8 and SIRPα. WT, A17KO, iR1KO and iR2KO HTB94 cells were transiently transfected with constructs containing N-terminally FLAG-tagged MXRA8 or SIRPα, and stimulated with PMA, with or without the ADAM inhibitor marimastat. Then, levels of shed proteins in

conditioned media and lysates were analysed by Western blotting. I found an increase of shed MXRA8 in the conditioned media of PMA-stimulated WT HTB94 cells, which was reverted by marimastat (Figure 22A, 22B). Such an increase of shed MXRA8 upon PMA stimulation was not evident in A17KO cells, indicating that MXRA8 is indeed an ADAM17 substrate. Loss of iRhom1 did not affect shedding of MXRA8, as its levels in the conditioned media of iR1KO cells augmented in response to PMA. Similarly, PMA stimulated MXRA8 shedding also in the absence of iRhom2, although to a lesser extent as in WT or iR1KO cells (Figure 22A, 22B). Similar to what I noticed in mEFs, cellular levels of MXRA8 levels increased upon PMA stimulation, but its expression was homogenous across the different HTB94 cell lines (Figure 22A, 22B). Akin to MXRA8, extracellular SIRPα was more abundant upon PMA stimulation in WT cells, and marimastat reduced it to the levels of unstimulated WT cells and A17KO cells (Figure 22C, 22D). Upon PMA stimulation, levels of SIRPα in the conditioned media increased 4-fold in both iR1KO cells and about 6-fold in iR2KO cells, indicating that both iRhoms could support its shedding. In line with proteomics, shedding of SIRPα was slightly more favourable in iR2KO cells than in iR1KO cells. As a control, I also analysed shedding of a known ADAM17 substrate, VASN. Shed levels of VASN in the conditioned media increased in PMA-stimulated WT, iR1KO and iR2KO cells, but not in A17KO cells, compared to unstimulated controls, and Marimastat inhibited its shedding (Figure 22E, 22F). Nevertheless, I still observed a modest PMA-induced increase of VASN in the CM of A17 KO cells. A plausible explanation is that PMA also enhances exosome-mediated secretion of VASN, a route independent of A17-dependent ectodomain shedding. Indeed, VASN is known to be packaged into exosomes and released [355]. PMA, via PKC activation, can increase exosome release in various cell types [356]. Thus, even in A17KO cells, PMA could enhance exosomal VASN export, yielding the observed SN increase. In contrast with SIRPα, levels of shed VASN were slightly higher in iR1KO cells than in iR2KO cells, again in line with proteomics results.

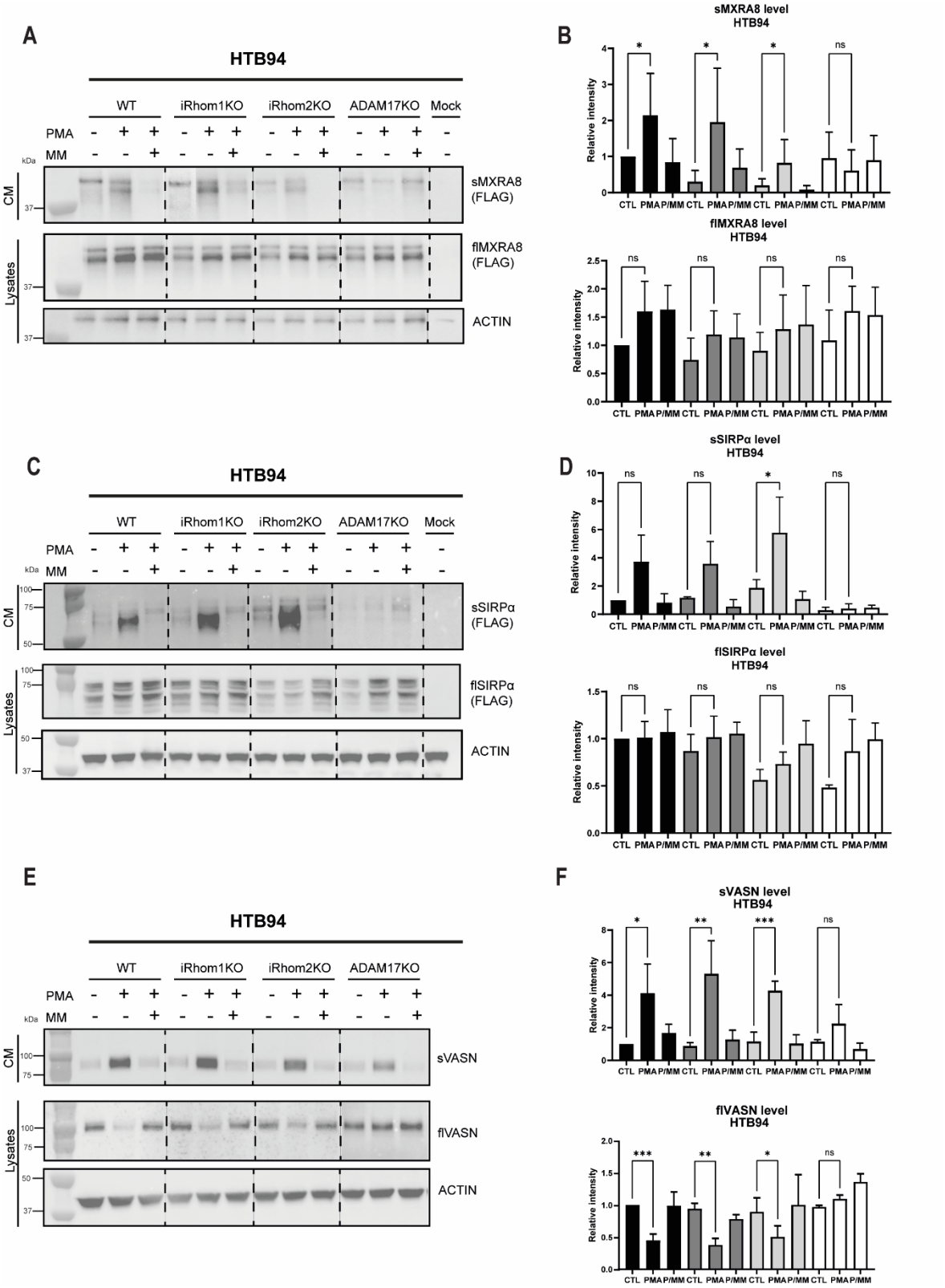

Figure 22: ADAM17 shedding of MXRA8 and SIRPα and VASN were supported by either iRhom by validation with western blotting. A) Western blotting validation on WT, iRhom1KO, iRhom2KO and ADAM17KO HTB94 treated with or without 25 ng/mL PMA and/or 10 µM marimastat (MM) of overexpressing Mxra8-FLAG on TCA precipitated conditioned media (CM) and cell lysates (Lysates). Actin was used as a loading control. B) Densitometric quantification of soluble levels of MXRA8 (sMXRA8) and cell lysates levels of full-length Mxra8 (flMXRA8) on WT, iR1KO, iR2KO and ADAM17KO HTB94 lines treated with or without 25 ng/mL PMA and/or 10 µM marimastat (MM) (mean values ± standard deviation; ns not statistical, *p-value<0.05; n=7). C) Western blotting validation on WT, iRhom1KO, iRhom2KO and ADAM17KO HTB94 treated with or without 25 ng/mL PMA and/or 10 µM marimastat (MM) of overexpressing SIRPα-FLAG on TCA precipitated conditioned media (CM) and cell lysates (Lysates). Actin was used as a loading control. D) Densitometric quantification of soluble levels of SIRPα (sSIRPA) and cell lysates levels of full-length SIRPα (flSIRPA)

on WT, iR1KO, iR2KO and ADAM17KO HTB94 lines treated with or without 25 ng/mL PMA and/or 10 μM marimastat (MM) (mean values ± standard deviation; ns not statistical, *p-value<0.05; ***p-value<0.001; n=5). E) Western blotting validation on WT, iRhom1KO, iRhom2KO and ADAM17KO HTB94 treated with or without 25 ng/mL PMA and/or 10 μM marimastat (MM) of Vasorin (VASN) on TCA precipitated conditioned media (CM) and cell lysates (Lysates). Actin was used as a loading control. F) Densitometric quantification of soluble levels of VASN (sVASN) and cell lysates levels of full-length VASN (flVASN) on WT, iR1KO, iR2KO and ADAM17KO HTB94 lines treated with or without 25 ng/mL PMA and/or 10 μM marimastat (MM) (mean values ± standard deviation; ns not statistical, *p-value<0.05; n=5).

4.5 iRhom2 regulates cell surface expression and shedding of MHC-I molecules

MHC-I molecules are ubiquitously expressed, not only in immune cells, and therefore they are expressed in tissues where both iRhom1 and iRhom2 are present. It was reported that, other than supporting ADAM17 maturation, iRhoms can control its substrate selectivity [327,348].

From my proteomic analysis explained in the previous chapter and from a secretome analysis on bone marrow-derived macrophages carried out in Scilabra group [253], MHC-I appeared to be shed by ADAM17, and whose shedding was only supported by iRhom2.

To test this hypotesis or whether there was some redundancy with iRhom1, I assessed both expression and cell surface levels of endogenous H2-D1 in mEFs. I found that cell surface levels of H2-D1 in iR2KO and A17KO cells were lower than WT, despite its higher expression (Figure 23A). H2-D1 levels on the surface of iR1/2 dKO cells were comparable with WT.

When treated with marimastat, PMA-stimulated WT MEFs showed higher H2-D1 cell surface levels than controls (Figure 23B and 23C). Given their different genetical background, I tested other cell lines to validate my findings on mEFs. Loss of iRhom2 also had similar effects on the human counterpart of MHC-I, leading to decreased cell surface levels of HLA in human macrophage-like THP-1 cells (Figure 23D and 23E). Altogether, these results suggested that, in addition to support its ADAM17-mediated shedding, iRhom2 could regulate cell surface levels of MHC-I, in mouse and human, by a different mechanism. Given the heterogeneity of mEFs lines, I further confirm this hypothesis by using HTB94 genetically ablated for ADAM17 and iRhom2 in a human fibroblast-like cell line (HTB94). PMA stimulation increased levels of HLA in the conditioned media of WT HTB94 cells, while metalloproteinase inhibition by marimastat reduced them (Figure 23F and 23G), in line with levels of vasorin, a known ADAM17 substrate [243]. Loss of ADAM17 or iRhom2 clearly diminished extracellular levels of HLA in PMA-stimulated HTB94 cells compared to the WT controls. Then, I evaluated levels full length HLA in cell lysates by Western blot and on the cell membrane by flow cytometry. PMA stimulation, which increased HLA levels

in the conditioned media, had negligible effects on its cell lysate or surface levels (Figure 23F-23I). Conversely, metalloprotease inhibition did not change its levels in the lysate, but it slightly increased its cell surface levels, in line with metalloproteinase inhibition in murine fibroblasts (Figure 20I).

Loss of iRhom2 reduced surface levels of HLA in HTB94 cells, in spite of a mild overall increase in their cellular levels (Figure 23F-23I). ADAM17 ablation led to indistinguishable results from iR2KO HTB94 cells on HLA shedding and membrane expression. Indeed, ADAM17 is known to stabilize iRhom2, preventing it from degradation [179].

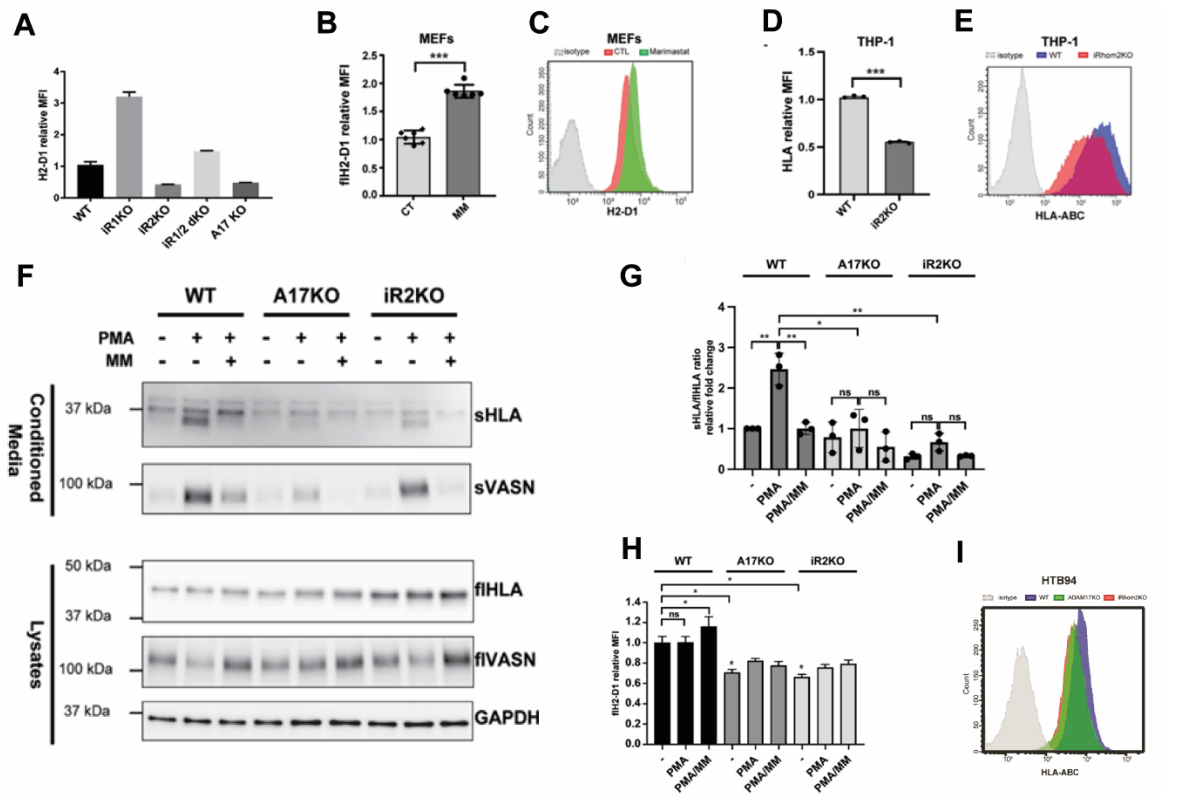

Figure 23: iRhom2 regulates membrane levels of MHC-I. A) Cell membrane levels of H2-D1 were measured by flow cytometry (n = 3). B) C) Flow cytometry analysis shows that levels of H2-D1 on the cell surface of PMA-stimulated WT MEFs increased in the presence of 10 µm marimastat (MM) (***p < 0.005, Student t-test; flow cytometry histograms of one representative experiment are shown in (C). D) E) Flow cytometry analysis shows that levels of HLA in iR2KO THP-1 cells were reduced compared to WT (***p < 0.005, Student t-test; flow cytometry histograms of one representative experiment are shown in (E). F) Immunoblots show that levels of shed HLA (sHLA) increased in the conditioned media of PMA stimulated WT HTB94 cells compared to untreated controls. Addition of marimastat (MM) to PMA-stimulated cells reduced extra cellular sHLA levels to those of unstimulated controls. sHLA in the conditioned media of stimulated A17KO or iR2KO cells was reduced compared to stimulated WT controls. Levels of full-length HLA (flHLA) in the lysate of A17KO cells and iR2KO slightly increased compared to WT cells. The ADAM17 substrate vasorin (VASN), is used as a control protein that is known to be shed in an ADAM17 dependent manner in PMA stimulated cells, and GAPDH is used as a protein loading control). G) Bands of sHLA in the conditioned media were quantified and normalized to the corresponding flHLA bands in the lysates. Results from three independent experiments were dis played as the mean of fold change relative to untreated WT and ana lyzed by 2-way Anova (*p < 0.05; **p < 0.01, n.s. non-significant). H) Flow cytometry shows that cell membrane levels of HLA increased when PMA stimulated WT HTB94 cells were treated with mari mastat (MM), and that HLA levels decreased in ADAM17 KO and iRhom2 KO HTB94 compared to WT cells (*p < 0.05, n.s. non-sig nificant; 2-way Anova). I) Flow cytometry analysis of HLA levels in iRhom2 KO, ADAM17 KO and WT HTB94 cells.

In addition to ADAM17, iRhom2 was reported to support the trafficking of STING and VISA [357,358]. I reasoned that iRhom2 could control surface levels of MHC-I by regulating its trafficking in a similar manner. Thus, I treated iR2KO and WT HTB94 cells with brefeldin A, which inhibits protein transport from the ER to the Golgi apparatus, or monensin, which prevents protein secretion from the medial to trans cisternae of the Golgi complex. Both drugs clearly reduced HLA levels at the surface of WT HTB94 cells, while they had minimal effect on iRhom2-deficient cells (Figure 21A and 21B). These results show that HLA exit from the ER is quite rapid, and that iR2 plays a minor role, if any, in HLA trafficking through the secretory pathway.

To evaluate whether MHC-I could be a direct interactor of iR2, as reported for STING and VISA, I overexpressed iR2 along with SPPL2B D<A, which served as a negative control due to its structural similarity, in terms of number of TMDs, to iRhom2 but distinct functional profile. As expected, iR2 co-immunoprecipitated with ADAM17, but not with HLA (Figure 21C). Altogether, these data suggest that, in addition to regulating its shedding, iRhom2 may also influence the cell surface expression of MHC-I in both mouse and human cells through a mechanism that remains to be elucidated.

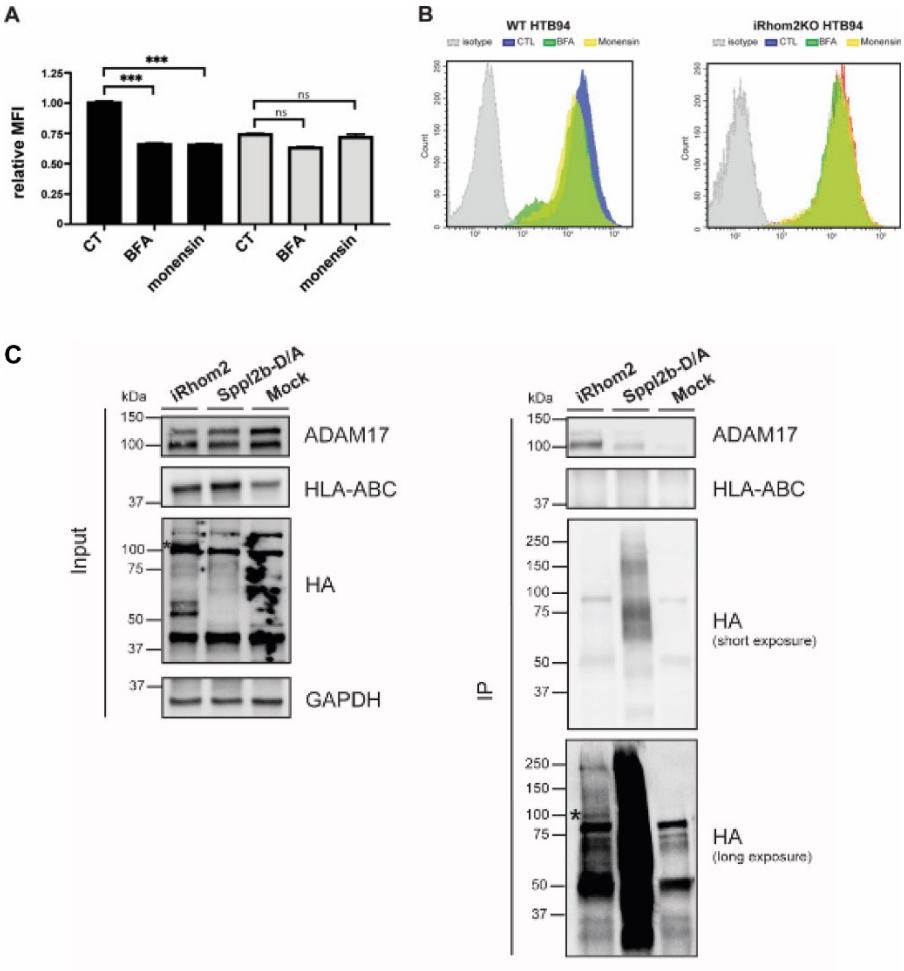

Figure 24: iRhom2 loss reduces cell surface levels of HLA. A) B) Cell membrane levels of HLA in wild-type or iRhom2 KO HTB94 cells, treated with or without brefeldin A (BFA) or monensin and measured by flow cytometry (n = 3, 2-way Anova, ***p < 0.005). Flow cytom etry histograms of one representative experiment are shown in B). C) Co-immunoprecipitation of iRhom2 with ADAM17 or HLA in HTB94 cells. (n=3)

4.6 Discussion

To validate the candidate ADAM17 substrates identified through mass spectrometry–based secretome profiling, I performed a series of biochemical experiments using Western blotting, which remains a gold standard technique for detecting both full-length and shed protein fragments. These experiments were carried out in mouse embryonic fibroblasts (mEFs) and human HTB94 fibroblast-like cells under the same experimental conditions used for proteomic analyses, including PMA stimulation and defined genetic backgrounds (WT, ADAM17 knockout, iRhom1 knockout, and iRhom2 knockout). This allowed a direct comparison between proteomic results and antibody-based detection of shedding events, thereby strengthening the confidence in iRhom-dependent substrate regulation by ADAM17.

To extend validation to substrates with low endogenous expression or lacking sufficiently sensitive antibodies, I also employed a complementary overexpression system. Selected candidate substrates were transiently overexpressed in the aforementioned cell lines, and their cleavage was assessed by analyzing conditioned media for the presence of shed ectodomains. This approach provided a more consistent detection across genotypes and allowed validation of shedding events initially inferred from proteomic data. It also enabled the detection of quantitative differences in shedding that may otherwise be masked by low endogenous abundance or antibody limitations.

In addition to validating known and newly proposed ADAM17 substrates, this analysis led to the identification of a previously unrecognized regulatory role for iRhom2 in modulating the surface expression of major histocompatibility complex class I (MHC-I) molecules. Previous evidence from Scilabra's lab (Calligaris et al., 2024) had suggested that MHC-I can be shed by ADAM17 under specific conditions. My proteomic data supported this observation by revealing increased levels of MHC-I in the secretome of PMA-stimulated WT HTB94 cells, which was reduced in the absence of ADAM17. Notably, in the course of validating this finding, I observed that loss of iRhom2 affected both the shedding and membrane abundance of MHC-I molecules, suggesting a novel regulatory mechanism whereby iRhom2 contributes to MHC-I turnover or trafficking. This unexpected result points to a broader role for iRhom2 in modulating immune recognition beyond its established function in controlling ADAM17 activation, with potential implications for immune surveillance and tumor immune evasion.

Together, these validation experiments not only confirmed the accuracy of the proteomics approach but also uncovered a new dimension of iRhom2 biology, highlighting its involvement in the regulation of immune-related molecules such as MHC-I. These findings

add mechanistic depth to the role of iRhoms in substrate selectivity and expand their functional repertoire beyond classical ADAM17 substrates.

Conclusion and final remarks

This PhD gave me the opportunity to advance our understanding of the regulatory mechanisms governing ADAM17 activity, with a particular focus on the role of its cofactors iRhom1 and iRhom2. Through systematic and kinetic analyses, it becomes evident that iRhoms not only facilitate ADAM17 maturation but also differentially control substrate selectivity, especially during the early phases of activation. iRhom2 emerges as a dominant regulator of rapid, stimulus-induced shedding across a broad range of substrates, while iRhom1 exhibits a more selective role, predominantly supporting cleavage of substrates like TGFα.

By using mass spectrometry-based profiling, I showed how high-resolution proteomics is an efficient and accurate tool for a more comprehensive study of ADAM17 biology (Figure 24), in that further revealed a continuum of substrate preferences between iRhom1- and iRhom2-associated ADAM17 complexes and identified novel substrates such as SIRPα, MXRA8, and MHC-I. The discovery of MHC-I regulation by iRhom2, not solely through shedding but also by modulating surface stability and trafficking, has critical implications for cancer immunology. The downregulation of MHC-I in iRhom2-deficient cells, particularly in leukaemia, pancreatic ductal adenocarcinoma (PDAC), suggests a novel mechanism of immune evasion and positions iRhom2 as a potential therapeutic target to enhance anti-tumor immunity in cold tumors.

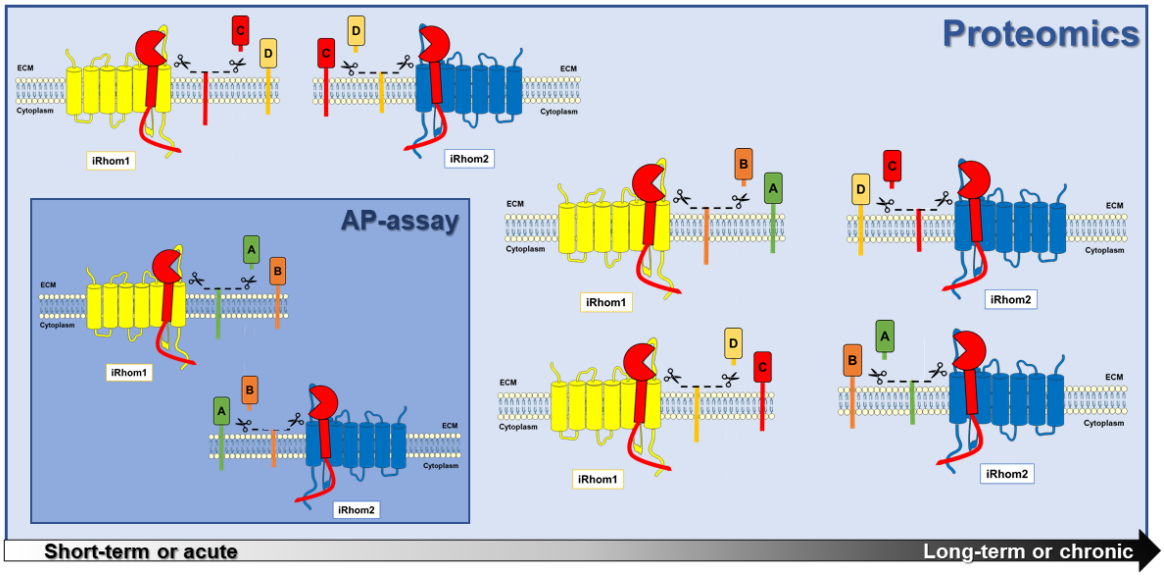

Figure 25: High-resolution proteomics is an accurate tool for studying comprehensively ADAM17 biology both in health and disease

Together, these findings underscore the dynamic and context-dependent nature of ADAM17 function, tightly governed by iRhoms in both substrate selection and temporal response. They also highlight new avenues for therapeutic intervention—particularly the modulation of iRhom2—to restore immune visibility in tumors and fine-tune growth factor signaling in cancer. This work lays a strong foundation for the development of targeted

therapies aimed at manipulating ADAM17/iRhom complexes in diseases characterized by dysregulated shedding activity.

Appendix

Papers (published, submitted)

1. Calligaris, M., **Spanò, D. P**., Puccio, M. C., Müller, S. A., Bonelli, S., Lo Pinto, M., Zito, G., Blobel, C. P., Lichtenthaler, S. F., Troeberg, L., & Scilabra, S. D. Development of a Proteomic Workflow for the Identification of Heparan Sulphate Proteoglycan-Binding Substrates of ADAM17. Proteomics, 24(23-24), e202400076. (2024). https://doi.org/10.1002/pmic.202400076
2. Calligaris, M., **Spanò, D. P.**, Bonelli, S., Müller, S. A., Carcione, C., D'apolito, D., Amico, G., Miele, M., Di Bella, M., Zito, G., Nuti, E., Rossello, A., Blobel, C. P., Lichtenthaler, S. F., & Scilabra, S. D.
   iRhom2 regulates ectodomain shedding and surface expression of the major histocompatibility complex (MHC) class I. Cellular and molecular life sciences : CMLS, 81(1), 163. (2024). https://doi.org/10.1007/s00018-024-05201-7
3. Calligaris, M., Yang, C. Y., Bonelli, S., **Spanò, D. P**., Müller, S. A., Lichtenthaler, S. F., Troeberg, L., & Scilabra, S. D. Identification of membrane proteins regulated by ADAM15 by SUSPECS proteomics. Frontiers in molecular biosciences, 10, 1162504. (2023). https://doi.org/10.3389/fmolb.2023.1162504
4. Cuffaro, D., Scilabra, S.D., **Spanò, D.P.**, Calligaris, M., Nuti, E., and Rossello, A. Chapter 3.5 "A disintegrin and metalloproteinases (ADAMs) and tumor necrosis factor-alpha converting enzyme (TACE)". Metalloenzymes. From Bench to Bedside. (2023). https://doi.org/10.1016/B978-0-12-823974-2.00016-4
5. **Spanò, D. P.,** Bonelli, S., Calligaris, M., Carreca, A. P., Carcione, C., Zito, G., Nicosia, A., Rizzo, S., & Scilabra, S. D. High-Resolution Secretome Analysis of Chemical Hypoxia Treated Cells Identifies Putative Biomarkers of Chondrosarcoma. Proteomes, 10(3), 25. (2022). https://doi.org/10.3390/proteomes10030025
6. **Spanò, D. P.**, & Scilabra, S. D. Tissue Inhibitor of Metalloproteases 3 (TIMP-3): In Vivo Analysis Underpins Its Role as a Master Regulator of Ectodomain Shedding. Membranes, 12(2), 211. (2022). https://doi.org/10.3390/membranes12020211
7. Calligaris, M., Cuffaro, D., Bonelli, S., **Spanò, D. P.,** Rossello, A., Nuti, E., & Scilabra, S. D. Strategies to Target ADAM17 in Disease: From its Discovery to the iRhom Revolution. Molecules (Basel, Switzerland), 26(4), 944. https://doi.org/10.3390/molecules26040944

Oral Presentation at Conferences/workshop

1. **Does iRhom2 have a role in protein stability?**
   2nd workshop of the Bilateral Agreements CNR – Royal Society of London, Norwich (UK).
   14/03/2023
2. **Characterization of iRhom-mediated substrate selectivity of stimulated ADAM17 by high-resolution proteomics**
   2nd workshop of Technologies and Sciences for Human Health – University of Palermo – Palermo (Italy). *25/10/2023*

Presented Posters at Conferences/workshop

1. Characterization of iRhom-mediated substrate selectivity of stimulated ADAM17 by high resolution proteomics
   'Proteolysis at the membrane – from signaling to disease', Kloster Seeon (Germany),
   13/05/2024 – 16/05/2024

Other activities:

Abroad period from June 2024 to December 2024 at the Hospital for Special Surgery (HSS) Research Institute, part of the Weill Cornell University, School of Medical Sciences, Department of Physiology, Biophysics and Systems Biology (New York City, NY – United States), under the supervision of Prof. Dr. Carl P. Blobel.

Bibliography

1. Lichtenthaler, S. F., Lemberg, M. K. & Fluhrer, R. Proteolytic ectodomain shedding of membrane proteins in mammals-hardware, concepts, and recent developments. *EMBO J* **37**, e99456 (2018).
2. Arribas, J. & Borroto, A. Protein Ectodomain Shedding. *Chem. Rev.* **102**, 4627–4638 (2002).
3. Blobel, G. *et al.* Translocation of proteins across membranes: the signal hypothesis and beyond. *Symp Soc Exp Biol* **33**, 9–36 (1979).
4. Schatz, G. & Dobberstein, B. Common principles of protein translocation across membranes. *Science* **271**, 1519–1526 (1996).
5. Brown, M. S., Ye, J., Rawson, R. B. & Goldstein, J. L. Regulated intramembrane proteolysis: a control mechanism conserved from bacteria to humans. *Cell* **100**, 391–398 (2000).
6. Lichtenthaler, S. F. & Steiner, H. Sheddases and intramembrane-cleaving proteases: RIPpers of the membrane. Symposium on regulated intramembrane proteolysis. *EMBO Rep* **8**, 537–541 (2007).
7. Blobel, C. P. ADAMs: key components in EGFR signalling and development. *Nat Rev Mol Cell Biol* **6**, 32–43 (2005).
8. Scheller, J. Control and consequences of IL-6 receptor ectodomain shedding. *European Journal of Medical Research* **19**, S17 (2014).
9. Lichtenthaler, S. F. & Meinl, E. To cut or not to cut: New rules for proteolytic shedding of membrane proteins. *J Biol Chem* **295**, 12353–12354 (2020).
10. Reiss, K. & Saftig, P. The 'a disintegrin and metalloprotease' (ADAM) family of sheddases: physiological and cellular functions. *Semin Cell Dev Biol* **20**, 126–137 (2009).
11. Vassar, R. *et al.* Function, therapeutic potential and cell biology of BACE proteases: current status and future prospects. *Journal of Neurochemistry* **130**, 4–28 (2014).
12. Itoh, Y. Membrane-type matrix metalloproteinases: Their functions and regulations. *Matrix Biol* **44–46**, 207–223 (2015).

13. Broder, C. & Becker-Pauly, C. The metalloproteases meprin α and meprin β: unique enzymes in inflammation, neurodegeneration, cancer and fibrosis. *Biochemical Journal* **450**, 253–264 (2013).

14. Seidah, N. G. & Prat, A. The biology and therapeutic targeting of the proprotein convertases. *Nat Rev Drug Discov* **11**, 367–383 (2012).

15. Szabo, R. & Bugge, T. H. Membrane-anchored serine proteases in vertebrate cell and developmental biology. *Annu Rev Cell Dev Biol* **27**, 213–235 (2011).

16. Antalis, T. M., Bugge, T. H. & Wu, Q. Membrane-anchored serine proteases in health and disease. *Prog Mol Biol Transl Sci* **99**, 1–50 (2011).

17. Visse, R. & Nagase, H. Matrix metalloproteinases and tissue inhibitors of metalloproteinases: structure, function, and biochemistry. *Circ Res* **92**, 827–839 (2003).

18. Nagase, H., Visse, R. & Murphy, G. Structure and function of matrix metalloproteinases and TIMPs. *Cardiovasc Res* **69**, 562–573 (2006).

19. Lunde, N. N., Bosnjak, T., Solberg, R. & Johansen, H. T. Mammalian legumain - A lysosomal cysteine protease with extracellular functions? *Biochimie* **166**, 77–83 (2019).

20. Solberg, R. *et al.* The Mammalian Cysteine Protease Legumain in Health and Disease. *Int J Mol Sci* **23**, 15983 (2022).

21. Sobotič, B. *et al.* Proteomic Identification of Cysteine Cathepsin Substrates Shed from the Surface of Cancer Cells. *Mol Cell Proteomics* **14**, 2213–2228 (2015).

22. Freeman, M. The rhomboid-like superfamily: molecular mechanisms and biological roles. *Annu Rev Cell Dev Biol* **30**, 235–254 (2014).

23. Bergbold, N. & Lemberg, M. K. Emerging role of rhomboid family proteins in mammalian biology and disease. *Biochim Biophys Acta* **1828**, 2840–2848 (2013).

24. Höppner, S., Schröder, B. & Fluhrer, R. Structure and function of SPP/SPPL proteases: insights from biochemical evidence and predictive modeling. *FEBS J* **290**, 5456–5474 (2023).

25. Güner, G. & Lichtenthaler, S. F. The substrate repertoire of γ-secretase/presenilin. *Semin Cell Dev Biol* **105**, 27–42 (2020).

26. Hsia, H.-E. *et al.* Functions of 'A disintegrin and metalloproteases (ADAMs)' in the mammalian nervous system. *Cell Mol Life Sci* **76**, 3055–3081 (2019).

27. Blobel, C. P., Myles, D. G., Primakoff, P. & White, J. M. Proteolytic processing of a protein involved in sperm-egg fusion correlates with acquisition of fertilization competence. *J Cell Biol* **111**, 69–78 (1990).

28. Blobel, C. P. *et al.* A potential fusion peptide and an integrin ligand domain in a protein active in sperm-egg fusion. *Nature* **356**, 248–252 (1992).

29. Wolfsberg, T. G. *et al.* The precursor region of a protein active in sperm-egg fusion contains a metalloprotease and a disintegrin domain: structural, functional, and evolutionary implications. *Proc Natl Acad Sci U S A* **90**, 10783–10787 (1993).

30. Shilling, F. M. *et al.* Identification of metalloprotease/disintegrins in Xenopus laevis testis with a potential role in fertilization. *Dev Biol* **186**, 155–164 (1997).

31. Pan, D. & Rubin, G. M. Kuzbanian controls proteolytic processing of Notch and mediates lateral inhibition during Drosophila and vertebrate neurogenesis. *Cell* **90**, 271–280 (1997).

32. Wen, C., Metzstein, M. M. & Greenwald, I. SUP-17, a Caenorhabditis elegans ADAM protein related to Drosophila KUZBANIAN, and its role in LIN-12/NOTCH signalling. *Development* **124**, 4759–4767 (1997).

33. Nakamura, T., Abe, H., Hirata, A. & Shimoda, C. ADAM family protein Mde10 is essential for development of spore envelopes in the fission yeast Schizosaccharomyces pombe. *Eukaryot Cell* **3**, 27–39 (2004).

34. Stone, A. L., Kroeger, M. & Sang, Q. X. Structure-function analysis of the ADAM family of disintegrin-like and metalloproteinase-containing proteins (review). *J Protein Chem* **18**, 447–465 (1999).

35. Cuffaro, D. *et al.* Chapter 3.5 - A disintegrin and metalloproteinases (ADAMs) and tumor necrosis factor-alpha-converting enzyme (TACE). in *Metalloenzymes* (eds. Supuran, C. T. & Donald, W. A.) 207–237 (Academic Press, 2024). doi:10.1016/B978-0-12-823974-2.00016-4.

36. Lum, L., Reid, M. S. & Blobel, C. P. Intracellular maturation of the mouse metalloprotease disintegrin MDC15. *J Biol Chem* **273**, 26236–26247 (1998).

37. Milla, M. E. *et al.* Specific sequence elements are required for the expression of functional tumor necrosis factor-alpha-converting enzyme (TACE). *J Biol Chem* **274**, 30563–30570 (1999).

38. Stöcker, W. *et al.* The metzincins--topological and sequential relations between the astacins, adamalysins, serralysins, and matrixins (collagenases) define a superfamily of zinc-peptidases. *Protein Sci* **4**, 823–840 (1995).

39. Maskos, K. *et al.* Crystal structure of the catalytic domain of human tumor necrosis factor-alpha-converting enzyme. *Proc Natl Acad Sci U S A* **95**, 3408–3412 (1998).

40. Juárez, P., Comas, I., González-Candelas, F. & Calvete, J. J. Evolution of snake venom disintegrins by positive Darwinian selection. *Mol Biol Evol* **25**, 2391–2407 (2008).

41. Weskamp, G. & Blobel, C. P. A family of cellular proteins related to snake venom disintegrins. *Proc. Natl. Acad. Sci. U.S.A.* **91**, 2748–2751 (1994).

42. Krätzschmar, J., Lum, L. & Blobel, C. P. Metargidin, a membrane-anchored metalloprotease-disintegrin protein with an RGD integrin binding sequence. *J Biol Chem* **271**, 4593–4596 (1996).

43. Zolkiewska, A. Disintegrin-like/cysteine-rich region of ADAM 12 is an active cell adhesion domain. *Exp Cell Res* **252**, 423–431 (1999).

44. Herren, B., Raines, E. W. & Ross, R. Expression of a disintegrin-like protein in cultured human vascular cells and in vivo. *FASEB J* **11**, 173–180 (1997).

45. Blobel, C. P. & White, J. M. Structure, function and evolutionary relationship of proteins containing a disintegrin domain. *Curr Opin Cell Biol* **4**, 760–765 (1992).

46. Weskamp, G., Krätzschmar, J., Reid, M. S. & Blobel, C. P. MDC9, a widely expressed cellular disintegrin containing cytoplasmic SH3 ligand domains. *J Cell Biol* **132**, 717–726 (1996).

47. Mehrabipour, M., Jasemi, N. S. K., Dvorsky, R. & Ahmadian, M. R. A Systematic Compilation of Human SH3 Domains: A Versatile Superfamily in Cellular Signaling. *Cells* **12**, 2054 (2023).

48. Howard, L., Nelson, K. K., Maciewicz, R. A. & Blobel, C. P. Interaction of the metalloprotease disintegrins MDC9 and MDC15 with two SH3 domain-containing proteins, endophilin I and SH3PX1. *J Biol Chem* **274**, 31693–31699 (1999).

49. Ebsen, H., Lettau, M., Kabelitz, D. & Janssen, O. Identification of SH3 Domain Proteins Interacting with the Cytoplasmic Tail of the A Disintegrin and Metalloprotease 10 (ADAM10). *PLoS One* **9**, e102899 (2014).

50. Suzuki, A. *et al.* Meltrin alpha cytoplasmic domain interacts with SH3 domains of Src and Grb2 and is phosphorylated by v-Src. *Oncogene* **19**, 5842–5850 (2000).

51. Poghosyan, Z. *et al.* Phosphorylation-dependent interactions between ADAM15 cytoplasmic domain and Src family protein-tyrosine kinases. *J Biol Chem* **277**, 4999–5007 (2002).

52. Kärkkäinen, S. *et al.* Identification of preferred protein interactions by phage-display of the human Src homology-3 proteome. *EMBO Rep* **7**, 186–191 (2006).

53. Sahin, U. *et al.* Distinct roles for ADAM10 and ADAM17 in ectodomain shedding of six EGFR ligands. *J Cell Biol* **164**, 769–779 (2004).

54. Lora, J. *et al.* Targeted truncation of the ADAM17 cytoplasmic domain in mice results in protein destabilization and a hypomorphic phenotype. *Journal of Biological Chemistry* **296**, 100733 (2021).

55. Spanò, D. P. & Scilabra, S. D. Tissue Inhibitor of Metalloproteases 3 (TIMP-3): In Vivo Analysis Underpins Its Role as a Master Regulator of Ectodomain Shedding. *Membranes (Basel)* **12**, 211 (2022).

56. Murphy, G. *et al.* Role of TIMPs (tissue inhibitors of metalloproteinases) in pericellular proteolysis: the specificity is in the detail. *Biochem Soc Symp* 65–80 (2003) doi:10.1042/bss0700065.

57. Scilabra, S. D. *et al.* Differential regulation of extracellular tissue inhibitor of metalloproteinases-3 levels by cell membrane-bound and shed low density lipoprotein receptor-related protein 1. *J Biol Chem* **288**, 332–342 (2013).

58. Vassar, R. *et al.* Beta-secretase cleavage of Alzheimer's amyloid precursor protein by the transmembrane aspartic protease BACE. *Science* **286**, 735–741 (1999).

59. Hussain, I. *et al.* Identification of a novel aspartic protease (Asp 2) as beta-secretase. *Mol Cell Neurosci* **14**, 419–427 (1999).

60. Sinha, S. *et al.* Purification and cloning of amyloid precursor protein beta-secretase from human brain. *Nature* **402**, 537–540 (1999).

61. Rochin, L. *et al.* BACE2 processes PMEL to form the melanosome amyloid matrix in pigment cells. *Proc Natl Acad Sci U S A* **110**, 10658–10663 (2013).

62. Esterházy, D. *et al.* Bace2 is a β cell-enriched protease that regulates pancreatic β cell function and mass. *Cell Metab* **14**, 365–377 (2011).

63. Hampel, H. *et al.* The β-Secretase BACE1 in Alzheimer's Disease. *Biol Psychiatry* **89**, 745–756 (2021).

64. Haniu, M. *et al.* Characterization of Alzheimer's beta -secretase protein BACE. A pepsin family member with unusual properties. *J Biol Chem* **275**, 21099–21106 (2000).

65. Hussain, I., Christie, G., Schneider, K., Moore, S. & Dingwall, C. Prodomain processing of Asp1 (BACE2) is autocatalytic. *J Biol Chem* **276**, 23322–23328 (2001).

66. Tomasselli, A. G. *et al.* Employing a superior BACE1 cleavage sequence to probe cellular APP processing. *J Neurochem* **84**, 1006–1017 (2003).

67. Turner, R. T. *et al.* Specificity of memapsin 1 and its implications on the design of memapsin 2 (beta-secretase) inhibitor selectivity. *Biochemistry* **41**, 8742–8746 (2002).

68. Pastorino, L., Ikin, A. F., Nairn, A. C., Pursnani, A. & Buxbaum, J. D. The Carboxyl-Terminus of BACE Contains a Sorting Signal That Regulates BACE Trafficking but Not the Formation of Total Aβ. *Molecular and Cellular Neuroscience* **19**, 175–185 (2002).

69. Kang, E. L., Biscaro, B., Piazza, F. & Tesco, G. BACE1 protein endocytosis and trafficking are differentially regulated by ubiquitination at lysine 501 and the Di-leucine motif in the carboxyl terminus. *J Biol Chem* **287**, 42867–42880 (2012).

70. Kuhn, P.-H. *et al.* Secretome protein enrichment identifies physiological BACE1 protease substrates in neurons. *EMBO J* **31**, 3157–3168 (2012).

71. Sletten, E. M. & Bertozzi, C. R. From mechanism to mouse: a tale of two bioorthogonal reactions. *Acc Chem Res* **44**, 666–676 (2011).

72. Willem, M. *et al.* Control of peripheral nerve myelination by the beta-secretase BACE1. *Science* **314**, 664–666 (2006).

73. Zhou, L. *et al.* The Neural Cell Adhesion Molecules L1 and CHL1 Are Cleaved by BACE1 Protease in Vivo. *J Biol Chem* **287**, 25927–25940 (2012).

74. Zhu, K. *et al.* Beta-Site Amyloid Precursor Protein Cleaving Enzyme 1 Inhibition Impairs Synaptic Plasticity via Seizure Protein 6. *Biol Psychiatry* **83**, 428–437 (2018).

75. Pigoni, M. *et al.* Seizure protein 6 and its homolog seizure 6-like protein are physiological substrates of BACE1 in neurons. *Mol Neurodegener* **11**, 67 (2016).

76. Müller, S. A. *et al.* The Alzheimer's disease-linked protease BACE1 modulates neuronal IL-6 signaling through shedding of the receptor gp130. *Molecular Neurodegeneration* **18**, 13 (2023).

77. Stützer, I. *et al.* Systematic proteomic analysis identifies β-site amyloid precursor protein cleaving enzyme 2 and 1 (BACE2 and BACE1) substrates in pancreatic β-cells. *J Biol Chem* **288**, 10536–10547 (2013).

78. Fukui, K. *et al.* The HNF-1 target collectrin controls insulin exocytosis by SNARE complex formation. *Cell Metab* **2**, 373–384 (2005).

79. Akpinar, P., Kuwajima, S., Krützfeldt, J. & Stoffel, M. Tmem27: A cleaved and shed plasma membrane protein that stimulates pancreatic β cell proliferation. *Cell Metabolism* **2**, 385–397 (2005).

80. Watt, B. *et al.* N-terminal domains elicit formation of functional Pmel17 amyloid fibrils. *J Biol Chem* **284**, 35543–35555 (2009).

81. Murphy, G. & Nagase, H. Localizing matrix metalloproteinase activities in the pericellular environment. *FEBS J* **278**, 2–15 (2011).

82. Kajita, M. *et al.* Membrane-type 1 matrix metalloproteinase cleaves CD44 and promotes cell migration. *J Cell Biol* **153**, 893–904 (2001).

83. Manon-Jensen, T., Multhaupt, H. A. B. & Couchman, J. R. Mapping of matrix metalloproteinase cleavage sites on syndecan-1 and syndecan-4 ectodomains. *FEBS J* **280**, 2320–2331 (2013).

84. Moss, N. M. *et al.* Ovarian cancer cell detachment and multicellular aggregate formation are regulated by membrane type 1 matrix metalloproteinase: a potential role in I.p. metastatic dissemination. *Cancer Res* **69**, 7121–7129 (2009).

85. Fu, H.-L. *et al.* Shedding of discoidin domain receptor 1 by membrane-type matrix metalloproteinases. *J Biol Chem* **288**, 12114–12129 (2013).

86. Chan, K. M. *et al.* MT1-MMP inactivates ADAM9 to regulate FGFR2 signaling and calvarial osteogenesis. *Dev Cell* **22**, 1176–1190 (2012).

87. Hayashita-Kinoh, H. *et al.* Membrane-type 5 matrix metalloproteinase is expressed in differentiated neurons and regulates axonal growth. *Cell Growth Differ* **12**, 573–580 (2001).

88. Willem, M. *et al.* η-Secretase processing of APP inhibits neuronal activity in the hippocampus. *Nature* **526**, 443–447 (2015).

89. Rahn, S. & Becker-Pauly, C. Meprin and ADAM proteases as triggers of systemic inflammation in sepsis. *FEBS Lett* **596**, 534–556 (2022).

90. Bertenshaw, G. P., Norcum, M. T. & Bond, J. S. Structure of homo- and hetero-oligomeric meprin metalloproteases. Dimers, tetramers, and high molecular mass multimers. *J Biol Chem* **278**, 2522–2532 (2003).

91. Arolas, J. L. *et al.* Structural basis for the sheddase function of human meprin β metalloproteinase at the plasma membrane. *Proc Natl Acad Sci U S A* **109**, 16131–16136 (2012).

92. Beynon, R. J., Shannon, J. D. & Bond, J. S. Purification and characterization of a metallo-endoproteinase from mouse kidney. *Biochem J* **199**, 591–598 (1981).

93. Sterchi, E. E., Green, J. R. & Lentze, M. J. Non-pancreatic hydrolysis of N-benzoyl-l-tyrosyl-p-aminobenzoic acid (PABA-peptide) in the human small intestine. *Clin Sci (Lond)* **62**, 557–560 (1982).

94. Sterchi, E. E., Green, J. R. & Lentze, M. J. Nonpancreatic hydrolysis of N-benzoyl-L-tyrosyl-p-aminobenzoic acid (PABA peptide) in the rat small intestine. *J Pediatr Gastroenterol Nutr* **2**, 539–547 (1983).

95. Yamaguchi, T. *et al.* Meprin is predominantly involved in parathyroid hormone degradation by the microvillar membranes of rat kidney. *Life Sciences* **54**, 381–386 (1994).

96. Yamaguchi, T., Fukase, M., Sugimoto, T., Kido, H. & Chihara, K. Purification of meprin from human kidney and its role in parathyroid hormone degradation. *Biol Chem Hoppe Seyler* **375**, 821–824 (1994).

97. Addison, M. L. *et al.* A role for metalloendopeptidases in the breakdown of the gut hormone, PYY 3-36. *Endocrinology* **152**, 4630–4640 (2011).

98. Ambort, D. *et al.* Specific processing of tenascin-C by the metalloprotease meprinbeta neutralizes its inhibition of cell spreading. *Matrix Biol* **29**, 31–42 (2010).

99. Oneda, B. *et al.* Metalloprotease meprin beta in rat kidney: glomerular localization and differential expression in glomerulonephritis. *PLoS One* **3**, e2278 (2008).

100. Bylander, J. *et al.* Targeted disruption of the meprin metalloproteinase beta gene protects against renal ischemia-reperfusion injury in mice. *Am J Physiol Renal Physiol* **294**, F480-490 (2008).

101. Kaushal, G. P., Walker, P. D. & Shah, S. V. An old enzyme with a new function: purification and characterization of a distinct matrix-degrading metalloproteinase in rat kidney cortex and its identification as meprin. *Journal of Cell Biology* **126**, 1319–1327 (1994).

102. Banerjee, S. & Bond, J. S. Prointerleukin-18 Is Activated by Meprin β in Vitro and in Vivo in Intestinal Inflammation. *J Biol Chem* **283**, 31371–31377 (2008).

103. Bien, J. *et al.* The metalloprotease meprin β generates amino terminal-truncated amyloid β peptide species. *J Biol Chem* **287**, 33304–33313 (2012).

104. Mizuno, K., Nakamura, T., Ohshima, T., Tanaka, S. & Matsuo, H. Yeast KEX2 genes encodes an endopeptidase homologous to subtilisin-like serine proteases. *Biochem Biophys Res Commun* **156**, 246–254 (1988).

105. Roebroek, A. J. *et al.* Characterization of human c-fes/fps reveals a new transcription unit (fur) in the immediately upstream region of the proto-oncogene. *Mol Biol Rep* **11**, 117–125 (1986).

106. van de Ven, W. J. *et al.* Furin is a subtilisin-like proprotein processing enzyme in higher eukaryotes. *Mol Biol Rep* **14**, 265–275 (1990).

107. Seidah, N. G. The proprotein convertases, 20 years later. *Methods Mol Biol* **768**, 23–57 (2011).

108. Wang, X. & Pei, D. Shedding of membrane type matrix metalloproteinase 5 by a furin-type convertase: a potential mechanism for down-regulation. *J Biol Chem* **276**, 35953–35960 (2001).

109. Leitlein, J. *et al.* Processing of immunosuppressive pro-TGF-beta 1,2 by human glioblastoma cells involves cytoplasmic and secreted furin-like proteases. *J Immunol* **166**, 7238–7243 (2001).

110. Seidah, N. G., Abifadel, M., Prost, S., Boileau, C. & Prat, A. The Proprotein Convertases in Hypercholesterolemia and Cardiovascular Diseases: Emphasis on Proprotein Convertase Subtilisin/Kexin 9. *Pharmacol Rev* **69**, 33–52 (2017).

111. Szabo, R. & Bugge, T. H. Type II transmembrane serine proteases in development and disease. *Int J Biochem Cell Biol* **40**, 1297–1316 (2008).

112. Bugge, T. H., Antalis, T. M. & Wu, Q. Type II transmembrane serine proteases. *J Biol Chem* **284**, 23177–23181 (2009).

113. Page, M. J. & Di Cera, E. Serine peptidases: classification, structure and function. *Cell Mol Life Sci* **65**, 1220–1236 (2008).

114. Hoffmann, M. *et al.* SARS-CoV-2 Cell Entry Depends on ACE2 and TMPRSS2 and Is Blocked by a Clinically Proven Protease Inhibitor. *Cell* **181**, 271-280.e8 (2020).

115. Beckmann, A.-M. *et al.* The intact Kunitz domain protects the amyloid precursor protein from being processed by matriptase-2. *Biol Chem* **397**, 777–790 (2016).

116. Wu, C.-J., Feng, X., Lu, M., Morimura, S. & Udey, M. C. Matriptase-mediated cleavage of EpCAM destabilizes claudins and dysregulates intestinal epithelial homeostasis. *J Clin Invest* **127**, 623–634 (2017).

117. Gaweł-Bęben, K. *et al.* TMEFF2 shedding is regulated by oxidative stress and mediated by ADAMs and transmembrane serine proteases implicated in prostate cancer. *Cell Biol Int* **42**, 273–280 (2018).

118. Trabocchi, A. & Lenci, E. Chapter 3.4 - Matrix metalloproteases. in *Metalloenzymes* (eds. Supuran, C. T. & Donald, W. A.) 197–206 (Academic Press, 2024). doi:10.1016/B978-0-12-823974-2.00033-4.

119. Kryczka, J. *et al.* Matrix metalloproteinase-2 cleavage of the β1 integrin ectodomain facilitates colon cancer cell motility. *J Biol Chem* **287**, 36556–36566 (2012).

120. Noë, V. *et al.* Release of an invasion promoter E-cadherin fragment by matrilysin and stromelysin-1. *J Cell Sci* **114**, 111–118 (2001).

121. Jang, B., Jung, H., Chung, H., Moon, B.-I. & Oh, E.-S. Syndecan-2 enhances E-cadherin shedding and fibroblast-like morphological changes by inducing MMP-7 expression in colon cancer cells. *Biochem Biophys Res Commun* **477**, 47–53 (2016).

122. Dean, R. A. *et al.* Macrophage-specific metalloelastase (MMP-12) truncates and inactivates ELR+ CXC chemokines and generates CCL2, -7, -8, and -13 antagonists: potential role of the

macrophage in terminating polymorphonuclear leukocyte influx. *Blood* **112**, 3455–3464 (2008).

123. Van Doren, S. R., Marcink, T. C., Koppisetti, R. K., Jurkevich, A. & Fulcher, Y. G. Peripheral membrane associations of matrix metalloproteinases. *Biochim Biophys Acta Mol Cell Res* **1864**, 1964–1973 (2017).
124. Wh, Y. & Jf, W. Heparan sulfate proteoglycans as extracellular docking molecules for matrilysin (matrix metalloproteinase 7). *The Journal of biological chemistry* **275**, (2000).
125. Soh, W. T. *et al.* ExteNDing Proteome Coverage with Legumain as a Highly Specific Digestion Protease. *Anal. Chem.* **92**, 2961–2971 (2020).
126. Zhang, Z. *et al.* Delta-secretase cleaves amyloid precursor protein and regulates the pathogenesis in Alzheimer's disease. *Nat Commun* **6**, 8762 (2015).
127. Yadati, T., Houben, T., Bitorina, A. & Shiri-Sverdlov, R. The Ins and Outs of Cathepsins: Physiological Function and Role in Disease Management. *Cells* **9**, 1679 (2020).
128. Creasy, B. M. & McCoy, K. L. Cytokines regulate cysteine cathepsins during TLR responses. *Cell Immunol* **267**, 56–66 (2011).
129. Authier, F., Kouach, M. & Briand, G. Endosomal proteolysis of insulin-like growth factor-I at its C-terminal D-domain by cathepsin B. *FEBS Letters* **579**, 4309–4316 (2005).
130. Hsieh, C.-S., deRoos, P., Honey, K., Beers, C. & Rudensky, A. Y. A Role for Cathepsin L and Cathepsin S in Peptide Generation for MHC Class II Presentation1. *The Journal of Immunology* **168**, 2618–2625 (2002).
131. Beers, C. *et al.* Cathepsin S Controls MHC Class II-Mediated Antigen Presentation by Epithelial Cells In Vivo1. *The Journal of Immunology* **174**, 1205–1212 (2005).
132. Brown, R. *et al.* Cathepsin S: investigating an old player in lung disease pathogenesis, comorbidities, and potential therapeutics. *Respir Res* **21**, 111 (2020).
133. Clark, A. K., Yip, P. K. & Malcangio, M. The liberation of fractalkine in the dorsal horn requires microglial cathepsin S. *J Neurosci* **29**, 6945–6954 (2009).
134. Pietra, D., Borghini, A., Ricci, C. & Bianucci, A. M. Enzyme kinetics studies on 29-kDa human liver cathepsin L. *Chem Biol Drug Des* **84**, 648–658 (2014).

135. Gocheva, V. *et al.* Distinct roles for cysteine cathepsin genes in multistage tumorigenesis. *Genes Dev.* **20**, 543–556 (2006).

136. Düsterhöft, S., Künzel, U. & Freeman, M. Rhomboid proteases in human disease: Mechanisms and future prospects. *Biochimica et Biophysica Acta (BBA) - Molecular Cell Research* **1864**, 2200–2209 (2017).

137. JURGENS, G., WIESCHAUS, E., NUSSLEIN-VOLHARD, C. & KLUDING, H. Mutations affecting the pattern of the larval cuticle in Drosophila melanogaster. II: Zygotic loci on the third chromosome. *Wilhelm Roux arch. dev. biol* **193**, 283–295 (1984).

138. Urban, S., Lee, J. R. & Freeman, M. Drosophila Rhomboid-1 Defines a Family of Putative Intramembrane Serine Proteases. *Cell* **107**, 173–182 (2001).

139. Urban, S. & Freeman, M. Substrate specificity of rhomboid intramembrane proteases is governed by helix-breaking residues in the substrate transmembrane domain. *Mol Cell* **11**, 1425–1434 (2003).

140. Lemberg, M. K. & Freeman, M. Functional and evolutionary implications of enhanced genomic analysis of rhomboid intramembrane proteases. *Genome Res.* **17**, 1634–1646 (2007).

141. Wang, Y., Zhang, Y. & Ha, Y. Crystal structure of a rhomboid family intramembrane protease. *Nature* **444**, 179–180 (2006).

142. Lemberg, M. K. *et al.* Mechanism of intramembrane proteolysis investigated with purified rhomboid proteases. *The EMBO Journal* **24**, 464–472 (2005).

143. Lastun, V. L., Grieve, A. G. & Freeman, M. Substrates and physiological functions of secretase rhomboid proteases. *Seminars in Cell & Developmental Biology* **60**, 10–18 (2016).

144. Spinazzi, M. & De Strooper, B. PARL: The mitochondrial rhomboid protease. *Seminars in Cell & Developmental Biology* **60**, 19–28 (2016).

145. Cheng, T.-L. *et al.* Functions of Rhomboid Family Protease RHBDL2 and Thrombomodulin in Wound Healing. *J Invest Dermatol* **131**, 2486–2494 (2011).

146. Lohi, O., Urban, S. & Freeman, M. Diverse Substrate Recognition Mechanisms for Rhomboids: Thrombomodulin Is Cleaved by Mammalian Rhomboids. *Current Biology* **14**, 236–241 (2004).

147. Pascall, J. C. & Brown, K. D. Intramembrane cleavage of ephrinB3 by the human rhomboid family protease, RHBDL2. *Biochemical and Biophysical Research Communications* **317**, 244–252 (2004).

148. Adrain, C. *et al.* Mammalian EGF receptor activation by the rhomboid protease RHBDL2. *EMBO reports* **12**, 421–427 (2011).

149. Fleig, L. *et al.* Ubiquitin-Dependent Intramembrane Rhomboid Protease Promotes ERAD of Membrane Proteins. *Molecular Cell* **47**, 558–569 (2012).

150. Liu, X.-N. *et al.* Lentivirus-mediated silencing of rhomboid domain containing 1 suppresses tumor growth and induces apoptosis in hepatoma HepG2 cells. *Asian Pac J Cancer Prev* **14**, 5–9 (2013).

151. Wei, X., Lv, T., Chen, D. & Guan, J. Lentiviral Vector Mediated Delivery of RHBDD1 shRNA down Regulated the Proliferation of Human Glioblastoma Cells. *Technol Cancer Res Treat* **13**, 87–93 (2014).

152. Han, J. *et al.* Lentivirus-mediated knockdown of rhomboid domain containing 1 inhibits colorectal cancer cell growth. *Molecular Medicine Reports* **12**, 377–381 (2015).

153. Paschkowsky, S., Hamzé, M., Oestereich, F. & Munter, L. M. Alternative Processing of the Amyloid Precursor Protein Family by Rhomboid Protease RHBDL4. *J Biol Chem* **291**, 21903–21912 (2016).

154. Pellegrini, L. *et al.* PAMP and PARL, two novel putative metalloproteases interacting with the COOH-terminus of Presenilin-1 and -2. *Journal of Alzheimer's Disease* **3**, 181–190 (2001).

155. Meissner, C., Lorenz, H., Weihofen, A., Selkoe, D. J. & Lemberg, M. K. The mitochondrial intramembrane protease PARL cleaves human Pink1 to regulate Pink1 trafficking. *Journal of Neurochemistry* **117**, 856–867 (2011).

156. Meissner, C., Lorenz, H., Hehn, B. & Lemberg, M. K. Intramembrane protease PARL defines a negative regulator of PINK1- and PARK2/Parkin-dependent mitophagy. *Autophagy* (2015).

157. Ponting, C. P. *et al.* Identification of a novel family of presenilin homologues. *Hum Mol Genet* **11**, 1037–1044 (2002).

158. Weihofen, A., Binns, K., Lemberg, M. K., Ashman, K. & Martoglio, B. Identification of signal peptide peptidase, a presenilin-type aspartic protease. *Science* **296**, 2215–2218 (2002).

159. Lemberg, M. K. & Martoglio, B. Requirements for signal peptide peptidase-catalyzed intramembrane proteolysis. *Mol Cell* **10**, 735–744 (2002).

160. Boname, J. M. *et al.* Cleavage by signal peptide peptidase is required for the degradation of selected tail-anchored proteins. *J Cell Biol* **205**, 847–862 (2014).

161. Chen, C. *et al.* Signal peptide peptidase functions in ERAD to cleave the unfolded protein response regulator XBP1u. *EMBO J* **33**, 2492–2506 (2014).

162. Stefanovic-Barrett, S. *et al.* MARCH6 and TRC8 facilitate the quality control of cytosolic and tail-anchored proteins. *EMBO Rep* **19**, e45603 (2018).

163. Martin, L. *et al.* Regulated intramembrane proteolysis of Bri2 (Itm2b) by ADAM10 and SPPL2a/SPPL2b. *J Biol Chem* **283**, 1644–1652 (2008).

164. Martin, L., Fluhrer, R. & Haass, C. Substrate requirements for SPPL2b-dependent regulated intramembrane proteolysis. *J Biol Chem* **284**, 5662–5670 (2009).

165. Bergmann, H. *et al.* B cell survival, surface BCR and BAFFR expression, CD74 metabolism, and CD8- dendritic cells require the intramembrane endopeptidase SPPL2A. *J Exp Med* **210**, 31–40 (2013).

166. Kuhn, P.-H. *et al.* Secretome analysis identifies novel signal Peptide peptidase-like 3 (Sppl3) substrates and reveals a role of Sppl3 in multiple Golgi glycosylation pathways. *Mol Cell Proteomics* **14**, 1584–1598 (2015).

167. Voss, M. *et al.* Shedding of glycan-modifying enzymes by signal peptide peptidase-like 3 (SPPL3) regulates cellular N-glycosylation. *The EMBO Journal* **33**, 2890–2905 (2014).

168. Hobohm, L. *et al.* N-terminome analyses underscore the prevalence of SPPL3-mediated intramembrane proteolysis among Golgi-resident enzymes and its role in Golgi enzyme secretion. *Cell Mol Life Sci* **79**, 185 (2022).

169. Sherrington, R. *et al.* Cloning of a gene bearing missense mutations in early-onset familial Alzheimer's disease. *Nature* **375**, 754–760 (1995).

170. De Strooper, B. *et al.* Deficiency of presenilin-1 inhibits the normal cleavage of amyloid precursor protein. *Nature* **391**, 387–390 (1998).

171. Haapasalo, A. & Kovacs, D. M. The many substrates of presenilin/γ-secretase. *J Alzheimers Dis* **25**, 3–28 (2011).

172. Bai, X.-C. *et al.* An atomic structure of human γ-secretase. *Nature* **525**, 212–217 (2015).

173. Schauenburg, L. *et al.* APLP1 is endoproteolytically cleaved by γ-secretase without previous ectodomain shedding. *Sci Rep* **8**, 1916 (2018).

174. Moss, M. L. *et al.* Cloning of a disintegrin metalloproteinase that processes precursor tumour-necrosis factor-alpha. *Nature* **385**, 733–736 (1997).

175. Black, R. A. *et al.* A metalloproteinase disintegrin that releases tumour-necrosis factor-alpha from cells. *Nature* **385**, 729–733 (1997).

176. Dulloo, I., Muliyil, S. & Freeman, M. The molecular, cellular and pathophysiological roles of iRhom pseudoproteases. *Open Biology* **9**, 190003 (2019).

177. Calligaris, M. *et al.* Strategies to Target ADAM17 in Disease: From its Discovery to the iRhom Revolution. *Molecules* **26**, 944 (2021).

178. Grötzinger, J., Lorenzen, I. & Düsterhöft, S. Molecular insights into the multilayered regulation of ADAM17: The role of the extracellular region. *Biochimica et Biophysica Acta (BBA) - Molecular Cell Research* **1864**, 2088–2095 (2017).

179. Weskamp, G. *et al.* ADAM17 stabilizes its interacting partner inactive Rhomboid 2 (iRhom2) but not inactive Rhomboid 1 (iRhom1). *J Biol Chem* **295**, 4350–4358 (2020).

180. Avci, D. *et al.* The intramembrane protease SPP impacts morphology of the endoplasmic reticulum by triggering degradation of morphogenic proteins. *J Biol Chem* **294**, 2786–2800 (2019).

181. Kahveci-Türköz, S. *et al.* A structural model of the iRhom–ADAM17 sheddase complex reveals functional insights into its trafficking and activity. *Cell. Mol. Life Sci.* **80**, 135 (2023).

182. Lu, F. *et al.* Cryo-EM reveals that iRhom2 restrains ADAM17 protease activity to control the release of growth factor and inflammatory signals. *Mol Cell* **84**, 2152-2165.e5 (2024).

183. Sehnal, D. *et al.* Mol* Viewer: modern web app for 3D visualization and analysis of large biomolecular structures. *Nucleic Acids Res* **49**, W431–W437 (2021).

184. Christova, Y., Adrain, C., Bambrough, P., Ibrahim, A. & Freeman, M. Mammalian iRhoms have distinct physiological functions including an essential role in TACE regulation. *EMBO Rep* **14**, 884–890 (2013).

185. Maciag, J. J. *et al.* Structural Insights into the Activation and Inhibition of the ADAM17-iRhom2 Complex. *bioRxiv* 2024.12.22.629961 (2024) doi:10.1101/2024.12.22.629961.

186. Li, X. *et al.* Structural modeling defines transmembrane residues in ADAM17 that are crucial for Rhbdf2-ADAM17-dependent proteolysis. *J Cell Sci* **130**, 868–878 (2017).

187. Düsterhöft, S. *et al.* The iRhom homology domain is indispensable for ADAM17-mediated TNFα and EGF receptor ligand release. *Cell. Mol. Life Sci.* **78**, 5015–5040 (2021).

188. Zhao, Y. *et al.* Identification of Molecular Determinants in iRhoms1 and 2 That Contribute to the Substrate Selectivity of Stimulated ADAM17. *Int J Mol Sci* **23**, 12796 (2022).

189. Oikonomidi, I. *et al.* iTAP, a novel iRhom interactor, controls TNF secretion by policing the stability of iRhom/TACE. *eLife* **7**, e35032 (2018).

190. Künzel, U. *et al.* FRMD8 promotes inflammatory and growth factor signalling by stabilising the iRhom/ADAM17 sheddase complex. *Elife* **7**, e35012 (2018).

191. Bläsius, K. *et al.* Pathological mutations reveal the key role of the cytosolic iRhom2 N-terminus for phosphorylation-independent 14-3-3 interaction and ADAM17 binding, stability, and activity. *Cell Mol Life Sci* **81**, 102 (2024).

192. Siggs, O. M. *et al.* Genetic interaction implicates iRhom2 in the regulation of EGF receptor signalling in mice. *Biol Open* **3**, 1151–1157 (2014).

193. Hosur, V. *et al.* Rhbdf2 mutations increase its protein stability and drive EGFR hyperactivation through enhanced secretion of amphiregulin. *Proc Natl Acad Sci U S A* **111**, E2200-2209 (2014).

194. Dulloo, I. *et al.* Cleavage of the pseudoprotease iRhom2 by the signal peptidase complex reveals an ER-to-nucleus signaling pathway. *Mol Cell* **84**, 277-292.e9 (2024).

195. Karantza, V. Keratins in health and cancer: more than mere epithelial cell markers. *Oncogene* **30**, 127–138 (2011).

196. Edwards, D. R., Handsley, M. M. & Pennington, C. J. The ADAM metalloproteinases. *Molecular Aspects of Medicine* **29**, 258–289 (2008).

197. Düsterhöft, S. *et al.* Membrane-Proximal Domain of a Disintegrin and Metalloprotease-17 Represents the Putative Molecular Switch of Its Shedding Activity Operated by Protein-disulfide Isomerase. *J. Am. Chem. Soc.* **135**, 5776–5781 (2013).

198. Düsterhöft, S. *et al.* Extracellular Juxtamembrane Segment of ADAM17 Interacts with Membranes and Is Essential for Its Shedding Activity. *Biochemistry* **54**, 5791–5801 (2015).

199. Sommer, A. *et al.* Phosphatidylserine exposure is required for ADAM17 sheddase function. *Nat Commun* **7**, 11523 (2016).

200. Peschon, J. J. *et al.* An essential role for ectodomain shedding in mammalian development. *Science* **282**, 1281–1284 (1998).

201. Li, X. *et al.* iRhoms 1 and 2 are essential upstream regulators of ADAM17-dependent EGFR signaling. *Proc Natl Acad Sci U S A* **112**, 6080–6085 (2015).

202. Horiuchi, K. *et al.* Substrate selectivity of epidermal growth factor-receptor ligand sheddases and their regulation by phorbol esters and calcium influx. *Mol Biol Cell* **18**, 176–188 (2007).

203. Gschwind, A., Hart, S., Fischer, O. M. & Ullrich, A. TACE cleavage of proamphiregulin regulates GPCR-induced proliferation and motility of cancer cells. *EMBO J* **22**, 2411–2421 (2003).

204. Jg, W., Km, O., K, M., Cs, R. & B, S.-Z. Up-regulation of soluble Axl and Mer receptor tyrosine kinases negatively correlates with Gas6 in established multiple sclerosis lesions. *The American journal of pathology* **175**, (2009).

205. Bech-Serra, J. J. *et al.* Proteomic identification of desmoglein 2 and activated leukocyte cell adhesion molecule as substrates of ADAM17 and ADAM10 by difference gel electrophoresis. *Mol Cell Biol* **26**, 5086–5095 (2006).

206. Leksa, V. *et al.* Soluble M6P/IGF2R released by TACE controls angiogenesis via blocking plasminogen activation. *Circ Res* **108**, 676–685 (2011).

207. Lambert, D. W. *et al.* Tumor necrosis factor-alpha convertase (ADAM17) mediates regulated ectodomain shedding of the severe-acute respiratory syndrome-coronavirus (SARS-CoV) receptor, angiotensin-converting enzyme-2 (ACE2). *J Biol Chem* **280**, 30113–30119 (2005).

208. Haga, S. *et al.* Modulation of TNF-alpha-converting enzyme by the spike protein of SARS-CoV and ACE2 induces TNF-alpha production and facilitates viral entry. *Proc Natl Acad Sci U S A* **105**, 7809–7814 (2008).

209. Endres, K., Postina, R., Schroeder, A., Mueller, U. & Fahrenholz, F. Shedding of the amyloid precursor protein-like protein APLP2 by disintegrin-metalloproteinases. *FEBS J* **272**, 5808–5820 (2005).

210. Schulte, A. *et al.* Sequential processing of the transmembrane chemokines CX3CL1 and CXCL16 by alpha- and gamma-secretases. *Biochem Biophys Res Commun* **358**, 233–240 (2007).

211. Dyczynska, E. *et al.* Proteolytic processing of delta-like 1 by ADAM proteases. *J Biol Chem* **282**, 436–444 (2007).

212. Wang, Y. *et al.* ADAM17 cleaves CD16b (FcγRIIIb) in human neutrophils. *Biochim Biophys Acta* **1833**, 680–685 (2013).

213. Zatovicova, M. *et al.* Ectodomain shedding of the hypoxia-induced carbonic anhydrase IX is a metalloprotease-dependent process regulated by TACE/ADAM17. *Br J Cancer* **93**, 1267–1276 (2005).

214. Buxbaum, J. D. *et al.* Evidence that tumor necrosis factor alpha converting enzyme is involved in regulated alpha-secretase cleavage of the Alzheimer amyloid protein precursor. *J Biol Chem* **273**, 27765–27767 (1998).

215. Slack, B. E., Ma, L. K. & Seah, C. C. Constitutive shedding of the amyloid precursor protein ectodomain is up-regulated by tumour necrosis factor-alpha converting enzyme. *Biochem J* **357**, 787–794 (2001).

216. Patel, I. R. *et al.* TNF-alpha convertase enzyme from human arthritis-affected cartilage: isolation of cDNA by differential display, expression of the active enzyme, and regulation of TNF-alpha. *J Immunol* **160**, 4570–4579 (1998).

217. Sahin, U. & Blobel, C. P. Ectodomain shedding of the EGF-receptor ligand epigen is mediated by ADAM17. *FEBS Lett* **581**, 41–44 (2007).

218. Etzerodt, A., Maniecki, M. B., Møller, K., Møller, H. J. & Moestrup, S. K. Tumor necrosis factor α-converting enzyme (TACE/ADAM17) mediates ectodomain shedding of the scavenger receptor CD163. *J Leukoc Biol* **88**, 1201–1205 (2010).

219. Franzke, C.-W., Tasanen, K., Borradori, L., Huotari, V. & Bruckner-Tuderman, L. Shedding of collagen XVII/BP180: structural motifs influence cleavage from cell surface. *J Biol Chem* **279**, 24521–24529 (2004).

220. Liu, Q. *et al.* LRP1 shedding in human brain: roles of ADAM10 and ADAM17. *Mol Neurodegener* **4**, 17 (2009).

221. Chen, C.-D., Podvin, S., Gillespie, E., Leeman, S. E. & Abraham, C. R. Insulin stimulates the cleavage and release of the extracellular domain of Klotho by ADAM10 and ADAM17. *Proc Natl Acad Sci U S A* **104**, 19796–19801 (2007).

222. Wang, Y. & Sul, H. S. Ectodomain shedding of preadipocyte factor 1 (Pref-1) by tumor necrosis factor alpha converting enzyme (TACE) and inhibition of adipocyte differentiation. *Mol Cell Biol* **26**, 5421–5435 (2006).

223. Kawaguchi, N. *et al.* Different ADAMs have distinct influences on Kit ligand processing: phorbol-ester-stimulated ectodomain shedding of Kitl1 by ADAM17 is reduced by ADAM19. *J Cell Sci* **120**, 943–952 (2007).

224. Hansen, H. P. *et al.* The ectodomain shedding of CD30 is specifically regulated by peptide motifs in its cysteine-rich domains 2 and 5. *FASEB J* **18**, 893–895 (2004).

225. Nyborg, A. C., Ladd, T. B., Zwizinski, C. W., Lah, J. J. & Golde, T. E. Sortilin, SorCS1b, and SorLA Vps10p sorting receptors, are novel gamma-secretase substrates. *Mol Neurodegener* **1**, 3 (2006).

226. Cho, R. W. *et al.* mGluR1/5-dependent long-term depression requires the regulated ectodomain cleavage of neuronal pentraxin NPR by TACE. *Neuron* **57**, 858–871 (2008).

227. Kawaguchi, M., Hozumi, Y. & Suzuki, T. ADAM protease inhibitors reduce melanogenesis by regulating PMEL17 processing in human melanocytes. *J Dermatol Sci* **78**, 133–142 (2015).

228. Schäfer, B., Gschwind, A. & Ullrich, A. Multiple G-protein-coupled receptor signals converge on the epidermal growth factor receptor to promote migration and invasion. *Oncogene* **23**, 991–999 (2004).

229. Contin, C. *et al.* Membrane-anchored CD40 is processed by the tumor necrosis factor-alpha-converting enzyme. Implications for CD40 signaling. *J Biol Chem* **278**, 32801–32809 (2003).

230. Alfa Cissé, M. *et al.* M1 and M3 muscarinic receptors control physiological processing of cellular prion by modulating ADAM17 phosphorylation and activity. *J Neurosci* **27**, 4083–4092 (2007).

231. Young, J. *et al.* Lymphotoxin-alphabeta heterotrimers are cleaved by metalloproteinases and contribute to synovitis in rheumatoid arthritis. *Cytokine* **51**, 78–86 (2010).

232. Marczynska, J. *et al.* The role of metalloproteinase ADAM17 in regulating ICOS ligand-mediated humoral immune responses. *J Immunol* **193**, 2753–2763 (2014).

233. Peng, M. *et al.* Ectodomain shedding of Fcalpha receptor is mediated by ADAM10 and ADAM17. *Immunology* **130**, 83–91 (2010).

234. Fox, J. E. Shedding of adhesion receptors from the surface of activated platelets. *Blood Coagul Fibrinolysis* **5**, 291–304 (1994).

235. Pruessmeyer, J. *et al.* A disintegrin and metalloproteinase 17 (ADAM17) mediates inflammation-induced shedding of syndecan-1 and -4 by lung epithelial cells. *J Biol Chem* **285**, 555–564 (2010).

236. Lum, L. *et al.* Evidence for a role of a tumor necrosis factor-alpha (TNF-alpha)-converting enzyme-like protease in shedding of TRANCE, a TNF family member involved in osteoclastogenesis and dendritic cell survival. *J Biol Chem* **274**, 13613–13618 (1999).

237. Badoual, C. *et al.* The soluble alpha chain of interleukin-15 receptor: a proinflammatory molecule associated with tumor progression in head and neck cancer. *Cancer Res* **68**, 3907–3914 (2008).

238. Qu, D., Wang, Y., Esmon, N. L. & Esmon, C. T. Regulated endothelial protein C receptor shedding is mediated by tumor necrosis factor-alpha converting enzyme/ADAM17. *J Thromb Haemost* **5**, 395–402 (2007).

239. Reddy, P. *et al.* Functional analysis of the domain structure of tumor necrosis factor-alpha converting enzyme. *J Biol Chem* **275**, 14608–14614 (2000).

240. Määttä, J. A. *et al.* Proteolytic cleavage and phosphorylation of a tumor-associated ErbB4 isoform promote ligand-independent survival and cancer cell growth. *Mol Biol Cell* **17**, 67–79 (2006).

241. Rio, C., Buxbaum, J. D., Peschon, J. J. & Corfas, G. Tumor necrosis factor-alpha-converting enzyme is required for cleavage of erbB4/HER4. *J Biol Chem* **275**, 10379–10387 (2000).

242. Wunderlich, P. *et al.* Sequential proteolytic processing of the triggering receptor expressed on myeloid cells-2 (TREM2) protein by ectodomain shedding and γ-secretase-dependent intramembranous cleavage. *J Biol Chem* **288**, 33027–33036 (2013).

243. J, M., C, E., Jj, B.-S., F, C. & J, A. ADAM17 (TACE) regulates TGFβ signaling through the cleavage of vasorin. *Oncogene* **30**, (2011).

244. Chalaris, A. *et al.* Apoptosis is a natural stimulus of IL6R shedding and contributes to the proinflammatory trans-signaling function of neutrophils. *Blood* **110**, 1748–1755 (2007).

245. Schantl, J. A., Roza, M., Van Kerkhof, P. & Strous, G. J. The growth hormone receptor interacts with its sheddase, the tumour necrosis factor-alpha-converting enzyme (TACE). *Biochem J* **377**, 379–384 (2004).

246. Zhang, Q. *et al.* SRC family kinases mediate epidermal growth factor receptor ligand cleavage, proliferation, and invasion of head and neck cancer cells. *Cancer Res* **64**, 6166–6173 (2004).

247. Tsakadze, N. L. *et al.* Tumor necrosis factor-alpha-converting enzyme (TACE/ADAM-17) mediates the ectodomain cleavage of intercellular adhesion molecule-1 (ICAM-1). *J Biol Chem* **281**, 3157–3164 (2006).

248. Brou, C. *et al.* A novel proteolytic cleavage involved in Notch signaling: the role of the disintegrin-metalloprotease TACE. *Mol Cell* **5**, 207–216 (2000).

249. Rovida, E., Paccagnini, A., Del Rosso, M., Peschon, J. & Dello Sbarba, P. TNF-alpha-converting enzyme cleaves the macrophage colony-stimulating factor receptor in macrophages undergoing activation. *J Immunol* **166**, 1583–1589 (2001).

250. Koenen, R. R. *et al.* Regulated release and functional modulation of junctional adhesion molecule A by disintegrin metalloproteinases. *Blood* **113**, 4799–4809 (2009).

251. Li, N. *et al.* Metalloproteases regulate T-cell proliferation and effector function via LAG-3. *EMBO J* **26**, 494–504 (2007).

252. Maretzky, T. *et al.* L1 is sequentially processed by two differently activated metalloproteases and presenilin/gamma-secretase and regulates neural cell adhesion, cell migration, and neurite outgrowth. *Mol Cell Biol* **25**, 9040–9053 (2005).

253. Calligaris, M. *et al.* iRhom2 regulates ectodomain shedding and surface expression of the major histocompatibility complex (MHC) class I. *Cell Mol Life Sci* **81**, 163 (2024).

254. Swendeman, S. *et al.* VEGF-A stimulates ADAM17-dependent shedding of VEGFR2 and crosstalk between VEGFR2 and ERK signaling. *Circ Res* **103**, 916–918 (2008).

255. Chitadze, G. *et al.* Shedding of endogenous MHC class I-related chain molecules A and B from different human tumor entities: heterogeneous involvement of the 'a disintegrin and metalloproteases' 10 and 17. *Int J Cancer* **133**, 1557–1566 (2013).

256. Díaz-Rodríguez, E., Montero, J. C., Esparís-Ogando, A., Yuste, L. & Pandiella, A. Extracellular signal-regulated kinase phosphorylates tumor necrosis factor alpha-converting enzyme at threonine 735: a potential role in regulated shedding. *Mol Biol Cell* **13**, 2031–2044 (2002).

257. Esselens, C. W. *et al.* Metastasis-associated C4.4A, a GPI-anchored protein cleaved by ADAM10 and ADAM17. *Biol Chem* **389**, 1075–1084 (2008).

258. Na, H.-W., Shin, W.-S., Ludwig, A. & Lee, S.-T. The cytosolic domain of protein-tyrosine kinase 7 (PTK7), generated from sequential cleavage by a disintegrin and metalloprotease 17 (ADAM17) and γ-secretase, enhances cell proliferation and migration in colon cancer cells. *J Biol Chem* **287**, 25001–25009 (2012).

259. Julian, J., Dharmaraj, N. & Carson, D. D. MUC1 is a substrate for gamma-secretase. *J Cell Biochem* **108**, 802–815 (2009).

260. Fleck, D. *et al.* Dual cleavage of neuregulin 1 type III by BACE1 and ADAM17 liberates its EGF-like domain and allows paracrine signaling. *J Neurosci* **33**, 7856–7869 (2013).

261. Ruhe, J. E., Streit, S., Hart, S. & Ullrich, A. EGFR signaling leads to downregulation of PTP-LAR via TACE-mediated proteolytic processing. *Cell Signal* **18**, 1515–1527 (2006).

262. Kalus, I., Bormann, U., Mzoughi, M., Schachner, M. & Kleene, R. Proteolytic cleavage of the neural cell adhesion molecule by ADAM17/TACE is involved in neurite outgrowth. *J Neurochem* **98**, 78–88 (2006).

263. Romero, Y., Wise, R. & Zolkiewska, A. Proteolytic processing of PD-L1 by ADAM proteases in breast cancer cells. *Cancer Immunol Immunother* **69**, 43–55 (2020).

264. Fabre-Lafay, S. *et al.* Nectin-4, a new serological breast cancer marker, is a substrate for tumor necrosis factor-alpha-converting enzyme (TACE)/ADAM-17. *J Biol Chem* **280**, 19543–19550 (2005).

265. Althoff, K. *et al.* Recognition sequences and structural elements contribute to shedding susceptibility of membrane proteins. *Biochem J* **353**, 663–672 (2001).

266. Borrell-Pagès, M., Rojo, F., Albanell, J., Baselga, J. & Arribas, J. TACE is required for the activation of the EGFR by TGF-alpha in tumors. *EMBO J* **22**, 1114–1124 (2003).

267. Kenny, P. A. & Bissell, M. J. Targeting TACE-dependent EGFR ligand shedding in breast cancer. *J Clin Invest* **117**, 337–345 (2007).

268. Zhu, L. *et al.* Regulated surface expression and shedding support a dual role for semaphorin 4D in platelet responses to vascular injury. *Proc Natl Acad Sci U S A* **104**, 1621–1626 (2007).

269. Tanabe, Y., Kasahara, T., Momoi, T. & Fujita, E. Neuronal RA175/SynCAM1 isoforms are processed by tumor necrosis factor-alpha-converting enzyme (TACE)/ADAM17-like proteases. *Neurosci Lett* **444**, 16–21 (2008).

270. Schweigert, O. *et al.* Soluble T cell immunoglobulin and mucin domain (TIM)-1 and -4 generated by A Disintegrin And Metalloprotease (ADAM)-10 and -17 bind to phosphatidylserine. *Biochim Biophys Acta* **1843**, 275–287 (2014).

271. Ermert, M. *et al.* In situ localization of TNFalpha/beta, TACE and TNF receptors TNF-R1 and TNF-R2 in control and LPS-treated lung tissue. *Cytokine* **22**, 89–100 (2003).

272. Caolo, V. *et al.* ADAM10 and ADAM17 have opposite roles during sprouting angiogenesis. *Angiogenesis* **18**, 13–22 (2015).

273. Garton, K. J., Gough, P. J. & Raines, E. W. Emerging roles for ectodomain shedding in the regulation of inflammatory responses. *J Leukoc Biol* **79**, 1105–1116 (2006).

274. Singh, R. J. R. *et al.* Cytokine stimulated vascular cell adhesion molecule-1 (VCAM-1) ectodomain release is regulated by TIMP-3. *Cardiovasc Res* **67**, 39–49 (2005).

275. Düsterhöft, S., Lokau, J. & Garbers, C. The metalloprotease ADAM17 in inflammation and cancer. *Pathology - Research and Practice* **215**, 152410 (2019).

276. Grell, M. *et al.* The transmembrane form of tumor necrosis factor is the prime activating ligand of the 80 kDa tumor necrosis factor receptor. *Cell* **83**, 793–802 (1995).

277. Robak, T., Gladalska, A. & Stepień, H. The tumour necrosis factor family of receptors/ligands in the serum of patients with rheumatoid arthritis. *Eur Cytokine Netw* **9**, 145–154 (1998).

278. Poltorak, A. *et al.* Defective LPS Signaling in C3H/HeJ and C57BL/10ScCr Mice: Mutations in Tlr4 Gene. *Science* **282**, 2085–2088 (1998).

279. McIlwain, D. R. *et al.* iRhom2 regulation of TACE controls TNF-mediated protection against Listeria and responses to LPS. *Science* **335**, 229–232 (2012).

280. Bradley, J. TNF-mediated inflammatory disease. *The Journal of Pathology* **214**, 149–160 (2008).

281. Deng, M., Loughran, P. A., Zhang, L., Scott, M. J. & Billiar, T. R. Shedding of the tumor necrosis factor (TNF) receptor from the surface of hepatocytes during sepsis limits inflammation through cGMP signaling. *Sci Signal* **8**, ra11 (2015).

282. Horiuchi, K. *et al.* Cutting edge: TNF-alpha-converting enzyme (TACE/ADAM17) inactivation in mouse myeloid cells prevents lethality from endotoxin shock. *J Immunol* **179**, 2686–2689 (2007).

283. Li, Y., Brazzell, J., Herrera, A. & Walcheck, B. ADAM17 deficiency by mature neutrophils has differential effects on L-selectin shedding. *Blood* **108**, 2275–2279 (2006).

284. Long, C., Wang, Y., Herrera, A. H., Horiuchi, K. & Walcheck, B. In vivo role of leukocyte ADAM17 in the inflammatory and host responses during E. coli-mediated peritonitis. *Journal of Leukocyte Biology* **87**, 1097–1101 (2010).

285. Wolf, J., Rose-John, S. & Garbers, C. Interleukin-6 and its receptors: a highly regulated and dynamic system. *Cytokine* **70**, 11–20 (2014).

286. Calabrese, L. H. & Rose-John, S. IL-6 biology: implications for clinical targeting in rheumatic disease. *Nat Rev Rheumatol* **10**, 720–727 (2014).

287. Babendreyer, A. *et al.* Differential Induction of the ADAM17 Regulators iRhom1 and 2 in Endothelial Cells. *Front. Cardiovasc. Med.* **7**, (2020).

288. Adrain, C., Zettl, M., Christova, Y., Taylor, N. & Freeman, M. Tumor necrosis factor signaling requires iRhom2 to promote trafficking and activation of TACE. *Science* **335**, 225–228 (2012).

289. Issuree, P. D. A. *et al.* iRHOM2 is a critical pathogenic mediator of inflammatory arthritis. *J Clin Invest* **123**, 928–932 (2013).

290. Qing, X. *et al.* iRhom2 promotes lupus nephritis through TNF-α and EGFR signaling. *J Clin Invest* **128**, 1397–1412 (2018).

291. Ge, C.-X. *et al.* iRhom2 deficiency relieves TNF-α associated hepatic dyslipidemia in long-term PM2.5-exposed mice. *Biochem Biophys Res Commun* **493**, 1402–1409 (2017).

292. Franzke, C.-W. *et al.* Epidermal ADAM17 maintains the skin barrier by regulating EGFR ligand-dependent terminal keratinocyte differentiation. *J Exp Med* **209**, 1105–1119 (2012).

293. Rossello, A., Nuti, E., Ferrini, S. & Fabbi, M. Targeting ADAM17 Sheddase Activity in Cancer. *Curr Drug Targets* **17**, 1908–1927 (2016).

294. Schmidt, S. *et al.* ADAM17 is required for EGF-R–induced intestinal tumors via IL-6 trans-signaling. *Journal of Experimental Medicine* **215**, 1205–1225 (2018).

295. Bolik, J. *et al.* Inhibition of ADAM17 impairs endothelial cell necroptosis and blocks metastasis. *Journal of Experimental Medicine* **219**, e20201039 (2021).

296. Sun, J. *et al.* Therapeutic potential of ADAM17 modulation in gastric cancer through regulation of the EGFR and TNF-α signalling pathways. *Mol Cell Biochem* **426**, 17–26 (2017).

297. Li, W. *et al.* ADAM17 promotes lymph node metastasis in gastric cancer via activation of the Notch and Wnt signaling pathways. *Int J Mol Med* **43**, 914–926 (2019).

298. Xu, M. *et al.* ADAM17 promotes epithelial-mesenchymal transition via TGF-β/Smad pathway in gastric carcinoma cells. *Int J Oncol* **49**, 2520–2528 (2016).

299. Ishida, Y., Agata, Y., Shibahara, K. & Honjo, T. Induced expression of PD-1, a novel member of the immunoglobulin gene superfamily, upon programmed cell death. *EMBO J* **11**, 3887–3895 (1992).

300. Dong, H. *et al.* Tumor-associated B7-H1 promotes T-cell apoptosis: A potential mechanism of immune evasion. *Nat Med* **8**, 793–800 (2002).

301. Brahmer, J. R. *et al.* Safety and activity of anti-PD-L1 antibody in patients with advanced cancer. *N Engl J Med* **366**, 2455–2465 (2012).

302. Geesala, R., Issuree, P. D. & Maretzky, T. Novel functions of inactive rhomboid proteins in immunity and disease. *Journal of Leukocyte Biology* **106**, 823–835 (2019).

303. Yan, Z. *et al.* Human rhomboid family-1 gene silencing causes apoptosis or autophagy to epithelial cancer cells and inhibits xenograft tumor growth. *Mol Cancer Ther* **7**, 1355–1364 (2008).

304. Zhou, Z. *et al.* Human rhomboid family-1 suppresses oxygen-independent degradation of hypoxia-inducible factor-1α in breast cancer. *Cancer Res* **74**, 2719–2730 (2014).

305. Zou, H. *et al.* Human rhomboid family-1 gene RHBDF1 participates in GPCR-mediated transactivation of EGFR growth signals in head and neck squamous cancer cells. *FASEB J* **23**, 425–432 (2009).

306. Luo, Z. *et al.* Inhibition of iRhom1 by CD44-targeting nanocarrier for improved cancer immunochemotherapy. *Nat Commun* **15**, 255 (2024).

307. Saarinen, S. *et al.* Analysis of a Finnish family confirms RHBDF2 mutations as the underlying factor in tylosis with esophageal cancer. *Fam Cancer* **11**, 525–528 (2012).

308. Blaydon, D. C. *et al.* RHBDF2 mutations are associated with tylosis, a familial esophageal cancer syndrome. *Am J Hum Genet* **90**, 340–346 (2012).

309. Mokoena, T., Smit, J. G. M., Karusseit, V. O., Dorfling, C. M. & van Rensburg, E. J. Tylosis associated with squamous cell carcinoma of the oesophagus (TOC): Report of an African family with a novel RHBDF2 variant. *Clin Genet* **93**, 1114–1116 (2018).

310. Hosur, V., Low, B. E., Shultz, L. D. & Wiles, M. V. Genetic deletion of amphiregulin restores the normal skin phenotype in a mouse model of the human skin disease tylosis. *Biol Open* **6**, 1174–1179 (2017).

311. Rabinowitsch, A. I. *et al.* Analysis of the function of ADAM17 in iRhom2 curly-bare and tylosis with esophageal cancer mutant mice. *J Cell Sci* **136**, jcs260910 (2023).

312. Wilkins, M. R. *et al.* From Proteins to Proteomes: Large Scale Protein Identification by Two-Dimensional Electrophoresis and Arnino Acid Analysis. *Nat Biotechnol* **14**, 61–65 (1996).

313. Elhamraoui, Z. What are DIA and DDA and how does the data looks like ? *Medium* https://medium.com/@zahraelhamraoui1997/what-are-dia-and-dda-and-how-does-the-data-looks-like-e18a3a532142 (2024).

314. Tyanova, S., Temu, T. & Cox, J. The MaxQuant computational platform for mass spectrometry-based shotgun proteomics. *Nat Protoc* **11**, 2301–2319 (2016).

315. Demichev, V., Messner, C. B., Vernardis, S. I., Lilley, K. S. & Ralser, M. DIA-NN: neural networks and interference correction enable deep proteome coverage in high throughput. *Nat Methods* **17**, 41–44 (2020).

316. Tyanova, S. *et al.* The Perseus computational platform for comprehensive analysis of (prote)omics data. *Nat Methods* **13**, 731–740 (2016).

317. Aebersold, R. & Mann, M. Mass spectrometry-based proteomics. *Nature* **422**, 198–207 (2003).

318. Aebersold, R. & Mann, M. Mass-spectrometric exploration of proteome structure and function. *Nature* **537**, 347–355 (2016).

319. Tucher, J. *et al.* LC–MS Based Cleavage Site Profiling of the Proteases ADAM10 and ADAM17 Using Proteome-Derived Peptide Libraries. *J. Proteome Res.* **13**, 2205–2214 (2014).

320. Wiśniewski, J. R., Zougman, A., Nagaraj, N. & Mann, M. Universal sample preparation method for proteome analysis. *Nat Methods* **6**, 359–362 (2009).

321. Wilm, M. & Mann, M. Analytical Properties of the Nanoelectrospray Ion Source. *Anal. Chem.* **68**, 1–8 (1996).

322. Fenn, J. B., Mann, M., Meng, C. K., Wong, S. F. & Whitehouse, C. M. Electrospray Ionization for Mass Spectrometry of Large Biomolecules. *Science* **246**, 64–71 (1989).

323. Herrero, P. *et al.* Comparison of triple quadrupole mass spectrometry and Orbitrap high-resolution mass spectrometry in ultrahigh performance liquid chromatography for the determination of veterinary drugs in sewage: benefits and drawbacks. *J Mass Spectrom* **49**, 585–596 (2014).

324. Domon, B. & Aebersold, R. Mass Spectrometry and Protein Analysis. *Science* **312**, 212–217 (2006).

325. Michalski, A., Cox, J. & Mann, M. More than 100,000 Detectable Peptide Species Elute in Single Shotgun Proteomics Runs but the Majority is Inaccessible to Data-Dependent LC−MS/MS. *J. Proteome Res.* **10**, 1785–1793 (2011).

326. Ludwig, C. *et al.* Data-independent acquisition-based SWATH-MS for quantitative proteomics: a tutorial. *Mol Syst Biol* **14**, e8126 (2018).

327. Maretzky, T. *et al.* iRhom2 controls the substrate selectivity of stimulated ADAM17-dependent ectodomain shedding. *Proc Natl Acad Sci U S A* **110**, 11433–11438 (2013).

328. Rappsilber, J., Ishihama, Y. & Mann, M. Stop and go extraction tips for matrix-assisted laser desorption/ionization, nanoelectrospray, and LC/MS sample pretreatment in proteomics. *Anal Chem* **75**, 663–670 (2003).

329. Cox, J. & Mann, M. MaxQuant enables high peptide identification rates, individualized p.p.b.-range mass accuracies and proteome-wide protein quantification. *Nat Biotechnol* **26**, 1367–1372 (2008).

330. Jocher, G. *et al.* ADAM10 and ADAM17 promote SARS-CoV-2 cell entry and spike protein-mediated lung cell fusion. *EMBO Rep* **23**, e54305 (2022).

331. Sf, L. *et al.* The cell adhesion protein P-selectin glycoprotein ligand-1 is a substrate for the aspartyl protease BACE1. *The Journal of biological chemistry* **278**, (2003).

332. Ardito, C. M. *et al.* EGF receptor is required for KRAS-induced pancreatic tumorigenesis. *Cancer Cell* **22**, 304–317 (2012).

333. Chalaris, A. *et al.* Critical role of the disintegrin metalloprotease ADAM17 for intestinal inflammation and regeneration in mice. *Journal of Experimental Medicine* **207**, 1617–1624 (2010).

334. Franzke, C.-W. *et al.* Epidermal ADAM17 maintains the skin barrier by regulating EGFR ligand-dependent terminal keratinocyte differentiation. *J Exp Med* **209**, 1105–1119 (2012).

335. Kelsall, B. Interleukin-10 in Inflammatory Bowel Disease. *New England Journal of Medicine* **361**, 2091–2093 (2009).

336. Zunke, F. & Rose-John, S. The shedding protease ADAM17: Physiology and pathophysiology. *Biochim Biophys Acta Mol Cell Res* **1864**, 2059–2070 (2017).

337. Grieve, A. G. *et al.* Phosphorylation of iRhom2 at the plasma membrane controls mammalian TACE-dependent inflammatory and growth factor signalling. *Elife* **6**, e23968 (2017).

338. Cavadas, M. *et al.* Phosphorylation of iRhom2 Controls Stimulated Proteolytic Shedding by the Metalloprotease ADAM17/TACE. *Cell Rep* **21**, 745–757 (2017).

339. Strategies to Target ADAM17 in Disease: From its Discovery to the iRhom Revolution - PubMed. https://pubmed.ncbi.nlm.nih.gov/33579029/.

340. Müller, S. A., Scilabra, S. D. & Lichtenthaler, S. F. Proteomic Substrate Identification for Membrane Proteases in the Brain. *Front Mol Neurosci* **9**, 96 (2016).

341. Tüshaus, J. *et al.* The pseudoprotease iRhom1 controls ectodomain shedding of membrane proteins in the nervous system. *FASEB J* **35**, e21962 (2021).

342. Xie, J. & Wang, H. Semaphorin 7A as a potential immune regulator and promising therapeutic target in rheumatoid arthritis. *Arthritis Res Ther* **19**, 10 (2017).

343. Okamura, Y., Kohmura, E. & Yamashita, T. TACE cleaves neogenin to desensitize cortical neurons to the repulsive guidance molecule. *Neurosci Res* **71**, 63–70 (2011).

344. van Erp, S. *et al.* Lrig2 Negatively Regulates Ectodomain Shedding of Axon Guidance Receptors by ADAM Proteases. *Developmental Cell* **35**, 537–552 (2015).

345. Nyren-Erickson, E. K., Jones, J. M., Srivastava, D. K. & Mallik, S. A disintegrin and metalloproteinase-12 (ADAM12): function, roles in disease progression, and clinical implications. *Biochim Biophys Acta* **1830**, 4445–4455 (2013).

346. Saftig, P. & Lichtenthaler, S. F. The alpha secretase ADAM10: A metalloprotease with multiple functions in the brain. *Prog Neurobiol* **135**, 1–20 (2015).

347. Gillet, L. C. *et al.* Targeted data extraction of the MS/MS spectra generated by data-independent acquisition: a new concept for consistent and accurate proteome analysis. *Mol Cell Proteomics* **11**, O111.016717 (2012).

348. Zhao, Y. *et al.* Identification of Molecular Determinants in iRhoms1 and 2 That Contribute to the Substrate Selectivity of Stimulated ADAM17. *Int J Mol Sci* **23**, 12796 (2022).

349. Kawahara, R. *et al.* Mass spectrometry-based proteomics revealed Glypican-1 as a novel ADAM17 substrate. *J Proteomics* **151**, 53–65 (2017).

350. Zhang, R. *et al.* Mxra8 is a receptor for multiple arthritogenic alphaviruses. *Nature* **557**, 570–574 (2018).

351. Feng, F. *et al.* Colocalization of Chikungunya Virus with Its Receptor MXRA8 during Cell Attachment, Internalization, and Membrane Fusion. *J Virol* **97**, e0155722 (2023).

352. Pengam, S. *et al.* SIRPα/CD47 axis controls the maintenance of transplant tolerance sustained by myeloid-derived suppressor cells. *Am J Transplant* **19**, 3263–3275 (2019).

353. Toth, A. B. *et al.* Synapse maturation by activity-dependent ectodomain shedding of SIRPα. *Nat Neurosci* **16**, 1417–1425 (2013).

354. Oronsky, B., Carter, C., Reid, T., Brinkhaus, F. & Knox, S. J. Just eat it: A review of CD47 and SIRP-α antagonism. *Semin Oncol* **47**, 117–124 (2020).

355. Huang, A. *et al.* Exosomal Transfer of Vasorin Expressed in Hepatocellular Carcinoma Cells Promotes Migration of Human Umbilical Vein Endothelial Cells. *Int J Biol Sci* **11**, 961–969 (2015).

356. Karunakaran, D. *et al.* Protein Kinase C Controls Vesicular Transport and Secretion of Apolipoprotein E from Primary Human Macrophages. *J Biol Chem* **288**, 5186–5197 (2013).

357. Luo, W.-W. *et al.* iRhom2 is essential for innate immunity to DNA viruses by mediating trafficking and stability of the adaptor STING. *Nat Immunol* **17**, 1057–1066 (2016).

358. Luo, W.-W. *et al.* iRhom2 is essential for innate immunity to RNA virus by antagonizing ER- and mitochondria-associated degradation of VISA. *PLOS Pathogens* **13**, e1006693 (2017).